This dissertation has been
microfilmed exactly as received

69-18,029

HUANG, Chi Kan, 1938-
THE THERMAL CURRENT STRUCTURE IN LAKE MICHIGAN - A THEORETICAL AND OBSERVATIONAL MODEL STUDY.

The University of Michigan, Ph.D., 1969
Oceanography

University Microfilms, Inc., Ann Arbor, Michigan

THE THERMAL CURRENT STRUCTURE IN LAKE MICHIGAN

A Theoretical and Observational Model Study

by

Chi Kan Huang

A dissertation submitted in partial fulfillment
of the requirements for the degree of
Doctor of Philosophy in
The University of Michigan
1969

Doctoral Committee:

Professor John C. Ayers, Co-Chairman
Associate Professor Stanley J. Jacobs, Co-Chairman
Professor Aksel C. Wiin-Nielsen
Professor Chia-Shun Yih
Doctor Vincent E. Noble, U. S. Naval Oceanographic Office

A B S T R A C T

THE THERMAL CURRENT STRUCTURE IN LAKE MICHIGAN

A Theoretical and Observational Model Study

by

Chi Kan Huang

Co-chairmen: Stanley J. Jacobs and John C. Ayers

A study is made of the thermally induced circulation in Lake Michigan. The surface temperature of the lake is approximated as a concave cosine function during the warming-up seasons and as a convex cosine function during the cooling-off seasons. The bottom boundary has very stable temperature all year round and a small heat flux is allowed to flow through the side boundaries. The free surface is assumed to be free from wind stresses.

It is noticed from a literature survey that for small thermal Rossby number and small Ekman number, such as found in the Lake Michigan model, flow in the lower symmetrical regime is expected to occur. Therefore, in this theoretical study, the first step is to linearize the system of nonlinear governing equations of the flow field by expanding all nondimensional dependent variables in powers of the small thermal Rossby number. Then, for every order of the thermal Rossby number in the expansion, a matching additive type boundary layer analysis is used to obtain inner and outer approximate solutions of the flow field. Under the scheme of double perturbation expansion, ignoring four small corners, the temperature distribution and the velocity field can be systematically solved for all regions.

Two types of general thermal currents have been found from the analytic solutions in our theoretical study. The type-A circulation has a cyclonic meridional velocity and two cells of zonal and vertical flow in the cross-section with sinking motion at the middle and upwellings on both edges of the lake. This type of circulation is expected to occur during the winter-cooling period, usually from January to March, and during the summer-heating period, which is usually the period between the disappearance of the thermal bar and the period of strong stratification. The type-B circulation takes place generally in late March (denoted as the spring-heating period) or late November and December (denoted as the autumn-cooling period). Its flow is exactly the reverse of the type-A circulation.

The type-C circulation occurs during the spring and the autumn thermal bar periods when two weakly stratified waters, one of which is in direct stratification and above 4°C as the other is in inverse stratification and below 4°C, mix together and sink along the 4°C isotherm (the thermal bar). The result is a four-cell circulation pattern with sinking motions at the thermal bars and upwellings in the middle and on both edges of the lake. Zonal flows are mostly restricted to the upper and lower Ekman layers. The meridional currents indicate loosely sheared flow along the thermal bar with the center of the lake as the nodal point.

Some field measurements for currents and eddy viscosities were conducted during 1967 and 1968 in Lake Michigan. Comparisons have been made between these theoretical predictions and the previously published field data. Qualitatively, the thermal current structure and temperature distribution agree very well with other observations as well as with our own field studies. This leads one to postulate that the thermal body force does play an important role in generating the mean lake circulation pattern.

To My Mother

ACKNOWLEDGMENTS

I wish to express my deepest gratitude to Professor John C. Ayers and Professor Stanley J. Jacobs, co-chairmen of my doctoral committee, for their encouragement, guidance, and criticism throughout my graduate studies and this research in particular.

I also wish to acknowledge my debt to Professor Aksel C. Wiin-Nielsen who, through teaching and personal discussion, has exposed me to his admirable scholarship, and who made my study in this University possible to begin with. Special appreciation is tendered to Professor Chia-Shun Yih who has been most helpful through his inspiring teaching and insight-giving discussion. My sincere thanks are extended to Dr. Vincent E. Noble who was very instrumental in recognizing the importance of the thermally induced phenomenon in Lake Michigan and who financially supported me in the initial stage of this research.

Great Lakes Research Division provided much of the material supplies, and granted me the privilege of using the research vessels INLAND SEAS and MYSIS which made the field measurements possible. The author is grateful to his fellow colleagues at the Division, especially Mr. Eduardo D. Michelena and Mr. Hung Kwong Soo and to captains and crews of the research vessels for their assistance and cooperation during his field observations.

My first year at The University of Michigan was supported by a Rackham Graduate School Predoctoral Fellowship. This research has received support from the U. S. Public Health Service Grants WP-00311 and WP-01067, from the National Science Foundation Grant GA-524, and grants from the American Electric Service Corporation, and the Toledo Edison Company.

Finally, my fond recognition is due my wife, Nancy, for her help, patience, sacrifices, and encouragement.

TABLE OF CONTENTS

	Page
LIST OF TABLES	vii
LIST OF FIGURES	viii
CHAPTER	
I. INTRODUCTION AND LITERATURE SURVEY	1
Introduction	1
Previous Observational Studies	12
Literature Survey	15
II. A BAROCLINIC DYNAMIC MODEL OF LAKE MICHIGAN	20
General Physical Description of Lake Michigan	20
Modeling Considerations	25
Mathematical Formulation of the General Governing Equations	26
Boundary Conditions and Seasonal Variations of the Surface Temperature Distributions	30
Velocity field	30
Seasonal variation of the surface temperature distribution	30
III. GENERAL THERMAL CURRENTS	33
Mathematical Formulation and Methods of Approximation	33
The equation of state	33
Nondimensional governing equations	33
Methods leading to the approximate solutions	36
Boundary layer scaling	41
Analytical Approximate Solutions	44
The zeroth R-order solutions	44
The first R-order solutions	51
Estimated Errors of the Approximate Solutions	61
Temperature	61
Velocity	61
Type-A Circulation	62
Type-B Circulation	62
IV. THE THERMAL BAR CURRENT	63
Mathematical Formulation	63

TABLE OF CONTENTS (Continued)

		Page
	The approximate equation of state	63
	Nondimensional governing equations	65
	Boundary layer scaling	69
	Analytical Approximate Solutions	70
	The zeroth R-order solutions	70
	The first R-order solutions	73
V.	EDDY VISCOSITY AND EDDY DIFFUSIVITY IN LAKE MICHIGAN	82
	Introduction to the Characteristics of Eddy Viscosity and Eddy Diffusivity	82
	Theoretical Background of the Formulae	85
	Reynolds stress and velocity gradient	85
	Mixing length and logarithmic velocity distribution	87
	Empirical formula for estimating vertical eddy viscosity from wind	89
	Eddy diffusivity based on statistical theory of turbulence	89
	Richardson's neighbor separation	93
	The Magnitudes	94
	An estimate of eddy viscosity by Reynolds stress and vertical velocity gradients	94
	An estimate of the upper limit value of eddy viscosity and eddy diffusivity by statistical theory	97
	An estimation of vertical eddy viscosity from current measurement near the bottom	97
	An approximation of the vertical eddy viscosity by surface wind	98
	Measurements of the eddy diffusivity by the dispersion of marked particles	99
	A measurement of the horizontal diffusion by drogue studies	107
	Comparisons of Values with Other Studies	112
	Reasonable Value for Model Study	113
VI.	REPRESENTATIVE VALUES OF PARAMETERS IN THE LAKE MICHIGAN MODEL	115
	General Physical Data	115
	Parameters as Functions of Seasonal Temperatures	116
	General thermal current	116
	Thermal bar current	118
VII.	THERMAL CURRENT CIRCULATION PATTERNS AND TEMPERATURE DISTRIBUTIONS FROM SOLUTIONS OF THE BAROCLINIC DYNAMIC MODEL OF LAKE MICHIGAN	119

TABLE OF CONTENTS (Concluded)

	Page
Temperature Distribution	120
General thermal current periods	120
Thermal bar periods	122
Velocity Field	124
General thermal currents	124
Thermal bar current	130
VIII. COMPARISON OF THE RESULTS FROM THE THEORETICAL MODEL STUDY WITH FIELD OBSERVATIONS	136
Theoretical Results	136
Closing the South End of the Lake Michigan Model	138
Comparison of Temperatures	139
Comparison of Velocity Field	151
Meridional velocity	151
Zonal and vertical velocities	159
IX. CONCLUSIONS	162
REFERENCES	164

LIST OF TABLES

Table		Page
1.	Nomenclature and Nondimensional Parameters	28
2.	Local Coordinates in Different Regions	43
3.	Abbreviations for Constant Functions	45
4.	Eddy Viscosity on Two Current-Meter Buoy Stations	96
5.	Estimated Vertical Eddy Viscosity from Current Measurement Near Bottom	98
6.	Estimated Vertical Eddy Viscosity From Wind Speed	99
7.	General Information and Effective Eddy Diffusivity of Dye Patch Studies	102
8.	General Information and Effective Eddy Diffusivity of Continuous Source Dye Plume Studies	108
9.	General Information and Eddy Diffusivity of Drogue Study in Lake Michigan	111
10.	General Physical Data Used in the Lake Michigan Model	115
11.	Values of Parameters Connected with Temperature for the General Thermal Currents	117
12.	Values of Parameters Connected with Temperature for the Thermal Bar Currents	118
13.	Drogue Studies of Surface Current on the West Side of Lake Michigan	158
14.	Percentage of Hours Current Flowed Northward, Westward, and Southward on the East Side of Lake Michigan Near Benton Harbor, Michigan	158

LIST OF FIGURES

Figure		Page
1.	The St. Lawrence Great Lakes and their mean currents during the navigation season.	2
2.	Surface temperature pattern of Lake Michigan in July 1962, obtained with the Barnes infrared radiation thermometer.	5
3.	Typical temperature transects in Lake Michigan.	6
4.	Various regimes of flow field occurring in a rotating fluid differentially heated in the horizontal as functions of non-dimensional thermal Rossby number and Taylor number.	17
5.	East-west cross-section of Lake Michigan between Milwaukee, Wisconsin and Muskegon, Michigan.	21
6.	Cross-section of a long, symmetrical, trapezoidal Lake Michigan model.	27
7.	Interior and boundary-layer regions of the Lake Michigan model.	41
8.	Relationship between freshwater density and temperature.	64
9.	A typical distribution of dye concentration across a dye patch.	101
10.	Lateral growth of the dye patch with time.	103
11.	Longitudinal growth of the dye patch with time.	104
12.	Continuous source apparatus.	105
13.	Lateral growth of dye plume at a constant distance from the source (between two marker buoys transverse to the current).	109
14.	Lateral growth of dye plume with distance from source.	110
15.	Nondimensional temperature distribution in Lake Michigan model for general thermal current periods.	121
16.	Nondimensional temperature distribution during thermal bar periods.	123

		Page
17.	Nondimensional meridional velocity of type-A circulation.	126
18.	Nondimensional zonal and vertical velocity components of type-A circulation.	129
19.	Nondimensional meridional velocity of thermal bar currents (type-C circulation).	131
20.	Nondimensional zonal and vertical thermal bar current circulation.	134
21.	January temperature distribution across the Milwaukee-Muskegon section in Lake Michigan.	140
22.	February temperature distribution across the Milwaukee-Muskegon section in Lake Michigan.	141
23.	March temperature distribution across the Milwaukee-Muskegon section in Lake Michigan.	142
24.	April temperature distribution across the Milwaukee-Muskegon section in Lake Michigan.	143
25.	Temperature distribution across a section of the thermal bar.	144
26.	May temperature distribution across the Milwaukee-Muskegon section in Lake Michigan.	146
27.	June temperature distribution across the Manitowoc-Frankfort section in Lake Michigan.	147
28.	November temperature distribution across the Milwaukee-Muskegon section in Lake Michigan.	149
29.	December temperature distribution across the Milwaukee-Muskegon section in Lake Michigan.	150
30.	June surface currents in Lake Michigan.	153
31.	First basic winter surface current pattern in Lake Michigan.	155
32.	Second basic winter surface current pattern in Lake Michigan.	156

LIST OF FIGURES (Concluded)

		Page
33.	Drogue studies for surface current measurements near western shore.	157
34.	Thermal bar circulation.	160
35.	Aerial photograph of thermal bar phenomena on 7 May 1968 near Grand Haven, Michigan.	161

I. INTRODUCTION AND LITERATURE SURVEY

Introduction

The St. Lawrence Great Lakes constitute the largest body of fresh water in the world and have long been considered as the inland "oceans" in the North American Continent. In spite of various differences between the properties of oceans and those of freshwater lakes, general physical phenomena in the two remain quite similar. The special characteristics of a freshwater Great Lake, such as negligible salinity and tides, and the more tractable boundary conditions make the lake an ideal huge hydrodynamic laboratory. In recent years great emphasis has been given to the value of the lakes as testing basins for oceanographic studies and to understanding all aspects of the limnological dynamics of the lakes. Figure 1 shows the Great Lakes and their mean surface currents during warmer months (after Millar, 1952).

The climate in the Great Lakes region is typically humid continental with a severe winter and a warm summer. The continental climate, modified by the stabilizing effect of the body of fresh water, gives this region more rapidly changing and complex weather patterns than those of the maritime region. Since the Great Lakes lie in the interior of the North American continent between source regions of contrasting polar and tropical air masses, this region is at the junction of the paths of storms from several areas of cyclogenesis in the western portion of the continent. Cyclonic storms produced along the polar front usually move toward the Great Lakes under the influence of the general

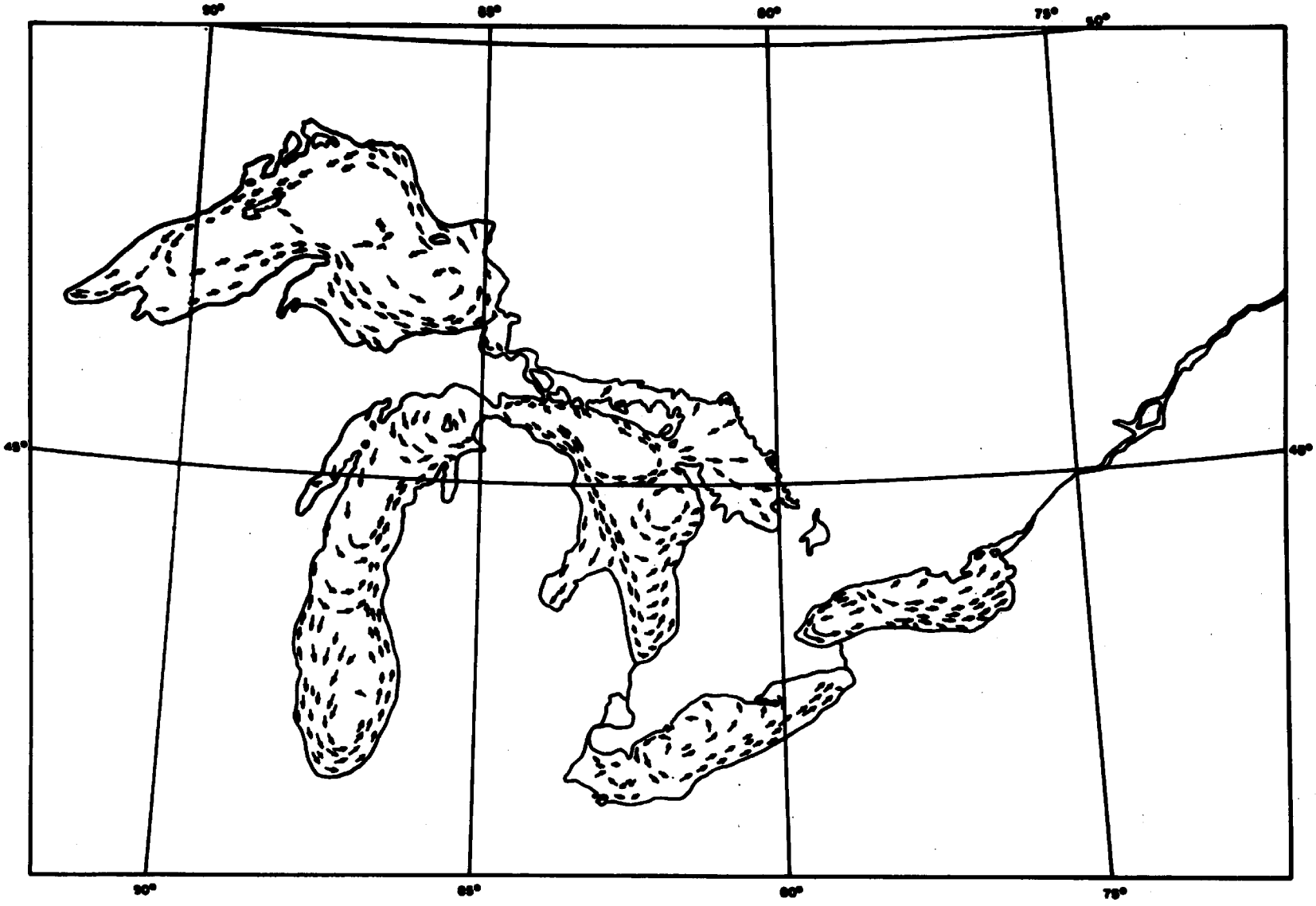


Figure 1. The St. Lawrence Great Lakes and their mean currents during the navigation season (from Millar, 1952).

western circulation. The numerous shifts in wind and changes in weather are due mostly to the many moving cyclones and anticyclones traversing the area. Although westerly winds prevail, winds from any direction are likely to be encountered, shifting in relation to the particular position with respect to the moving pressure centers (U. S. Dept. of Commerce, 1959).

The general annual thermal cycle in the lake has been discussed by Hutchinson (1957). For a relatively deep large lake in the temperate continental climate region, such as any one of the Great Lakes, the lake temperature falls below 4°C during the winter and rises far above 4°C during the summer. The lake is homogeneous in the winter and stratified in the summer. The quasi-homogeneous period in Lake Michigan is from November through June (Ayers, 1962). Fall turn-over continues almost all winter. As the season progresses the lake gradually becomes stratified with a relatively small vertical temperature gradient in the upper layer, the epilimnion, and another relatively larger vertical temperature decrease in the lower cold layer, the hypolimnion. Between these two layers there is a very thin layer of sharp vertical temperature gradient called the thermocline. In the autumn the epilimnion thickens due to convective mixing induced by surface cooling, the thermocline becomes weaker and deeper and finally disappears, and the lake again becomes homogeneous. If the lake freezes in winter, inverse stratification may be set up below the ice. However, for the lakes in this region, the surface is only partially ice-covered during the winter. Therefore most of the main body of the lake cools progressively during winter and reaches temperatures below 4°C. The thermal cycle does not start until the arrival of the warm-up season.

Since soil has a much lower specific heat and thermal conductivity than water, the land surface is more sensitive to the rate of change of heating or cooling the atmosphere. Consequently, a temperature gradient, either lakeward or shoreward, always exists along the perimeter of the lake during warming-up or cooling-off seasons. Figure 2 shows the surface temperature pattern in July 1962 (McFadden and Ragotzkie, 1963). Figure 3 shows some typical surface temperature transects in Lake Michigan during warming-up and cooling-off periods. In the late summer and through autumn, there is not much horizontal temperature difference between land and water and a strong thermocline always exists in the lake. In general, the lake is homogeneous, or nearly so, in winter, spring, and early summer.

A unique density characteristic of water makes aquatic life in it possible in winter as well as in other seasons. The density of fresh water is a maximum at 4°C, and decreases as the temperature deviates, either positively or negatively, away from the temperature of maximum density. The variation of the density of water in relation to the temperature substantially affects the nature of heat distribution and develops circulation phenomena in the body of water.

The energy inputs into the lake that are responsible for mixing and movement of its water, directly and indirectly, are the meteorological forces, the thermal forces, and the tidal forces. The last factor is negligible in the Great Lakes (Hough, 1958). Other forces which do not produce currents (but affect them) are the Coriolis, frictional, turbulent, and centrifugal forces.

Of the two main current generating forces, most scientists, in predicting lake currents, have considered the effects due to the wind stresses and neglected

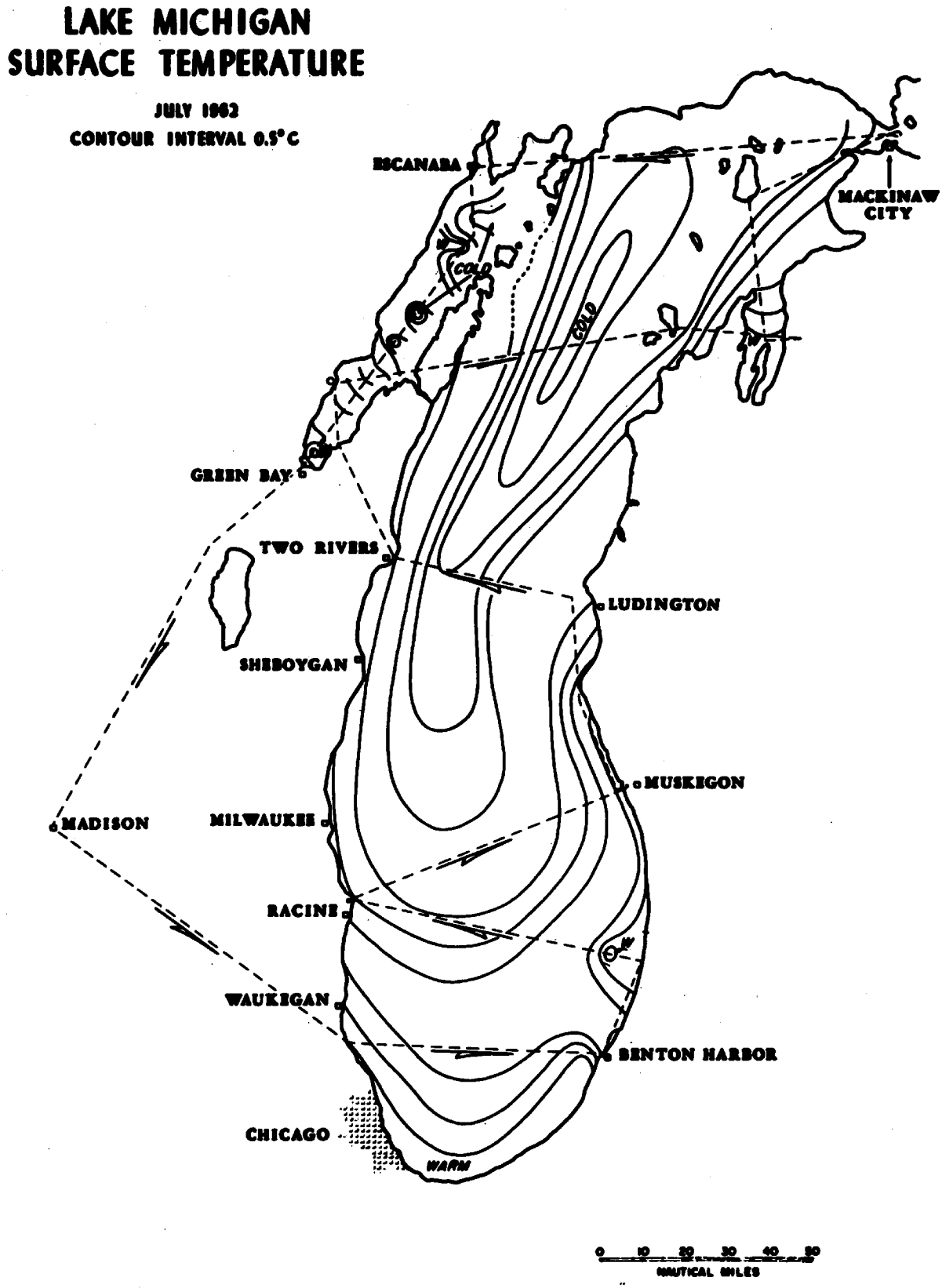


Figure 2. Surface temperature pattern of Lake Michigan in July 1962, obtained with the Barnes infrared radiation thermometer (from McFadden and Ragotzkie, 1963).

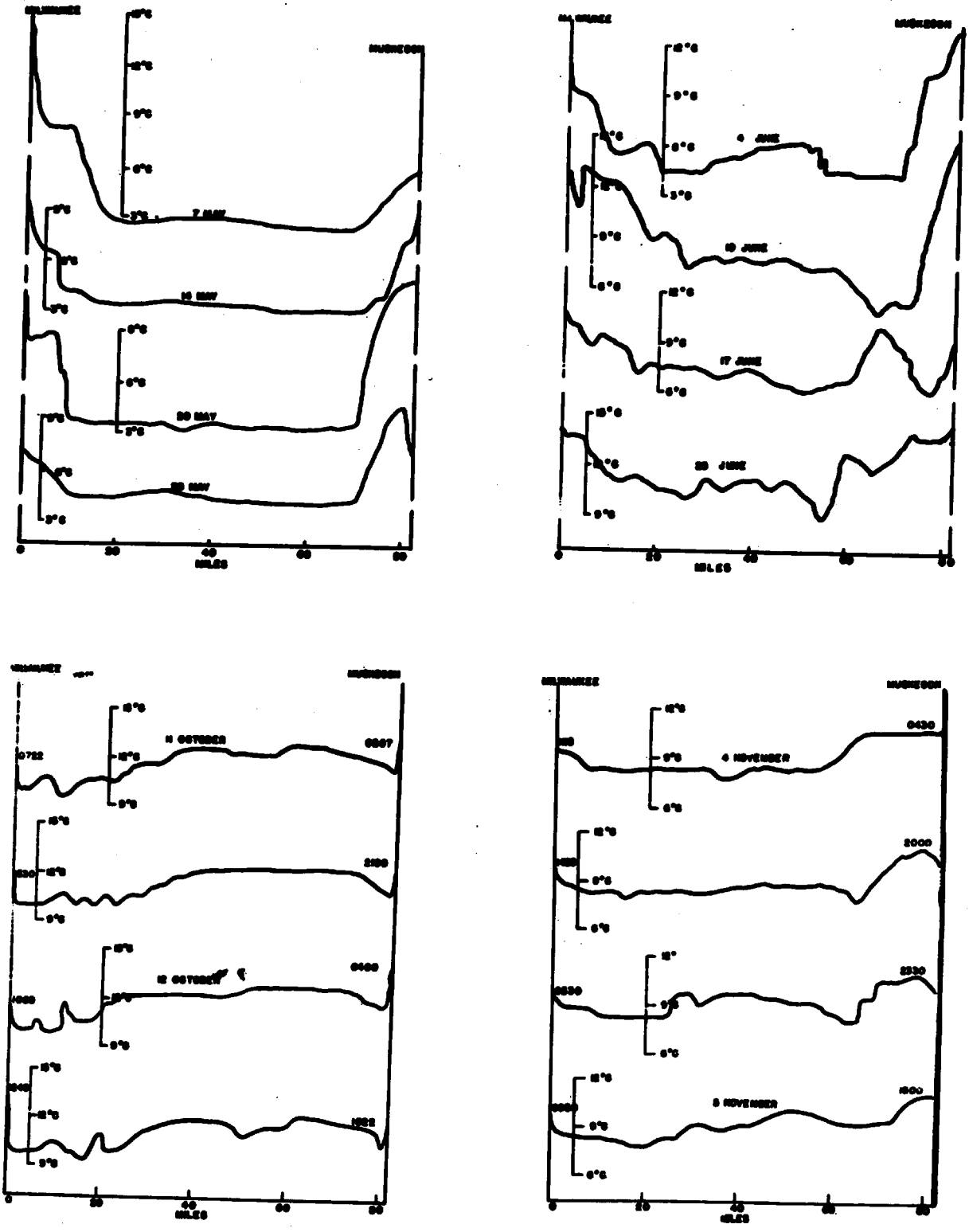


Figure 3. Typical temperature transects in Lake Michigan during (a) warming-up season and (b) cooling-off season (after Noble, 1966).

the thermal forces. So far, in my opinion, no satisfactory result from trying to relate the general current circulation pattern of the lake to the wind stresses has ever been achieved. On the other hand, though the temperature field in the lake is observed to be much more stable than the wind and far more detailed measurements of temperature data are available, few people have tried to investigate the relation of the thermally induced forces and the lake currents.

Given the temperature distribution in the lake, are the thermally induced forces really so small that they can be neglected in modeling the lake circulation, especially under a constantly shifting and changing wind field?

It is the purpose of the present study to model the flow in Lake Michigan, considering the geostrophic thermal gradient force as the prime source for the mean lake current generation, and to investigate the thermal circulation pattern of the lake that results.

A review of the temperature distributions for all the stages of the annual cycle in the Great Lakes shows that the basic thermal phenomena in the lake can be approximately grouped into seven types:

1. In the middle and late winter, between January and early March, the lake is below 4°C everywhere. Due to differential cooling from both sides of the lake, freezing starts from both shores and slowly progresses lakeward. The surface temperature of the partially ice-covered lake may be expressed as a cosine function with a maximum temperature, less than 4°C, in the middle portion of the lake. This is the typical case for winter cooling. This

condition usually lasts for a quite long period of time until the lake is almost free from ice in the spring.

2. In late March or early April, the warming-up season starts. During this period the whole lake is still below 4°C and some small portions of the lake may still be covered with floating ice. Due to the quick response of the land to the warming of the atmosphere, and the almost as rapid response of the shallow edges of the lake, the surface temperature of the lake can be approximated as a small amplitude concave cosine function with maxima of about 4°C at the two edges of the lake. This is the period of spring-heating.
3. As the season progresses the temperature of the water near the shore is heated up to above 4°C while the middle part of the lake may well be at less than 4°C. Then, the special unique characteristics of water will induce a near-shore mixing process which has been observed in all large and deep lakes in temperate regions during the warming-up and cooling-off periods.

During the warming-up period, the temperature of the inshore edges of the lake is all above 4°C, and a direct temperature stratification exists in the edge waters, but the main body of water in the middle portion of the lake is less than 4°C and essentially isothermal.

During the cooling-off period similar, but opposite, temperature conditions exist. The boundary band between these two temperature stratified regions, one isothermal and the other stratified, is called the "thermal bar." The thermal bar phenomenon is obviously connected with combination and mixture of waters from different sources at temperatures above and below

the temperature of maximum density. The mixing of warmer and colder waters causes a sinking motion along the 4°C isotherm, and a type of isolation of the flows on either side of the 4° isotherm is established. Waters of different color, marked differences in phytoplankton populations and different flow patterns are observed along the 4° mixing zone (Stoermer, 1968). Sinking along the 4° isotherm requires surface convergence. The convergence implication of the thermal bar requires an upwelling in the middle portion of the lake during this period of time. This upwelling provides water colder than the temperature of maximum density at the horizontal center of the lake until the disappearance of the thermal bar. The spring thermal bar period usually lasts for four to six weeks. The surface temperature profile can still be approximated as a concave cosine function, but the minimum temperature at the middle of the lake is below 4°C.

4. After the disappearance of the thermal bar the lake surface is above 4°C. The horizontal temperature difference between the edges of the lake and its middle portion has much increased and ascends to a maximum. A positive temperature gradient toward the shore always exists in this stage and the surface temperature profile of the lake can be approximated as a concave cosine function with its minimum near 4°C at the middle of the lake. A weak thermocline starts to grow in late June or early July. At the beginning, a weak, shallow, thermocline may appear during the day and disappear at night. In general, the whole lake is homogeneous, or almost so, during this period of time. This is the summer heating period.

5. After July, the lake is strongly stratified. A sharp vertical temperature gradient thermocline is present all across the lake. The almost homogeneous epilimnion is nearly isolated from the cold stable hypolimnion. This is the strong thermal stratification period.
6. The lake starts cooling off in late October or November as indicated in Figure 3. In December, the lake finally becomes quasi-homogeneous again. At this time, the whole lake is still above 4°C but the edges of the lake have temperatures lower than the middle. This is the autumn-cooling period. The surface temperature profile returns to cosine form.
7. After the edges of the lake have been cooled to a temperature less than 4°C, an autumn thermal bar phenomenon is expected to appear. However, the horizontal temperature difference between the edges and the main body of water, which is then nearly 4°C, is much smaller than the spring warming-up period. Therefore, the cooling-off thermal bar phenomenon is much weaker, and may even hardly be recognized.

After the cold weather becomes severer, the whole lake will soon be less than 4°C but is still cooling. Then the temperature cycle starts again.

In our study the following circulation patterns are obtained:

Type-A Circulation: During the period of winter-cooling and of summer-heating, a cylconic circulation pattern of meridional velocity (north-south flow) is found in the lake with the middle of the lake as the nodal line. The zonal component (east-west flow), together with the vertical component of the velocity field, forms two cells of circulation in the vertical cross-section of the lake.

There is a general weak, broad sinking motion in the middle portion of the lake and upwellings near both shores. Two narrow Ekman layers having zonal flows on the free surface and at the rigid bottom connect the cell circulations.

Type-B Circulation: The circulation pattern during the period of autumn-cooling and of spring-heating time is found to be almost opposite to that of the type-A circulation.

Type-C Circulation:—This is the thermal bar circulation pattern, either of the spring warming-up period or of the autumn cooling-off period. The circulation pattern is more complicated, as expected. The meridional velocities form two sets of weakly sheared flows along the thermal bars on each side of the lake. In the cross-section of the lake, the zonal and the vertical velocity components form four cells, two broad and large cells in the main body of water in the middle portion of the lake between two thermal bars, two other relatively more intense cells between the thermal bars and the shores. The cells circulate clockwise and counterclockwise in such a way that there is a general weak upwelling in the middle portion of the lake, sinking motions along the thermal bar mixing zones, and upwellings near the east and west shores.

The current circulation pattern for the strong thermal stratification period is not predicted in a quasi-homogeneous fluid model study.

To verify the importance of the thermal forces, it is convenient to compare the real field data with the mathematical model prediction in the corresponding periods of time. The temperature distribution and the velocity fields from the theoretical solutions qualitatively agree very well with field observations.

This leads one to postulate that the thermal force does play an important role in generating the mean lake circulation patterns.

Previous Observational Studies

Lake Michigan is the third largest of the Great Lakes, the only one totally within the United States. It is also one of the most surveyed large lakes in the world. For convenience, we are going to use the physical setting of Lake Michigan to investigate the typical thermally induced current structure in the Great Lakes.

The first study of the surface current in the Great Lakes was conducted by Harrington in the period 1892 to 1894 (1895). Figure 1 shows the general current patterns during warmer months found by Harrington and drawn by Millar (1952). Harrington's results from drift bottles show that the main surface current in Lake Michigan circulates in a cyclonic direction around the lake together with two separate cells, one in the southern basin, the other in the northern basin. Deason (1932) studied Lake Michigan currents using the same method and found a "swirling" circulation whose direction he does not give. Church (1942a, 1942b) made a comprehensive study of the annual thermal structures in many cross-sections of Lake Michigan and was the first to try to relate the currents to the observed temperature distribution. His remark, stating that the denser water is in the middle of the lake during most of the year, implies a cyclonic circulation in Lake Michigan. Ayers et al. (1958) made a series of synoptic surveys in the Great Lakes including four cruises in Lake Michigan,

studied the currents by using drift bottles, and computed the currents in Lake Michigan using the modified dynamic height method (Ayers, 1957). Their June currents showed a cyclonic circulation but the August current had a different pattern. Qualitatively, Ayers' drift bottle data agree well with Harrington's study. In 1962 and 1964, in order to understand the water pollution problem in Lake Michigan, the Federal Water Pollution Control Administration (FWPCA) undertook a lakewide long period detailed survey of the temperature and current by deploying recording instruments all over the lake at thirty to forty stations. At each station, Woods Hole type temperature recorder and Richardson current meters (Richardson, 1962) were set as pairs at fixed depths: 10, 15, 22, and 30 m, and at each succeeding 30 m level. A wind anemometer was installed on the buoys of some of the stations. Drogue studies for water movement were also made during that period. "This is the first occasion in which physical events and processes in so large a natural water body, fresh or marine, have been monitored for an interval of nearly two years with so close a network of recorders" as Mortimer remarked in the foreword of the report (U. S. Dept. of Interior, 1967). Unfortunately, most of these long series of recorded data have not yet been analyzed and published. From the analyzed data of some stations, the report indicates that, generally speaking, surface currents are weak and southbound near Lake Michigan's western shore, but narrower, stronger and northbound near its eastern shore. No positive correlation between the wind above and the surface current at 10 m depth could be found. No permanent type of circulation pattern exists in the lake, but four basic patterns have been observed. One winter pattern shows the currents circulate counterclockwise with

gyres in the northern and southern basins. The principal flows are northward along the east shore and southward along the west shore. This pattern is most often observed between January and April. The other winter pattern shows reverse circulation and is usually found after November. The summer patterns have more complicated pictures. The prevailing pattern shows the existence of a cyclonic gyre in the southern basin, but inshore currents on both shores are northward, in spite of the fact that the northern flow along the west shore is much weaker. In the northern basin, the dominant flow is southward in the center of the lake. The other summer pattern still has the cyclonic gyre in the southern basin but the inshore currents along both the east and the west shores are moving southward. The subsurface current has no permanent circulation pattern. Though the cyclonic pattern prevails, there are many instances in which the pattern is reversed. The day-to-day movements suggest that there is as much variability at 240 m as to the 10 m level. During the period of strong thermal stratification, it is found that the currents above and below the thermocline move in opposite directions. The studies also showed that currents exist through the entire vertical column of water and the upper layer is mostly wind-driven. Mortimer (1963) postulated that internal oscillations in the form of Kelvin waves near the shores and Poincare waves with periods less than inertial period (about 17.5 hr in mid-lake) in the middle lake are responsible for the current circulation pattern in Lake Michigan during the period of strong stratification. Csanady's (1967, 1968a, 1968b) studies of a simplified two-layer, constant depth, "model Great Lakes" with wind-driven currents, have suggested the existence of the following phenomena during the summer stratification: a

"coastal jet," large thermocline movements near the shores, surface and internal oscillations, and rotary current in the center portion of the lake. Verber (1964, 1965) has found the presence of inertial rotary currents and internal waves for prolonged periods during the stratified period in Lake Michigan. Noble (1966), using FWPCA Great Lakes-Illinois River Basins project data (station 8), attempted to synthesize the observed current structure with the Ekman type wind-driven model (Ekman, 1905) and was not successful. Alternatively, he suggested a geostrophic eddy model with the existence of contrarotating eddies in the lake. The persistence of the surface temperature profiles indicates stability of the geostrophic circulation (Noble, 1967). In studying the thermal structure in the Great Lakes, Rodgers (1965) has described the thermal bar feature in detail. Field data during the spring from all the Great Lakes confirm Tikhomirov's (1963) suggestion that the thermal bar as was observed in Lake Ladoga is a common phenomenon to all large dimictic lakes in the temperate zone.

Literature Survey

In geophysical fluid dynamics the Coriolis force plays an important role and must be taken into consideration. In Lake Michigan, except during the strong thermal stratification period, a horizontal temperature gradient always exists, especially during the warming-up and cooling-off seasons as shown in Figures 2 and 3. In the literature of differentially heated rotating flow, Hadley (1735) was the first to notice that the longitudinal atmospheric circu-

lation is the result of the body force induced by the latitudinal variation of the heating balanced by the Coriolis acceleration. In an attempt to understand the general circulation of the atmosphere and the origin of the earth's magnetic fields, a series of experiments on rotating differentially heated fluid, contained either in a "dish pan" or an annular container, were conducted by Fultz (1953), Hide (1953, 1958), Fowlis (1963), and Fowlis and Hide (1965). If the viscosity of the fluid is relatively small and the angular rotation is moderately high, the experimental results show that four distinct regimes of hydrodynamical flow may appear. The principal properties of the flow depend mainly on certain nondimensional parameters, such as the thermal Rossby number and the Taylor number. Figure 4, reproduced from Barcilon (1964), shows the transition curve obtained from Fowlis' experimental results (1963) on the Ⓗ, Ta plane in which all flow regimes are observed. The parameter

$$Ⓗ = \frac{g\alpha d\Delta T}{\Omega^2(b - a)^2}$$

is the thermal Rossby number, and

$$Ta = \frac{4\Omega^2(b - a)^5}{\nu^2 d}$$

is the Taylor number, where b and a are the outer radius and the inner radius of the annular container, respectively, d is the depth of the fluid in the annulus, α is the thermal expansion coefficient, ν is the kinematic viscosity, ΔT is the impressed temperature difference, g is the gravitational constant, and Ω is the rotation rate. As shown in the figure, there exists a value of the Taylor number (Ta), say Ta*, below which axisymmetric flow arises irrespec-

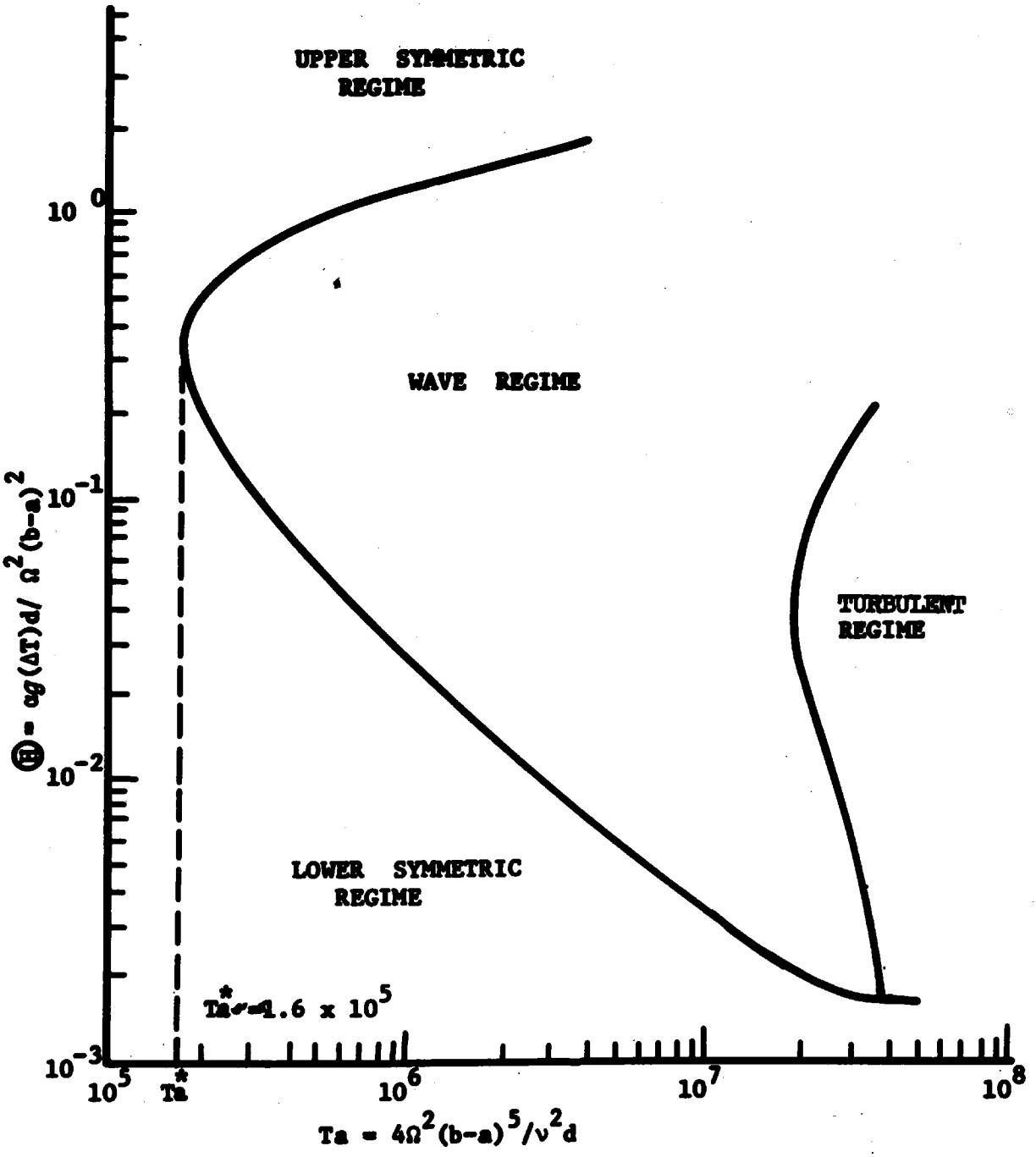


Figure 4. Various regimes of flow field occurring in a rotating fluid differentially heated in the horizontal as functions of nondimensional thermal Rossby number and Taylor number (after Barcilon, 1964).

tive of the value of the thermal Rossby number (Ⓗ). The upper or lower axisymmetric regions also occur when Ta is greater than Ta* and Ⓗ is sufficiently high, greater than a particular value $Ⓗ_1$, or Ⓗ is sufficiently low, smaller than another particular values $Ⓗ_2$. The nonsymmetric regimes appear only when Ta is greater than Ta* and Ⓗ has the value between $Ⓗ_1$ and $Ⓗ_2$. The nonsymmetrical flow pattern may be in regular wavy form with jet-streams, or, after some transitional vacillation phenomena, the flow may turn into irregular complicated fluctuations. Theoretical stability analyses on this problem have been carried out using different approaches, by Eady (1949), Davies (1956, 1959), Kuo (1957), Brindley (1960), and Barcilon (1964). Robinson (1959), and later Hunter (1967), investigated the lower symmetrical regime for fluid contained inside a rotating annulus of square cross-section subjected to horizontal differential heating. An entirely geostrophic thermal wind is obtained over the main body of the fluid in the limit of small thermal Rossby numbers. In the cross-section of the annulus, the circulation is much weaker and exists only within boundary layers circumscribing the rigid walls. A large cell is found to occupy most of the cross-section and two additional small cells are confined to the side-wall boundary layers. If the upper surface is free, the vertical side boundary layers have a double structure with one boundary layer inside another (Hunter, 1967).

Hide (1964) has studied the viscous boundary layer at the free surface of a rotating baroclinic fluid and found that the ageostrophic flow in a free surface boundary layer is much weaker, by a factor of the square root of the Ekman number, than the corresponding flow in the layer at the rigid surface.

In the thermal structure problem, in spite of the fact that the free surface Ekman layer is weak, vertical heat advection induced by boundary layer suction at the free surface can dominate thermal conduction if the product of the Prandtl number and the thermal Rossby number is not smaller than unity. (The corresponding result for a rigid surface is $PR \ll \varepsilon^{1/2}$.)

II. A BAROCLINIC DYNAMIC MODEL OF LAKE MICHIGAN

General Physical Description of Lake Michigan

Lake Michigan has a surface area of 58,016 km^2 and a total volume of 4878 km^3. The average depth of the lake, including the shallow Green Bay is 84 m, with the maximum depth of 281 m in the northern basin. The length of Lake Michigan, over 494 km, is much greater than the mean width of 120 km. Except for a few irregular points, most of the 2673 km shorelines are straight and smooth, and nearly in north-south orientation. An east-west cross-section of the central part of Lake Michigan from Milwaukee, Wisconsin, to Muskegon, Michigan, is shown in Figure 5. The average beach slope around the lake is about 1:100 (Davis and McGeary, 1965).

Lake Michigan and Lake Huron are, hydraulically speaking, only one lake. The connection between these two lakes is the broad and deep Strait of Mackinac. Therefore, their surfaces stand at the same level of 176.5 m above sea level. With the exception of some water diverted at the Chicago Canal into the Illinois River, the entire discharge of the Michigan basin goes to Lake Huron through this strait. Water budget estimates show a net outflow at the Strait of Mackinac of 1134 m^3 per second (U.S. Dept. of Interior, 1967). Using this average value, the total annual out-flow is calculated to be much less than 1% of the total Lake Michigan volume. Therefore, the hydrological effect is not very important.

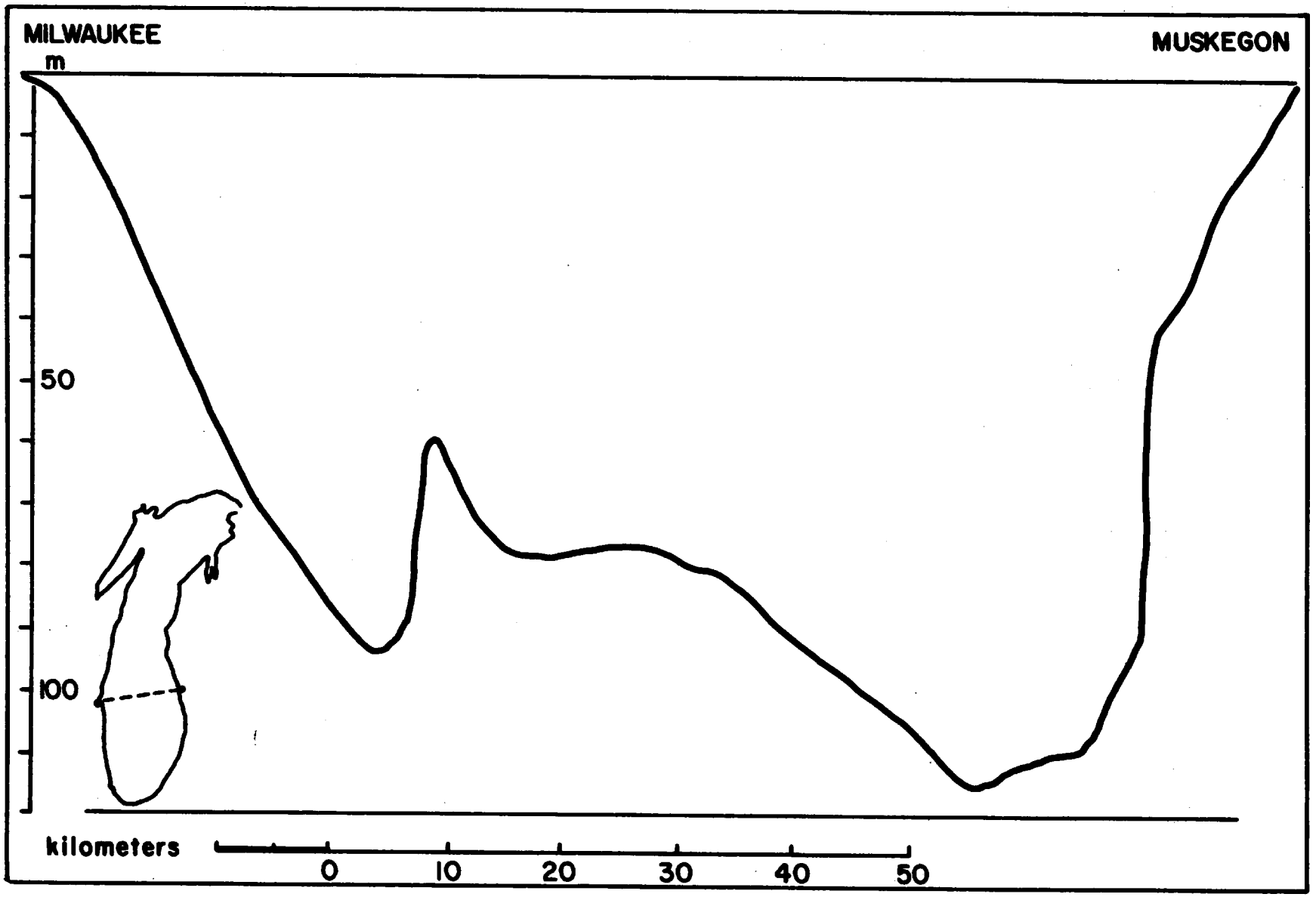


Figure 5. East-west-cross-section of Lake Michigan between Milwaukee, Wisconsin and Muskegon, Michigan (after Church, 1942a,b).

The Coriolis force per unit volume flow is twice the normal component of the earth's rotation vector at a particular location. Therefore, it varies with latitude. In Lake Michigan its magnitude ranges from 0.976×10^{-4} rad/sec in the southern end to 1.05×10^{-4} rad/sec in the northern end. The variation from the south end to the north end is small. Hence, the beta-effect in Lake Michigan is not important.

It is an obvious and well observed fact that wind produces waves, induces currents, and results in turbulent mixing. Ekman's theory (Sverdrup et al., 1942) on the wind-driven current in the open sea has been verified and documented. Shallow water drogue studies (about 1.5 m deep) in Lake Michigan show the surface currents are mostly wind-driven with a response time constant ranging from one hour to several hours after a wind shift. The direction of surface currents differ from that of the mean prevailing wind by from 20° - 80° (U.S. Dept. of Interior, 1967). However, various ways of weighting past wind averages used in the FWPCA project in trying to correlate the wind and the current water data 10 m below in Lake Michigan, show no definite correlation (U.S. Dept. of Interior, 1967).

In the Great Lakes area the wind system is modified by the continuous presence of a mesoscale high pressure in the spring-summer period and a low pressure in the fall-winter period due to the meteorological lake effect. The wind observed on the lake is quite different from that of nearby land stations. Hunt (1959) indicates that a wind differential exists between the land and the lake. In Lake Michigan, the winds over the lake may be 96% greater than those over the city of Chicago at certain times of the year (U.S. Dept. of Interior,

1967). As stated in the introduction, the wind in the Great Lakes region has numerous changes both in magnitude and in direction and is seldom constant over a long period of time. The apparent winds may well be felt differently at different locations in the lake even if there is no change in the wind system. Though wind is responsible for inducing the surface current, the long response time of the currents at deeper layers may well average out the effects of wind stresses over a long period of time, for rapidly changing winds. Therefore, as far as the general mean lake current circulation is concerned, it is possible that the wind-driven current may not be the most important. This is especially obvious during the lake warm-up season. In the spring, when the lake water is still relatively much colder than the already warmed adjacent land, the air mass above the lake is frequently in a stable condition. Wiresonde cross-sections in Lake Michigan have demonstrated the intense spring time inversion prevalent before the warming of the water surface (Bellaire, 1965). At the Wisconsin shore, it has been observed that water remains smooth even beneath offshore winds of greater than 10 knots (at 16 m) (Strong and Bellaire, 1965). Therefore, during this period the meteorological force is even less important. However, in general, turbulent mixing in the open lake is mostly due to wind stresses. Wind is also responsible for set-ups, seiches, and surface waves. These effects may have a secondary influence on the water movement and mixing process in the lake.

The temperature structure in Lake Michigan is in a continual quasi-steady state. The temperature is, generally speaking, a slowly varying function of time. During the warm-up season the sun and river runoff are putting energy

into the lake longer and more consistently than does wind stress. There are some changes in magnitude but solar energy heats the lake during the whole season. And it is similar, with diminishing trend, for the cooling-off season. During the lake warming-up and cooling-off season, temperature gradients, either horizontal or vertical, show persistence, which, in turn, suggests that the thermal energy input may dominate the lake circulation dynamics at this time. This is evident from the persistence in the thermal features in the transects as shown in Figure 3 (Noble, 1966).

The frictional forces are important near all boundaries. In a flow field of a turbulent nature, as in Lake Michigan, the frictional forces are expressed as the space rate of change of the products of eddy viscosity and Reynolds stresses, in analogy to laminar flow. The average horizontal eddy viscosity in Lake Michigan is the order of 10^3-10^5 cm^2/sec and vertical eddy viscosity (1-10^2 cm^2/sec) is much smaller. Eddy diffusivity may be of the same order as eddy viscosity but it is a bit smaller in general. Eddy viscosity and eddy diffusivity of the fluid depend not only on temperature (such as the molecular viscosity), but change from place to place and time to time, depending on the local character and dimension of the flow. The overall average values of the order of magnitude of eddy viscosity and eddy diffusivity can be crudely treated as "constant" for application to the present problem (see Chapter V).

In general, though a weak thermocline may exist during the early summer heating and late autumn cooling period, the lake is quasi-homogeneous during the warming-up and the cooling-off seasons. Of course, in the late summer and early autumn season, the lake is strongly stratified.

Modeling Considerations

During the warming-up and cooling-off seasons in Lake Michigan, a sharp horizontal temperature gradient always exists along the perimeter of the lake. Given the variability of the wind field, it is reasonable to assume that the time-averaged current is due to thermal forces. Equilibrium between the thermal body force and the Coriolis acceleration produces a horizontal velocity perpendicular to the direction of the existing thermal gradient. This is the geostrophic thermal wind relationship, which is considered to be of dominant importance.

The length of Lake Michigan is much longer than the average width. The north end of the lake is connected through a wide and deep strait to an even bigger lake. In the Lake Michigan model, to the lowest order of approximation, the flow field, away from the southern end, can be considered as independent of latitude.

The primary current generating force under consideration, the thermal body force, is a slowly varying function of time. In studying the thermal current structure of the lake for different seasons individually, all variables can be considered as time independent without losing good qualitative approximation.

The tremendous difference between the horizontal eddy viscosity and the vertical eddy viscosity makes the choosing of different values for the viscosity a necessity. But, in general, the vertical velocity gradient is much greater than the horizontal. Therefore, the effect of mixing due to the vertical transport may well be of the same order as the lateral mixing. In con-

sidering the horizontal Reynolds stress of the same order as the vertical Reynolds stress, the ratio of the vertical to the horizontal eddy viscosity is in the same ratio as the depth to the horizontal width of the lake, which, incidently, agrees well with our field data.

In our preliminary model, we will not consider the strong thermal stratification period of the year.

The Boussinesq approximation is used in the formulation. Since the largest horizontal dimension of the lake is much smaller than the radius of the earth, curvature effects can be neglected. The centrifugal acceleration is neglected as compared with the gravitational acceleration. In the energy equation, the dissipation term is considered as small and therefore is neglected.

Mathematical Formulation of the General Governing Equations

Together with the above restrictions, let us assume that the fluid is contained in a long symmetrical "trough," trapezoidal in cross-section. It is subjected to a surface temperature with a maximum or minimum at the center. The lake center is taken as the center of the Cartesian coordinates (Figure 6). The lake is rotating with angular velocity (component of the earth's rotation normal to the lake surface) about its vertical axis, which is anti-parallel to the gravitational force. The horizontal surface of the lake is considered free from wind stresses. The dominant flow is assumed to be meridional, thus the basic geostrophic thermal gradient relation is satisfied. All specifications of nomenclatures are summarized in Table 1.

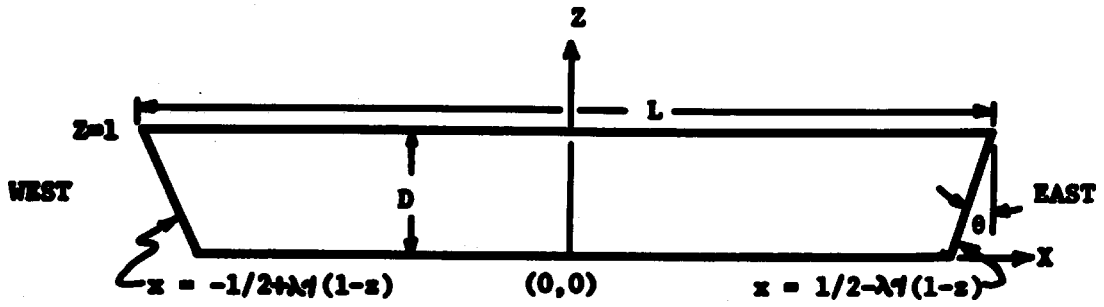


Figure 6. Cross-section of a long, symmetrical, trapezoidal Lake Michigan model.

The equations governing the steady motion of an incompressible, viscous, heat-conducting, rotating fluid are:

$$\vec{q}' \cdot \nabla \vec{q}' + 2\vec{\Omega} \times \vec{q}' = -\frac{1}{\rho_o} \nabla' p' - g \frac{\Delta\rho}{\rho_o} \hat{k} + \left(\nu_H \frac{\partial^2}{\partial x'^2} + \nu_V \frac{\partial^2}{\partial z'^2}\right) \vec{q}', \qquad (1)$$

$$\nabla' \cdot \vec{q}' = 0, \qquad (2)$$

$$\vec{q}' \cdot \nabla' T' = \left(\kappa_H \frac{\partial^2}{\partial x'^2} + \kappa_V \frac{\partial^2}{\partial z'^2}\right) T' \qquad (3)$$

which are, respectively, the Navier-Stokes equations, the continuity equation, and the energy equation. Note that the above dependent variables are independent of y. ∇' is a two-dimensional gradient operator. All primes are dimensional quantities.

TABLE 1

Nomenclature and Nondimensional Parameters

Symbol	Definition
x	Horizontal east-west coordinate, zonal direction
y	Symmetrical north-south coordinate, meridional direction
z	Vertical coordinate, negative is in the direction of gravity
$\vec{q}$	Velocity vector with components (u, v, w)
p	Deviation of the pressure from hydrostatic pressure
T	Temperature
	(N.B. The above symbols primed have dimensions, unprimed are dimensionless.)
T_o	Reference temperature, 4°C
A	Constant for density approximation
$(\hat{i},\hat{j},\hat{k},)$	Unit vector in the (x,y,z) directions
g	Acceleration due to gravity
α	Coefficient of thermal expansion; always positive except below 4°C
ν	Kinematic eddy viscosity, subscript H denotes horizontal, V, vertical
κ	Thermometric eddy diffusivity. Subscript H denotes horizontal, V, vertical.
Ω	Angular velocity of the vertical component of earth's rotation in Lake Michigan
L	Width of the lake, reference horizontal length dimension
D	Depth of the lake, reference vertical length dimension
ΔT	Total horizontal temperature difference between the edge temperature and the reference temperature T_o
ψ	Stream function for the zonal and the vertical velocities

TABLE 1 (Concluded)

Symbol	Definition
ρ	Fluid density at temperature T
γ	Depth to width ratio
λ	Tangent of the co-slope angle with the vertical, $\lambda = \tan\theta$ (see Figure 6)
∇	Two-dimensional gradient operator $\hat{i}\frac{\partial}{\partial x} + \hat{k}\frac{\partial}{\partial z}$
∇^2	Two-dimensional Laplace operator $\frac{\partial^2}{\partial x^2} + \frac{1}{\gamma}\frac{\partial^2}{\partial z^2}$
$\mathcal{L}$	A fourth order linear operator $2\frac{\partial^4}{\partial x^4} + (\gamma + 1)\frac{\partial^4}{\partial x^2 \partial z^2} + \frac{1}{\gamma}\frac{\partial^4}{\partial z^4}$
V	Dimension of velocity $V = \alpha g D \Delta T / 2\Omega L$; or $V = \frac{AgD\Delta T \sin(A\Delta T)}{2\,\Omega L}$
R	Nondimensional thermal Rossby number $R = \frac{\alpha g D \Delta T}{(2\Omega L)^2}$, or $R = \frac{AgD\Delta T \sin(A\Delta T)}{(2\Omega L)^2}$
ε	Nondimensional Ekman number $\varepsilon = \frac{\nu_V}{2\Omega L D}$
σ	Eddy Prandtl number $\sigma = \frac{\nu_V}{\kappa_V}$

Boundary Conditions and Seasonal Variations of the Surface Temperature Distributions

VELOCITY FIELD

The boundary conditions for the velocity field are the no slip conditions at rigid surfaces, the bottom and the slanted side boundaries, and the condition of zero stress and zero normal component of velocity at the free surface. The latter is assumed to be plane and horizontal. Hence, we must require that:

$$w' = 0, \frac{\partial u'}{\partial z'} = \frac{\partial v'}{\partial z'} = 0 \quad \text{at } z = D \ . \tag{4}$$

SEASONAL VARIATION OF THE SURFACE TEMPERATURE DISTRIBUTION

As discussed in the introduction, during the winter cooling period, when the whole lake is below 4°C and both edges of the lake are colder than the middle, the surface temperature profile is in the form of a cosine function with its maximum, slightly less than 4°C, at the middle. The current circulation induced in our model during this period has the same pattern as in the summer heating period. During the summer heating period the surface temperature in the lake is above 4°C and the edges have much higher temperatures than the middle. The fact that the same circulation patterns are induced by these two imposed temperature forms is due to the special characteristics of freshwater density and of the change in direction of the thermal gradient during the heating and the cooling periods. This type of circulation pattern is called the type-A circulation. In the mathematical demonstration of the type-A circulation pattern, we are going to use a concave cosine function as the free surface temperature condition. That is:

$$T' = \frac{1}{2}\left(1 - \cos\frac{2\pi x'}{L}\right)\Delta T + T_o \text{ at } z' = D. \qquad (5)$$

The type-B circulation pattern is expected to exist during the period of autumn cooling when the whole lake is still above 4°C with only two edges at a lower temperature near 4°C, and during the period of spring-heating when the whole lake is all below 4°C with edges in a bit warmer state at nearly 4°C. The type-B circulation is the exact opposite of the type-A circulation.

The type-C circulation pattern is the current circulation during thermal bar periods. The surface temperature of the spring thermal bar period is characterized by the existence of a sharp temperature gradient between the much warmer boundary water and the colder main body of water in the middle. In the middle portion of the lake, the temperature may be well below 4°C but the two edges have reached a temperature far above 4°C. Therefore, letting the thermal bar be near the temperature of maximum density, we require

$$T' = \frac{1}{3}\left(1 - 2\cos\frac{2\pi x'}{L}\right)\Delta T + T_o \text{ at } z = D \qquad (6)$$

where ΔT is the temperature difference between the maximum water temperature near the shores and the thermal bar temperature. The autumn thermal period has almost the opposite temperature profile except ΔT is smaller and negative.

The lake temperature near the bottom is very stable all year round with little variation from the temperature of maximum density. Therefore, we assume the bottom temperature to be constant at nearly 4°C in all cases. As to the slant side boundaries, we require the insulation conditions to be satisfied at $x = \pm L/2$, which permits some conduction between the earth of the slant shores and the edges of the lake water. This makes the side boundary conditions even

more similar to the real situation in the lake.

The differential equations (1), (2), and (3) together with all the boundary conditions form a high order, coupled, nonlinear system. Exact analytic solutions are very difficult to obtain. Therefore, some approximate methods capable of making the system more tractible are preferred. In the next chapter, the general thermal currents, including type-A and type-B circulations will be investigated mathematically in great detail.

III. GENERAL THERMAL CURRENTS

Mathematical Formulation and Methods of Approximation

THE EQUATION OF STATE

Except during the thermal bar time, the temperature in the lake is either all above 4°C, as in the summer-heating and the autumn-cooling periods, or all below 4°C as in the spring-heating and the winter-cooling periods. Then, using the Boussinesq approximation, the equation of state is a linear relation between the density and the temperature as

$$\rho' = \rho_o[1 - \alpha(T' - T_o)] \quad , \tag{7}$$

where α, the coefficient of thermal expansion, is treated qualitatively as a constant in each individual period, and T_o, the reference temperature, is 4°C. Hence, the thermal buoyant force in the momentum equation is:

$$\frac{\Delta\rho}{\rho_o} = -\alpha(T' - T_o) \tag{8}$$

This approximation is valid for all the type-A and type-B circulations, which are called general thermal currents to distinguish them from the thermal bar circulations.

NONDIMENSIONAL GOVERNING EQUATIONS

It is convenient to introduce nondimensional variables and parameters. The following unprimed nondimensional variables are defined:

$$x = \frac{x'}{L} , \quad z = \frac{z'}{D} , \quad T = \frac{T' - T_o}{\Delta T} , \quad (u,v) = \frac{1}{V}(u',v') ,$$
$$w = \frac{Lw'}{DV} \quad \text{and} \quad p = \frac{p'}{\rho_o \alpha g D \Delta T} , \tag{9}$$

where V is the reference dimensional velocity and all other variables have been specified in Table 1. The vertical velocity is nondimensionized in this form in order to satisfy the continuity requirement.

In our basic assumption, we consider that the dominant mean flow field is in geostrophic thermal gradient equilibrium. Then the basic thermal wind relationship should be satisfied, that is

$$2\Omega \frac{\partial V}{\partial z} = \alpha g \frac{\partial T}{\partial x} . \tag{10}$$

This gives V, in dimensional form, as:

$$V = \frac{\alpha g D \Delta T}{2\Omega L} \tag{11}$$

where D is the depth of the fluid. Since ΔT is the horizontal temperature difference, and the baroclinic circulation is induced by the horizontal density difference, the reference velocity V is the anticipated order of magnitude of the meridional motion.

In considering the mixing effect of vertical transport to have the same order as the lateral mixing effect, the horizontal eddy viscosity to the vertical eddy viscosity has the same proportion as the reference length L to the reference depth D. That is,

$$\nu_H \approx \frac{L}{D}\nu_V \quad . \tag{12}$$

Equations (9), (11), and (12) are substituted into (1), (2), and (3). The nondimensional continuity equation is still the same form as equation (3) which permits us to define a stream function ψ by expressing the nondimensional velocity as:

$$\vec{q} = \hat{j}x\nabla\psi(x,z) + v\hat{j} \quad . \tag{13}$$

The vorticity equation is obtained by eliminating the pressure by cross-differentiation from the x and z momentum equations. After using equation (13), it becomes,

$$\varepsilon\mathcal{L}\psi + \frac{\partial v}{\partial z} - \frac{\partial T}{\partial x} = R\left[\frac{\partial x}{\partial z}\frac{\partial^3\psi}{\partial x\partial z^2} - \frac{\partial\psi}{\partial x}\frac{\partial^3\psi}{\partial z^3} - \gamma^2\left(\frac{\partial\psi}{\partial x}\frac{\partial^3\psi}{\partial x^2\partial z} - \frac{\partial\psi}{\partial z}\frac{\partial^3\psi}{\partial x^3}\right)\right] \quad . \tag{14}$$

The y momentum equation, noting the y-independence of the model, becomes,

$$\varepsilon\nabla^2 v - \frac{\partial\psi}{\partial z} = R\left(\frac{\partial\psi}{\partial z}\frac{\partial v}{\partial x} - \frac{\partial\psi}{\partial x}\frac{\partial v}{\partial z}\right) \quad . \tag{15}$$

The eddy diffusivity is assumed to be of the same order as eddy viscosity, then equation (3) leads to:

$$\varepsilon\nabla^2 T = \sigma R\left(\frac{\partial\psi}{\partial z}\frac{\partial T}{\partial x} - \frac{\partial\psi}{\partial x}\frac{\partial T}{\partial z}\right) \quad . \tag{16}$$

All nondimensional parameters and operators are specified in Table 1. Notice that:

$$R = \frac{\alpha g D \Delta T}{(2\Omega L)^2}$$

is the nondimensional thermal Rossby number similar to the parameter (H) in Figure 4;

$$\varepsilon = \frac{\nu_V}{2\Omega L D}$$

is the nondimensional Ekman number which is similar to the reciprocal of the square root of the Taylor's number, and

$$\sigma = \frac{\nu_V}{\kappa_V} ,$$

is the eddy Prandtl number which is of the order of unity.

METHODS LEADING TO THE APPROXIMATE SOLUTIONS

We are interested in the range of small thermal Rossby numbers and small Ekman numbers. Since $R \ll 1$, examining equations (14) and (15), we find that the limiting case is that of geostrophic thermal gradient force domination in the flow field, which is the basic assumption of the modeling. This leads to the method of regular perturbation by expanding all dependent variables in powers of R.

The expansion of temperature in a power series in R needs justification. From the energy equation (16), since σ is of order unity, R totally determines the relative importance of the heat conduction or the heat convection. Small R means heat convection is less important. However, the Ekman number, ε, is an even smaller number. At first inspection of equation (16), it seems that

the temperature gradient terms coupled with momentum advections cannot be neglected even in the zeroth order of approximation because the combination of these three parameters ($\sigma R/\varepsilon$) is apparently not a small parameter. Nevertheless, due to the anistropy of the induced zonal and vertical velocity field, the series expansion in powers of R for the temperature is valid everywhere in the flow field. Because the free surface boundary conditions force the stream function to be small, of order ε throughout the field, this makes heat convection as represented by the right hand side of equation (16) still of order R. At the boundaries, as we will see later, since all velocity components and all high order temperatures do have boundary layer characteristics, the contribution due to the velocity coupled heat convection is still small, even smaller than that in the interior region. Hence, the relative unimportance of the coupled heat convections is made clear. Actually, as will become obvious later, leading terms of every order of the R-expansion of temperature are of the order unity. The expansion of temperature in powers of R is at least apparently asymptotic.

In the regular perturbation, we express all dependent variables in powers of R as

$$f = \sum_{n=0}^{\infty} R^n f^{(n)} \tag{17}$$

and substitute into equations (14), (15), and (16). After equating each power of R, we have the zeroth R-order equations as:

$$\varepsilon \mathcal{L}_\psi^{(o)} + \frac{\partial v^{(o)}}{\partial z} - \frac{\partial T^{(o)}}{\partial x} = 0 \ , \tag{18}$$

$$\varepsilon\nabla^2 v^{(0)} - \frac{\partial \psi^{(0)}}{\partial z} = 0 \quad , \tag{19}$$

$$\nabla^2 T^{(0)} = 0 \quad . \tag{20}$$

Notice that the zeroth R-order temperature is induced entirely by conduction.

The first R-order equations are:

$$\varepsilon\mathcal{L}\psi^{(1)} + \frac{\partial v^{(1)}}{\partial z} - \frac{\partial T^{(1)}}{\partial x} = \left[\frac{\partial \psi^{(0)}}{\partial z}\frac{\partial^3 \psi^{(0)}}{\partial x \partial z^2} - \frac{\partial \psi^{(0)}}{\partial x}\frac{\partial^3 \psi^{(0)}}{\partial z^3} - \gamma^2\left(\frac{\partial \psi^{(0)}}{\partial x}\frac{\partial^3 \psi^{(0)}}{\partial z \partial x^2} - \frac{\partial \psi^{(0)}}{\partial z}\frac{\partial^3 \psi^{(0)}}{\partial x^3}\right)\right] \tag{21}$$

$$\varepsilon\nabla^2 v^{(1)} - \frac{\partial \psi^{(1)}}{\partial z} = \frac{\partial \psi^{(0)}}{\partial z}\frac{\partial v^{(0)}}{\partial x} - \frac{\partial \psi^{(0)}}{\partial x}\frac{\partial v^{(0)}}{\partial z} \quad , \tag{22}$$

$$\varepsilon\nabla^2 T^{(1)} = \sigma\left(\frac{\partial \psi^{(0)}}{\partial z}\frac{\partial T^{(0)}}{\partial x} - \frac{\partial \psi^{(0)}}{\partial x}\frac{\partial T^{(0)}}{\partial z}\right) \quad . \tag{23}$$

The second R-order equations are:

$$\varepsilon\mathcal{L}\psi^{(2)} + \frac{\partial v^{(2)}}{\partial z} - \frac{\partial T^{(2)}}{\partial x} = \left[\frac{\partial \psi^{(0)}}{\partial z}\frac{\partial^3 \psi^{(1)}}{\partial x \partial z^2} - \frac{\partial \psi^{(0)}}{\partial x}\frac{\partial^3 \psi^{(1)}}{\partial z^3} + \frac{\partial \psi^{(1)}}{\partial z}\frac{\partial^3 \psi^{(0)}}{\partial x \partial z^2} - \frac{\partial \psi^{(0)}}{\partial x}\frac{\partial^3 \psi^{(0)}}{\partial z^3} + \gamma^2\left(\frac{\partial \psi^{(0)}}{\partial z}\frac{\partial^3 \psi^{(1)}}{\partial x^3} - \frac{\partial \psi^{(0)}}{\partial x}\frac{\partial^3 \psi^{(0)}}{\partial z \partial x^2} + \frac{\partial \psi^{(1)}}{\partial z}\frac{\partial^3 \psi^{(0)}}{\partial x^3} - \frac{\partial \psi^{(1)}}{\partial x}\frac{\partial^3 \psi^{(0)}}{\partial z \partial x^2}\right)\right] , \tag{24}$$

$$\varepsilon\nabla^2 v^{(2)} - \frac{\partial \psi^{(2)}}{\partial z} = \frac{\partial \psi^{(0)}}{\partial z}\frac{\partial v^{(1)}}{\partial x} - \frac{\partial \psi^{(0)}}{\partial x}\frac{\partial v^{(1)}}{\partial z} + \frac{\partial \psi^{(1)}}{\partial z}\frac{\partial v^{(0)}}{\partial x} - \frac{\partial \psi^{(1)}}{\partial x}\frac{\partial v^{(0)}}{\partial z} , \tag{25}$$

$$\varepsilon\nabla^2 T^{(0)} = \sigma\left(\frac{\partial \psi^{(0)}}{\partial z}\frac{\partial T^{(1)}}{\partial x} - \frac{\partial \psi^{(0)}}{\partial x}\frac{\partial T^{(1)}}{\partial z} + \frac{\partial \psi^{(1)}}{\partial z}\frac{\partial T^{(0)}}{\partial x} - \frac{\partial \psi^{(1)}}{\partial x}\frac{\partial \psi^{(0)}}{\partial z}\right) . \tag{26}$$

We are going to use second R-order equations for estimations of the approximation error. With reference to the last chapter, especially equations (14) and (15), boundary conditions for the zeroth R-order equations are:

$$\psi^{(0)} = \frac{\partial \psi^{(0)}}{\partial z} = v^{(0)} = 0 , \quad T^{(0)} = 0 \quad \text{at} \quad z = 0 , \tag{27}$$

$$\psi^{(0)} = \frac{\partial^2 \psi^{(0)}}{\partial z^2} = \frac{\partial v^{(0)}}{\partial z} = 0, \quad T^{(0)} = \frac{1}{2}(1 - \cos 2\pi x) \text{ at } z = 1 , \tag{28}$$

$$\psi^{(0)} = \frac{\partial \psi^{(0)}}{\partial x} = v^{(0)} = 0$$

on the slant side boundaries and

$$\frac{\partial T^{(0)}}{\partial x} = 0 \quad \text{at} \quad x = \pm\frac{1}{2} . \tag{29}$$

For all high R-order equations, the boundary conditions for the velocity field and the temperature on the slant boundaries are exactly the same as those of the zeroth R-order equations, only temperatures on the free surface and the rigid bottom require:

$$T^{(i)} = 0 , \quad i = 1,2,3,\ldots \text{ etc.} , \tag{30}$$

for higher i-th R-order temperature.

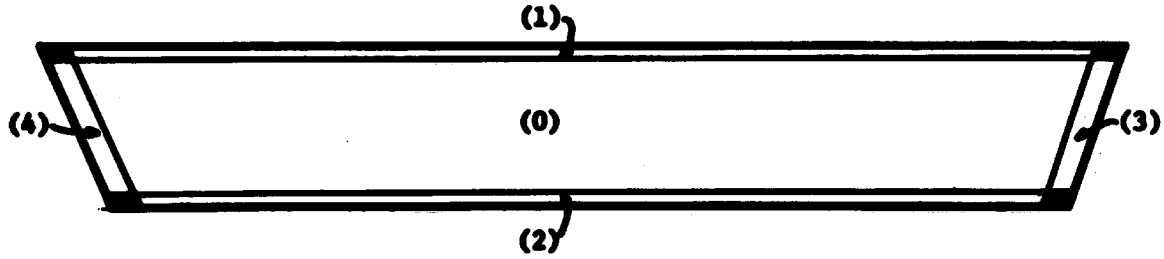
In all the R-order equations, the Ekman number ε appears only in the differentiated highest order terms. Since ε is a very small number connected with viscosity, the highest order differentiated terms may have contributions only in the boundaries where they are large enough to overcome the smallness of ε. Therefore, it becomes a singular perturbation problem. The method of matched asymptotic expansions, or generally, the method of boundary layer analyses can be used (Van Dyke, 1964, Carrier 1953). Following the procedures of the boundary layer additive type analysis, let,

$$f^{(i)} = {}_{o}f^{(i)} + {}_{j}f^{(i)} \qquad j = 1,2,3,4 \quad . \tag{31}$$

where f is any dependent variable; and the right superscript i denotes the i-th R-order in the series expansion of the variable f; the left subscript j denotes the i-th R-order of the variable in the j-th region, j = 1,2,3,4; and the subscript o represents the overall part of the variable f, including the interior region. Therefore, ${}_{o}f^{(i)}$ has no boundary layer characteristics. ${}_{j}f^{(i)}$, j = 1,2,3,4, represents the boundary layer part of the variable in its respective boundary region. If j = 1, that is the free surface boundary region, j = 2, the rigid bottom region, j = 3 and j = 4 are respectively the eastern and the western slant boundary regions. Figure 7 shows the interior and all boundary regions of the Lake Michigan Model. For example, the zeroth R-order stream function, $\psi^{(o)}$, is represented as

$$\psi^{(o)} = {}_{o}\psi^{(o)} + {}_{1}\psi^{(o)} + {}_{2}\psi^{(o)} + {}_{3}\psi^{(o)} + {}_{4}\psi^{(o)}$$

The $_0\psi^{(o)}$ is dominant in the interior region and also reaches all boundary regions without changing its order of magnitude. $_1\psi^{(o)}$ is significant only on the free surface boundary and vanishes exponentially in the interior. Similarly, $_2\psi^{(o)}$, $_3\psi^{(o)}$, $_4\psi^{(o)}$ are important only at their respective boundaries. In the interior region, only the $_0\psi^{(o)}$ part is important.



(0) indicates the interior region
(1) indicates the surface region
(2) indicates the bottom region
(3) indicates the eastern boundary region
(4) indicates the western boundary region

The shaded areas are corner regions

Figure 7. Interior and boundary-layer regions of the Lake Michigan Model.

BOUNDARY LAYER SCALING

Equations (18) and (19) are coupled and show boundary-layer characteristics. In boundary-layer analysis the boundary layer thickness can be estimated by equating the highest-order differentiated terms connected with the small viscous parameter to the other terms with no connection to the viscous parameter in the same equation. Therefore, we shall evaluate the order of the boundary layer thickness as a function of the small Ekman number ε.

Equations (18) and (19) together with equation (20) imply that

$$\varepsilon^2 \mathcal{L} \nabla^2 \psi^{(o)} + \frac{\partial^2 \psi^{(o)}}{\partial z^2} = 0 \quad , \tag{32}$$

where

$$\mathcal{L}\nabla^2 = \left[\gamma^2 \frac{\partial^6}{\partial x^6} + (2\gamma + 1) \frac{\partial^6}{\partial x^4 \partial z^2} + (1 + \frac{2}{\gamma}) \frac{\partial^6}{\partial x^2 \partial z^4} + \frac{1}{\gamma^2} \frac{\partial^6}{\partial z^6}\right]$$

is the sixth order linear operator.

On the free surface and the rigid bottom we may scale the normal coordinates near the boundaries as

$$\zeta = \varepsilon_1^{-\delta_1}(z - b) \quad , \tag{33}$$

and with no change in the tangential coordinates, where b = 0 on the bottom and b = 1 on the free surface.

At the boundary, the frictional force is important and in equation (32) the products of the viscous parameter, ε, and the leading terms in the sixth order linear operator may have the same order of magnitude as the other term with no viscous interaction. Substitute equation (33) into equation (32) and equate the leading viscous term to be the same order in ε as the non-viscous term. This leads to $\delta_1 = 1/2$ and $\varepsilon_1 = \varepsilon/\gamma$. Then, with the conditions that the boundary layer part of the zeroth R-order stream functions, ${}_j\psi^{(o)}$, j = 1 or 2, is of only local importance and vanishes away from its respective boundary, the equation (32) can be integrated twice and yields

$$\frac{\partial^4 {}_j\psi^{(o)}}{\partial \zeta^4} + {}_j\psi^{(o)} = 0 \quad , \tag{34}$$

where j = 1 on the free surface and j = 2 on the rigid bottom.

The eastern and western slant side boundaries are represented, in non-dimensional form by

$$x = \pm\left[\frac{1}{2} - \lambda\gamma(1 - z)\right]$$

where λ is the co-slope of the slant boundaries, that is, $\lambda = \tan\theta$. As shown in Figure 6, the co-slope angle, θ, is the physical topographic average angle of the beaches inclined with the vertical line. Let

$$\xi = \varepsilon_2^{-\delta_2}\left[x + \frac{1}{2} - \lambda\gamma(1 - z)\right], \qquad \eta = z \tag{35}$$

be the local coordinates normal and tangential to the slant boundaries. Substituting equation (35) into equation (32), with all the highest order normally differentiated terms combined in making the same contribution as the other term in the equation, will lead to $\delta_2 = 1/2$ and $\varepsilon_2 = \varepsilon K$, where

$$K = \left[\frac{1}{\lambda^2} + (2\gamma + 1) + (1 + \frac{2}{\gamma})\lambda^2\gamma^2 + \lambda^4\gamma^2\right]^{1/2} \tag{36}$$

is a constant. Then, equation (32) becomes exactly the same form as equation (34) except $j = 3$ for the eastern slant boundary and $j = 4$ for the western slant boundary. Table 2 shows the local coordinates in different regions.

TABLE 2

Local Coordinates in Different Regions

Region	Coordinates	
0	x	z
1	x	$\zeta_1 = \varepsilon_1^{-1/2}(1 - z)$
2	x	$\zeta_2 = \varepsilon_1^{-1/2} z$
3	$\xi_1 = \varepsilon_2^{-1/2}\left[x - \frac{1}{2} + \lambda\gamma(1 - z)\right]$,	$\eta_1 = z$
4	$\xi_2 = \varepsilon_2^{-1/2}\left[x + \frac{1}{2} - \lambda\gamma(1 - z)\right]$,	$\eta_2 = z$

It should be remarked that solutions of the flow field in region 1 and region 2 are not valid at the corners where the upper and lower Ekman layers merge with the slant side boundaries. As expected in the boundary layer problem, stretching the normal coordinates of their respective boundaries will cause difficulties at corners where two boundary effects are contradictory to each other. We notice that the flow in the Ekman extensions at the corner does not satisfy the slant side boundary conditions. There are four corners of dimension $O(\varepsilon_1^{1/2} \times \varepsilon_2^{1/2})$ where none of the above scaling is relevant. However, as Greenspan and Howard (1963), Robinson (1959) and Hunter (1967) have found these corner regions to be small and relatively unimportant; the remainder of the flow can be solved without solutions of these corner regions.

Analytical Approximate Solutions

THE ZEROTH R-ORDER SOLUTIONS

Temperature Distribution

The zeroth R-order temperature can be obtained from equation (20), which is simply the Laplace equation. The solution of equation (20) satisfying boundary conditions (27), (28) is

$$T^{(o)} = \frac{1}{2}\left[z - \frac{\sinh az}{H} \cos 2\pi x\right] \tag{37}$$

where a and H are abreviated constants specified in Table 3. The zeroth R-order temperature is purely conduction. Therefore it has no boundary layer effects.

TABLE 3

Abbreviations for Constant Functions

Abbreviated Notation	Meaning Represented
a	$2\pi\sqrt{\gamma}$
H	$\sinh 2\pi\sqrt{\gamma}$
G	$\cosh 2\pi\sqrt{\gamma}$
H_2	$\sinh 2a$
G_2	$\cosh 2a$
H_3	$\sinh 3a$
G_3	$\cosh 3a$
H_4	$\sinh 4a$
G_4	$\cosh 4a$
C_1	$\frac{2A\sigma}{27\gamma}$
C_2	$\frac{-A\sigma}{27\gamma}$
C_3	$\frac{4\pi A\sigma}{27\sqrt{\gamma}}$
C_4	$\frac{-8\pi^2 A\sigma}{27H}$
C_5	$\frac{-4\pi A\sigma}{81\sqrt{\gamma}\,H}$
C_6	$\frac{\pi A\sigma}{27\sqrt{\gamma}\,H}$

Velocity Field

Interior Solutions

In the interior region, boundary effects are small. Equations (18) and (19), with the first terms neglected, become:

$$\frac{\partial_o v^{(o)}}{\partial z} = \frac{\partial T^{(o)}}{\partial x} ,$$

and

$$\frac{\partial_o \psi^{(o)}}{\partial z} \equiv 0 ,$$

which yield

$$_o v^{(o)} = \frac{1}{2\sqrt{\gamma}} \left[\frac{\cosh az}{H} \sin 2\pi x \right] + A_o(x) , \tag{38a}$$

and

$$_o \psi^{(o)} = B_o(x) , \tag{39a}$$

where $A_o(x)$, $B_o(x)$ are integration constants and possibly functions of x. $A_o(x)$ and $B_o(x)$ can only be determined by matching up the interior solutions to the solutions obtained from the boundary regions.

Boundary-Layer Solutions

Region 1—the upper boundary (free surface). In the upper boundary region, the stream function and the meridional velocity are:

$$\psi^{(o)} = {}_o\psi^{(o)} + {}_1\psi^{(o)} ,$$

$$v^{(o)} = {}_o v^{(o)} + {}_1 v^{(o)}$$

and the vertical coordinate is stretched as shown in Table 2. Equation (32), using the local coordinates, and to the order of ε, yields,

$$\frac{\partial_1^{\varepsilon} \psi^{(o)}}{\partial \zeta_1^{\varepsilon}} + \frac{\partial_1^{2} \psi^{(o)}}{\partial \zeta_1^{2}} = 0 . \tag{40}$$

Since, ${}_1\psi^{(o)}$ vanished exponentially away from the upper boundary, the "constants" of integration vanish. Therefore equation (40) is simplified to equation (34). That is, in region 1,

$$\frac{\partial^4 {}_1\psi^{(o)}}{\partial \zeta_1^4} + {}_1\psi^{(o)} = 0 \quad . \tag{41}$$

The solutions of equation (41) are:

$${}_1\psi^{(o)} = \sum_{j=1}^{4} C_j(x)\, e^{m_j \zeta_1} \quad , \tag{42}$$

where the m_j are the roots of

$$m^4 + 1 = 0 \quad . \tag{43}$$

These are

$$m_{1,2,3,4} = \pm \exp\left[\pm i \frac{\pi}{4}\right] \quad . \tag{44}$$

Due to boundedness condition as $\zeta_1 \to \infty$, and since ζ_1, is always positive in the model, only the two roots with negative real parts are relevant:

$$m_{1,2} = -1 \pm i \quad . \tag{45}$$

The other two appropriate boundary conditions are

$$\psi^{(o)} = \frac{\partial^2 \psi^{(o)}}{\partial z^2} = 0 \quad \text{at} \quad z = 1$$

or equivalently,

$$\psi^{(o)} = \frac{\partial^2 \psi^{(o)}}{\partial \zeta_1^2} = 0 \quad \text{at} \quad \zeta_1 = 0 \quad . \tag{46}$$

All the $C_j(x)$ in equation (42) can be obtained, leaving only one constant

inherited from the interior undetermined.

Equation (19), to the order of ε on the boundary, leads to

$$\frac{\partial_1^2 v^{(o)}}{\partial \zeta_1^2} + \varepsilon_1^{-1/2} \frac{\partial_1 \psi^{(o)}}{\partial \zeta_1} = 0 \quad . \tag{47}$$

Since, ${}_1v^{(o)}$ is of significance only in the boundary region, the integration constant can be chosen as zero. After substituting ${}_1\psi^{(o)}$ in and together with boundary condition

$$\frac{\partial v^{(o)}}{\partial \zeta_1} = 0 \quad \text{at} \quad \zeta = 0 \tag{48}$$

will yield:

$${}_1v^{(o)} = -\varepsilon_1^{1/2} \frac{\pi e^{-\zeta_1/\sqrt{2}}}{\sqrt{2}} \sin 2\pi x (\cos \frac{\zeta_1}{\sqrt{2}} - \sin \frac{\zeta_1}{\sqrt{2}}) \quad , \tag{49}$$

and

$${}_1\psi^{(o)} = -\varepsilon_1 \pi e^{-\zeta_1/\sqrt{2}} \sin 2\pi x \cos \frac{\zeta_1}{\sqrt{2}} \quad . \tag{50}$$

Region 2—the lower boundary (rigid bottom). After stretching the vertical coordinate, equation (34) and another equation similar to (47), satisfying all the lower boundary conditions

$$v^{(o)} = \psi^{(o)} = \frac{\partial \psi^{(o)}}{\partial \zeta_2} = 0 \quad \text{at} \quad \zeta_2 = 0 \quad ,$$

we obtain

$${}_2v^{(o)} = \varepsilon_1^{1/2} \sqrt{2}\, \pi e^{-\zeta_2/\sqrt{2}} \sin 2\pi x \cos \frac{\zeta_2}{\sqrt{2}} \quad , \tag{52}$$

and

$$ {}_2\psi^{(o)} = -\varepsilon_1 \pi e^{-\zeta_2/\sqrt{2}} \sin 2\pi x \left(\cos \frac{\zeta_2}{\sqrt{2}} + \sin \frac{\zeta_2}{\sqrt{2}}\right) . \tag{53} $$

The integration constant in equation (52) has been absorbed into the integration constant of the interior velocity, $A_o(x)$ to satisfy the boundary condition at $z = 0$.

Matching the boundary solutions with that of the interior, the boundary conditions in equations (46) and (51) have also yielded the two integration constants in equations (27) and (28) as

$$ A_o(x) = \left(\frac{1}{2\sqrt{\gamma}\, H} + \varepsilon_1^{1/2} \sqrt{2}\,\pi\right) \sin 2\pi x , $$

and

$$ B_o(x) = \varepsilon_1 \pi \sin 2\pi x . $$

Then the interior solutions in equations (38a) and (39a) become,

$$ {}_o v^{(o)} = \left(\frac{\cosh az - 1}{2\sqrt{\gamma}\, H} - \varepsilon_1^{1/2} \sqrt{2}\,\pi\right) \sin 2\pi x , \tag{38} $$

and

$$ {}_o\psi^{(o)} = \varepsilon_1 \pi \sin 2\pi x . \tag{39} $$

Region 3 and region 4—the eastern and the western slant side boundaries. Using local normal component stretched coordinates in the side boundaries, equation (32) to the order of ε, leads to

$$ \frac{\partial_j^4 \psi^{(o)}}{\partial \xi^4} + {}_j\psi^{(o)} = 0 , \tag{54} $$

where $j = 3$ denotes the eastern boundary, $j = 4$, the western boundary. Notice that the boundary layer thickness is the order of $\varepsilon_2^{1/2}$, where $\varepsilon_2 = \varepsilon K$. K is constant as shown in equation (36).

Equation (19), to the order of ε, also leads to

$$\frac{\partial^2 {}_3v^{(o)}}{\partial \xi_1^2} + \frac{\lambda\gamma\sqrt{K}}{1+\lambda^2\gamma}\,\varepsilon^{-1/2}\,\frac{\partial {}_3\psi^{(o)}}{\partial \xi_1} = 0 \quad , \tag{55}$$

in region 3.

Equations (54) and (55) satisfying the boundary conditions on the eastern slant boundary,

$${}_3v^{(o)} = {}_3\psi^{(o)} = \frac{\partial {}_3\psi^{(o)}}{\partial \xi_1} = 0 \quad \text{at} \quad \xi_1 = 0 \quad , \tag{56}$$

and the decay condition, noticing ξ_1 is always negative in region 3, we have the solutions,

$${}_3v^{(o)} = \left\{\left[\frac{1-\cosh a\eta_1}{2\sqrt{\gamma}H} + \varepsilon^{1/2}\sqrt{2}\,\pi\left[\frac{1}{\sqrt{\gamma}} - \frac{\lambda\sqrt{K}}{(1+\lambda^2\gamma)}\left(1 - e^{\xi_1/\sqrt{2}}\cos\frac{\xi_1}{\sqrt{2}}\right)\right]\right]\right\}$$

$$\cdot \sin 2\pi\lambda\gamma(1-\eta_1) \quad , \tag{57}$$

and

$${}_3\psi^{(o)} = \varepsilon_1\pi \sin 2\pi\lambda\gamma(1-\eta_1)e^{\xi_1/\sqrt{2}}\left(\sin\frac{\xi_1}{\sqrt{2}} - \cos\frac{\xi_1}{\sqrt{2}}\right) \quad . \tag{58}$$

Similarly, in region 4, the solutions are

$$ {}_4v^{(o)} = \left\{ \frac{\cosh a\eta_2 - 1}{2\sqrt{\gamma}\, H} - \varepsilon^{1/2} 2\pi \left[\frac{1}{\sqrt{\gamma}} + \frac{\lambda\sqrt{K}}{(1+\lambda^2\gamma)} \left(1 - e^{\xi_2/\sqrt{2}} \cos \frac{\xi_2}{\sqrt{2}}\right)\right]\right\} $$

$$ \cdot \sin 2\pi\lambda\gamma(1 - \eta_2) \quad , \tag{59} $$

and

$$ {}_4\psi^{(o)} = - \varepsilon_1 \pi \sin 2\pi\lambda\gamma(1 - \eta_2) e^{-\xi_2/\sqrt{2}} \left(\cos \frac{\xi_2}{\sqrt{2}} + \sin \frac{\xi_2}{\sqrt{2}}\right) \quad . \tag{60} $$

THE FIRST R-ORDER SOLUTIONS

Temperature Distribution

The first R-order temperature, $T^{(1)}$, is governed by equation (23), with boundary conditions (29) and (30). The nonhomogeneous terms of equation (23) are the products of temperature fluxes and velocity components of the zeroth R-order solutions. Zeroth R-order velocities have boundary layer characteristics and these velocities are forcing the first R-order temperature. Though the zeroth R-order temperature has no boundary layer character, it is expected that at least part of the first R-order temperature will have boundary layer characteristics. Besides, the small viscous parameter ε, the symbol of boundary layer character, is also coupled with the differentiated highest order terms of the temperature in equation (23). Therefore, as indicated in equation (31), let

$$ T^{(1)} = {}_oT^{(1)} + {}_jT^{(1)} \quad , \quad j = 1,2,3,4 $$

where ${}_oT^{(1)}$ is the overall part and ${}_jT^{(1)}$ is the boundary part of the first R-

order temperature.

The governing equation (23), then, can be written in local coordinates in different regions as following:

in the interior region

$$\nabla_o^2 T^{(1)} = \frac{\sigma\pi^2}{\gamma} \cos 2\pi x \left(\frac{a \cosh az}{H} \cos 2\pi x - 1\right); \tag{61}$$

in region 1,

$$\frac{\partial_1^2 T^{(1)}}{\partial \zeta_1^2} = -\varepsilon_1^{1/2} \frac{\sigma\pi^2}{\sqrt{2}H} e^{-\zeta_1/\sqrt{2}} \sin^2 2\pi x \sinh a(1 - \varepsilon_1\zeta_1) \cdot \left(\cos\frac{\zeta_1}{\sqrt{2}} + \sin\frac{\zeta_1}{\sqrt{2}}\right) + O(\varepsilon) , \tag{62}$$

in region 2,

$$\frac{\partial_2^2 T^{(1)}}{\partial \zeta_2^2} = \varepsilon_1^{1/2} \frac{\sqrt{2}\,\sigma\pi^2}{H} e^{-\zeta_2/\sqrt{2}} \sin^2 2\pi x \sinh (a\varepsilon_1^{1/2}\zeta_2) \sin\frac{\zeta_2}{\sqrt{2}} + O(\varepsilon) , \tag{63}$$

in region 3,

$$\frac{\partial_3^2 T^{(1)}}{\partial \xi_1^2} = -\varepsilon_2^{1/2} \frac{\sigma\pi\, e^{\xi_1/\sqrt{2}}}{\sqrt{2}\,(1 + \lambda^2\gamma)\gamma} \sin 2\pi\lambda\gamma(1 - \eta_1) \sin\frac{\xi_1}{\sqrt{2}} \left[1 - \frac{a \cosh a\eta_1}{H} \cdot \cos 2\pi(\varepsilon_2^{1/2}\xi_1 + \frac{1}{2} - \lambda\gamma + \lambda\gamma\eta_1) + \frac{2\pi\lambda\gamma}{H} \sinh a\eta_1 \sin 2\pi \cdot (\varepsilon_2^{1/2}\xi_1 + \frac{1}{2} - \lambda\gamma + \lambda\gamma\eta_1)\right] + O(\varepsilon) , \tag{64}$$

in region 4,

$$\frac{\partial^2 T^{(1)}}{\partial \xi_2^2} = \varepsilon_2^{1/2} \frac{\sigma\pi\, e^{-\xi_2/\sqrt{2}}}{\sqrt{2}\,(1+\lambda^2\gamma)\gamma} \sin 2\pi\lambda\gamma(1-\eta_1) \sin\frac{\xi_2}{\sqrt{2}} \left[\frac{a\cosh a\eta_2}{H}\right.$$

$$\cdot \cos 2\pi(\varepsilon_2^{1/2}\xi_2 - \frac{1}{2} + \lambda\gamma - \lambda\gamma\eta_2) + \frac{2\pi\lambda\gamma}{H}\sinh a\eta_2 \sin 2\pi \qquad (65)$$

$$\left.\cdot (\varepsilon_2^{1/2}\xi_2 - \frac{1}{2} + \lambda\gamma - \lambda\gamma\eta_2) - 1\right] + O(\varepsilon) \ .$$

The boundary conditions for the first R-order temperature in equation (29) and (30) require $T^{(1)} = 0$ at $z = 0$, $z = 1$, and $\partial T^{(1)}/\partial x = 0$ at $x = \pm 1/2$. As we notice from equation (61) and equations (62), (63), (64), (65) that ${}_oT^{(1)}$ is order of unity and ${}_jT^{(1)}$s, are orders of $\varepsilon^{1/2}$. For simplicity, we can require that both ${}_oT^{(1)}$ and ${}_jT^{(1)}$, $j = 1,2$, vanish at the upper and lower boundaries to satisfy the boundary conditions without losing good approximation. On the eastern and western side, since the boundaries are inclined and all the dominant forcing terms in equations (64) and (65) vanish on the boundaries, we require ${}_jT^{(1)} = 0$, $j = 3,4$ at $\xi = 0$, instead of having $\partial T^{(1)}/\partial\xi = 0$ in consistency with the basic temperature requirement on the eastern and western boundaries.

Interior Solution

The overall part of the first R-order temperature ${}_oT^{(1)}$ can be obtained by solving equation (61) subjected to boundary conditions,

$$\begin{aligned} {}_oT^{(1)} &= 0 \quad \text{at} \quad z = 0,1 \ , \\ \frac{\partial {}_oT^{(1)}}{\partial x} &= 0 \quad \text{at} \quad x = \pm\frac{1}{2} \ . \end{aligned} \qquad (66)$$

The particular solution of equation (61) is

$$ {}_{o}T_{p}^{(1)} = \frac{\sigma}{4\gamma} \cos 2\pi x + \frac{\sigma\pi}{4\sqrt{\gamma}H} \cosh az - \frac{\sigma\pi}{12\sqrt{\gamma}H} \cosh az \cos 4\pi x . \qquad (67) $$

It is convenient to transfer particular solutions into new boundary conditions. For the homogeneous solution, equations (61) and (66) lead to:

$$ \nabla^2 {}_{o}T_{h}^{(1)} = 0 \qquad (68) $$

and

$$ {}_{o}T_{h}^{(1)} = - {}_{o}T_{p}^{(1)} \quad \text{at} \quad z = 0 , $$

$$ {}_{o}T_{h}^{(1)} = - {}_{o}T_{p}^{(1)} \quad \text{at} \quad z = 1 , \qquad (69) $$

$$ \frac{\partial {}_{o}T_{h}^{(1)}}{\partial x} = 0 \quad \text{at} \quad x = \pm \frac{1}{2} . $$

The solution of equation (68) satisfying boundary conditions (69) is

$$ {}_{o}T_{h}^{(1)} = - \frac{\sigma\pi}{4\sqrt{\gamma}H} + \frac{\sigma\pi}{4\sqrt{\gamma}H} (1 - G)z - \frac{\sigma}{4\gamma} \cosh az \cos 2\pi x $$

$$ + \frac{\sigma\pi}{12\sqrt{\gamma}H} \cosh 2az \cos 4\pi x + \frac{\sigma(G - 1)}{4\gamma H} \sinh az \cos 2\pi x \qquad (70) $$

$$ + \frac{\sigma\pi(G - G_2)}{12\sqrt{\gamma}H\ H_2} \sinh 2az \cos 4\pi x , $$

where H, G, H_2, G_2 are abbreviated constants listed in Table 3. Therefore,

the overall part of the first R-order temperature is

$$ {}_oT^{(1)} = {}_oT_p^{(1)} + {}_oT_h^{(1)} = \frac{\sigma\pi}{4\sqrt{\gamma}H}[\cosh az - 1 + (1 - G)z] + \frac{\sigma}{4\gamma} $$

$$ \left[1 - \cosh az + \frac{(G - 1)}{H}\sinh az\right] \cdot \cos 2\pi x + \frac{\sigma\pi}{12\sqrt{\gamma}H} \qquad (71) $$

$$ \left[\cosh 2az - \cosh az + \frac{(G - G_2)}{H_2}\sinh 2az\right]\cos 4\pi x \ . $$

Boundary Solutions

The boundary layer equations of the first R-order temperature in different regions are the equations (62), (63), (64), (65). The boundary conditions are ${}_jT^{(1)}$'s vanishing in the interior, and

$$ {}_jT^{(1)} = 0 \ , \quad j = 1,2,3,4 \text{ on the respective boundaries.} \qquad (72) $$

In region 1, equation (62), after integrations and having satisfied boundary conditions, yields

$$ {}_1T^{(1)} = \varepsilon_1^{1/2}\frac{\sigma\pi^2}{\sqrt{2}}\sin^2 2\pi x\left[1 - e^{-\zeta_1/\sqrt{2}}\left(\cos\frac{\zeta_1}{\sqrt{2}} - \sin\frac{\zeta_1}{\sqrt{2}}\right]\right] \ . \qquad (73) $$

In region 2, similarly, we obtain

$$ {}_2T^{(1)} = 0 \ . \qquad (74) $$

Since the forcing terms all vanished at the lower boundary as shown in equation (62), equation (74) means $T^{(1)}$ has no boundary layer modification near

the bottom as expected.

In regions 3 and 4, equations (64) and (65) with boundary conditions lead to

$$
{}_3T^{(1)} = \varepsilon_2^{1/2} \frac{\sigma\pi}{\sqrt{2}\,(1+\lambda^2\gamma)\gamma} \sin 2\pi\lambda\gamma(1-\eta_1) \left[1 + \frac{a \cosh a\eta_1}{H} \right. \tag{75}
$$

$$
\left. \cos 2\pi\lambda\gamma(1-\eta_1) + \frac{2\pi\lambda\gamma}{H} \sinh a\eta_1 \sin 2\pi\lambda\gamma(1-\eta_1) \right] \left(e^{\xi_1/\sqrt{2}} \cos \frac{\xi_1}{\sqrt{2}} - 1 \right) ,
$$

and

$$
{}_4T^{(1)} = \varepsilon_2^{1/2} \frac{\sigma\pi}{\sqrt{2}\,(1+\lambda^2\gamma)\gamma} \sin 2\pi\lambda\gamma(1-\eta_2) \left[1 + \frac{a}{H} \cosh a\eta_2 \cos 2\pi\lambda\gamma \right. \tag{76}
$$

$$
\left. \cdot\ (1-\eta_2) - \frac{2\pi\lambda\gamma}{H} \sinh a\eta_2 \sin 2\pi\lambda\gamma(1-\eta_2) \right] \left(e^{-\xi_2/\sqrt{2}} \cos \frac{\xi_2}{\sqrt{2}} - 1 \right) .
$$

Velocity Field

The first R-order velocity components are coupled with the first R-order temperature and the zeroth R-order velocities. From the governing equations (21), (22), (23), we obtain the equation for the first R-order boundary layer scaling as

$$
\begin{aligned}
\varepsilon^2 \mathcal{L} \nabla^2 \psi^{(1)} + \frac{\partial^2 \psi^{(1)}}{\partial z^2} = {} & \sigma \frac{\partial}{\partial x} \left(\frac{\partial \psi^{(o)}}{\partial z} \frac{\partial T^{(o)}}{\partial x} - \frac{\partial \psi^{(o)}}{\partial x} \frac{\partial T^{(o)}}{\partial z} \right) - \frac{\partial}{\partial z} \\
& \left(\frac{\partial \psi^{(o)}}{\partial z} \frac{\partial v^{(o)}}{\partial x} - \frac{\partial \psi^{(o)}}{\partial x} \frac{\partial v^{(o)}}{\partial z} \right) + \varepsilon \nabla^2 \left[\frac{\partial \psi^{(o)}}{\partial z} \frac{\partial^3 \psi^{(o)}}{\partial x \partial z^2} \right. \qquad (77) \\
& \left. - \frac{\partial \psi^{(o)}}{\partial x} \frac{\partial^3 \psi^{(o)}}{\partial z^3} + \gamma^2 \left(\frac{\partial^3 \psi^{(o)}}{\partial x^3} \frac{\partial \psi^{(o)}}{\partial z} - \frac{\partial \psi^{(o)}}{\partial x} \frac{\partial^3 \psi^{(o)}}{\partial x^2 \partial z} \right) \right] .
\end{aligned}
$$

Noticing that the $T^{(o)}$ has no boundary layer character, $\psi^{(o)}$ is order of ε with boundary layer part having the same order, and $v^{(o)}$ is order of unity with boundary layer part of the order of $\varepsilon^{1/2}$, the largest term on the right-hand side of equation (77) is estimated to be the order of unity in all the boundary regions. To the order of ε in the boundary regions, equation (77) reduces to the same boundary layer scaling equation for the zeroth R-order, that is, equation (32). Thus, we can solve the velocity field of the first R-order in exactly the same way as we did for the zeroth R-order solutions.

Interior Region

In the interior region, since $\partial_o \psi^{(o)}/\partial z = 0$, all the zeroth R-order terms in equation (21) are zeros. Therefore, in the interior region, equation (21) becomes

$$\frac{\partial_o v^{(1)}}{\partial z} = \frac{\partial_o T^{(1)}}{\partial x}$$

which together with ${}_oT^{(1)}$ in equation (71) yields

$$ {}_ov^{(1)} = \frac{\sigma}{4\gamma}\left[\frac{\sinh az}{\sqrt{\gamma}} - 2\pi z - \frac{(G-1)\cosh az}{\sqrt{\gamma}\,H}\right]\sin 2\pi x - \frac{\sigma\pi}{6\gamma H} \tag{78a}$$

$$\left[\frac{\sinh 2az}{2} - \sinh az + \frac{(G-G_2)}{2H_2}\cosh 2az\right]\sin 4\pi x + A_1(x) \quad .$$

Equation (22), to the order of ε, leads to

$$\frac{\partial_o \psi^{(1)}}{\partial z} = \frac{\partial_o \psi^{(o)}}{\partial x}\frac{\partial_o v^{(o)}}{\partial z}$$

which, with equations (38), (39), yields

$$ {}_0\psi^{(1)} = \varepsilon_1 \frac{\pi^2}{2\sqrt{\gamma}\,H} \cosh az \sin 4\pi x + B_1(x) \quad . \tag{79a} $$

The integration constants will be determined after matching the solutions.

Boundary Regions

In region 1 using the same local coordinates as shown in Table 2, equation (77), to the order of ε, can be reduced in similar manner to the similar equation (34) in the zeroth R-order solutions. With the boundary conditions similar to (46) and (48), equations (77) and (22), to the order of ε, lead to

$$ {}_1v^{(1)} = 0 \quad , \tag{80} $$

and

$$ {}_1\psi^{(1)} = 0 \quad . \tag{81} $$

The velocity component due to ${}_1T^{(1)}$ modification to the overall temperature distribution on the boundary has been neglected within the approximation accuracy.

In region 2, similarly, we obtain,

$$ {}_2v^{(1)} = \varepsilon_1^{1/2} \frac{\pi^2(1 - G)}{\sqrt{2\gamma}\,H} e^{-\zeta_2/\sqrt{2}} \sin 4\pi x \cos \frac{\zeta_2}{\sqrt{2}} \tag{82} $$

and

$$ {}_2\psi^{(1)} = - \varepsilon_1 \frac{\pi^2(1 - G)}{2\sqrt{\gamma}\,H} e^{-\zeta_2/\sqrt{2}} \sin 4\pi x \left(\cos \frac{\zeta_2}{\sqrt{2}} + \sin \frac{\zeta_2}{\sqrt{2}}\right) . \tag{83} $$

After matching the interior and the boundary solutions on the boundaries, the two integration constants, $A_1(x)$ and $B_1(x)$ have been determined. Equation (78a) becomes

$$
\begin{aligned}
{}_0v^{(1)} = {} & \frac{\sigma}{4\gamma}\left[\frac{\sinh az}{\sqrt{\gamma}} - 2\pi z + \frac{(G-1)}{\sqrt{\gamma}\,H}(1-\cosh az)\right]\sin 2\pi x \\
& - \left\{\frac{\sigma\pi}{6\gamma H}\left[\frac{\sinh 2az}{2} - \sinh az + \frac{(G-G_2)}{2H_2}(\cosh 2az - 1)\right]\right. \\
& \left. - \varepsilon_1^{1/2}\frac{\pi^2(1-G)}{\sqrt{2\gamma}\,H}\right\}\sin 4\pi x \quad . \qquad (78)
\end{aligned}
$$

Equation (79a) becomes

$$
{}_0\psi^{(1)} = \varepsilon_1 \frac{\pi^2 \sin 4\pi x}{2\sqrt{\gamma}\,H}(\cosh az - G) \quad . \qquad (79)
$$

In regions 3 and 4, noting that the order of unity part of the zeroth R-order meridional boundary velocity, ${}_3v^{(0)}$ and ${}_4v^{(4)}$, are functions of the unstretched tangential coordinate η only, equation (77) leads to an equation similar to (32) as mentioned before. Then, in similar manner, we obtain, in region 3

$$
{}_3v^{(1)} = -\varepsilon_2^{1/2}\frac{\pi^2\lambda\, e^{\xi_1/\sqrt{2}}}{\sqrt{2\gamma}\,H(1+\lambda^2\gamma)}\sin 4\pi\lambda\gamma(1-\eta_1)\cos\frac{\xi_1}{\sqrt{2}}(\cosh a\eta_1 - G) - h(\eta_1) \qquad (84)
$$

where

$$h(\eta) = \frac{\sigma}{4\gamma}\left[\frac{\sinh a\eta}{\sqrt{\gamma}} - 2\pi\eta + \frac{(G-1)}{\sqrt{\gamma}\ H}(1 - \cosh a\eta)\right]\sin 2\pi\lambda\gamma(1-\eta)$$

$$+ \left\{\frac{\sigma\pi}{4\gamma H}\left[\frac{\sinh 2a\eta}{2} - \sinh a\eta + \frac{G - G_2}{2H_2}(\cosh 2a\eta - 1)\right] + \varepsilon_1^{1/2}\frac{\pi^2(1-G)}{\sqrt{2\gamma}\ H}\right.$$

$$\left. - \varepsilon_2^{1/2}\frac{\pi^2\lambda}{\sqrt{2\gamma}\ H(1+\lambda^2\gamma)}(\cosh a\eta - G)\right\}\sin 4\pi\lambda\gamma(1-\eta) \quad ; \qquad (85)$$

and

$${}_3\psi^{(1)} = \varepsilon_1\frac{\pi^2 e^{\xi_1/\sqrt{2}}}{2\sqrt{\gamma}\ H}\sin 4\pi\lambda\gamma(1-\eta_1)(\cosh a\eta_1 - G)\left(\cos\frac{\xi_1}{\sqrt{2}} - \sin\frac{\xi_1}{\sqrt{2}}\right), \qquad (86)$$

in region 4,

$${}_4v^{(1)} = \varepsilon_2^{1/2}\frac{\pi^2\lambda\ e^{-\xi_2/\sqrt{2}}}{\sqrt{2\gamma}\ H(1+\lambda^2\gamma)}\sin 4\pi\lambda\gamma(1-\eta_2)\cos\frac{\xi_2}{\sqrt{2}}(\cosh a\eta_2 - G) + h(\eta_2) \qquad (87)$$

where $h(\eta_2)$ is a direct substitution of η_2 for η in equation (85) and

$${}_4\psi^{(1)} = -\varepsilon_1\frac{\pi^2\ e^{-\xi_2/\sqrt{2}}}{2\sqrt{\gamma}\ H}\sin 4\pi\lambda\gamma(1-\eta_2)(\cosh a\eta_2 - G)\left(\cos\frac{\xi_2}{\sqrt{2}} + \sin\frac{\xi_2}{\sqrt{2}}\right). \qquad (88)$$

Note that all boundary layer solutions in our model study are weaker by $O(\varepsilon^{1/2})$ than those obtained in the case of rigid surface (see, for example, Robinson, 1959). This agrees with Hide's (1964) result that the Ekman boundary layer associated with a free surface is weaker than that with rigid surface.

Estimated Errors of the Approximate Solutions

TEMPERATURE

The order of magnitude of the second R-order temperature, $T^{(2)}$, can be evaluated from its governing equation (26). From the zeroth R-order solutions, we know $\psi^{(0)}$ is $O(\varepsilon)$ both in the interior and boundary regions; $v^{(0)}$ is $O(1)$ in the interior and $O(\varepsilon^{1/2})$ for the boundary layer part; and $T^{(0)}$ has no boundary layer characteristics. The first R-order solutions have exactly the same order of magnitude as that of the zeroth R-order. Therefore, equation (26), having the forcing terms $O(\varepsilon)$ in the interior and $O(\varepsilon^{1/2})$ on the boundaries, will lead to the same results as the first R-order temperature, namely, ${}_oT^{(2)}$ is $O(1)$ and ${}_jT^{(2)}$'s are $O(\varepsilon^{1/2})$. Hence the highest order of $T^{(2)}$ is $O(1)$. Thus, the validity of the series expansion of the temperature in powers of R as shown in equation (17) has been verified. The asymptotic character of the infinite series is now plausible.

To the expansion of second power, the approximate error of temperature is $O(\sigma^2R^2)$ which is rather small.

VELOCITY

The meridional velocity is dominant in the flow field. It is $O(1)$ in both the zeroth R-order and the first R-order. Therefore, the approximate error for v, to the second power of the infinite series, is $O(R^2)$. A similar approximation error is found for the stream function.

Type-A Circulation

Type-A circulation is expected to occur during the summer-heating period when the temperature in the lake has already risen above 4°C with the middle part of the lake still colder than the edges, and during the winter-cooling period when the lake has cooled down to less than 4°C and is still cooling. The solutions of the flow field have been obtained by applying the surface temperature of the lake as a concave cosine function as mentioned in the last chapter. Notice that the thermally induced force during the winter-cooling period, since the fluid is less than 4°C and the air temperature is cooling the lake, has exactly the same effects as the summer-heating period, except the former has smaller ΔT and in the negative sense.

Type-B Circulation

During the spring-heating period and the autumn-cooling period the surface temperatures of the lake and their induced thermal body forces have exactly the reverse forms and opposite effects as that of the winter-cooling and summer-heating periods in the type-A circulation. Therefore, type-B circulation is the reverse form of type-A circulation.

IV. THE THERMAL BAR CURRENT

Mathematical Formulation

The general governing equations (1), (2), (3) with boundary conditions (4) and (6) are the differential system for the flow field during thermal bar periods of the Lake Michigan model. The current circulation pattern induced by the thermal bar phenomenon specified in Chapter I is called the thermal bar current or the type-C circulation in our terms. The thermal bar phenomenon is common to all large dimictic lakes during the time of spring warming-up period or the autumn cooling-off period. The latter, due to the smaller horizontal temperature difference, is much weaker. Since the effects of the thermal body forces in inducing currents during these two periods are exactly the same, we shall consider the spring thermal bar phenomenon as representative.

THE APPROXIMATE EQUATION OF STATE

During the prevailing period of the thermal bar phenomenon, the temperature near the shore of the lake is above 4°C while the temperature in the middle portion of the lake is still less than the temperature of maximum density. The relationship between pure water density and temperature is shown in Figure 8. Generally, Lake Michigan is rather shallow. The deviation of the maximum density of fresh water away from 4°C due to the hydrostatic pressure can be neglected. The density of the natural fresh water in the lake follows the curve closely as temperature changes (Welch, 1952). Therefore, within the ther-

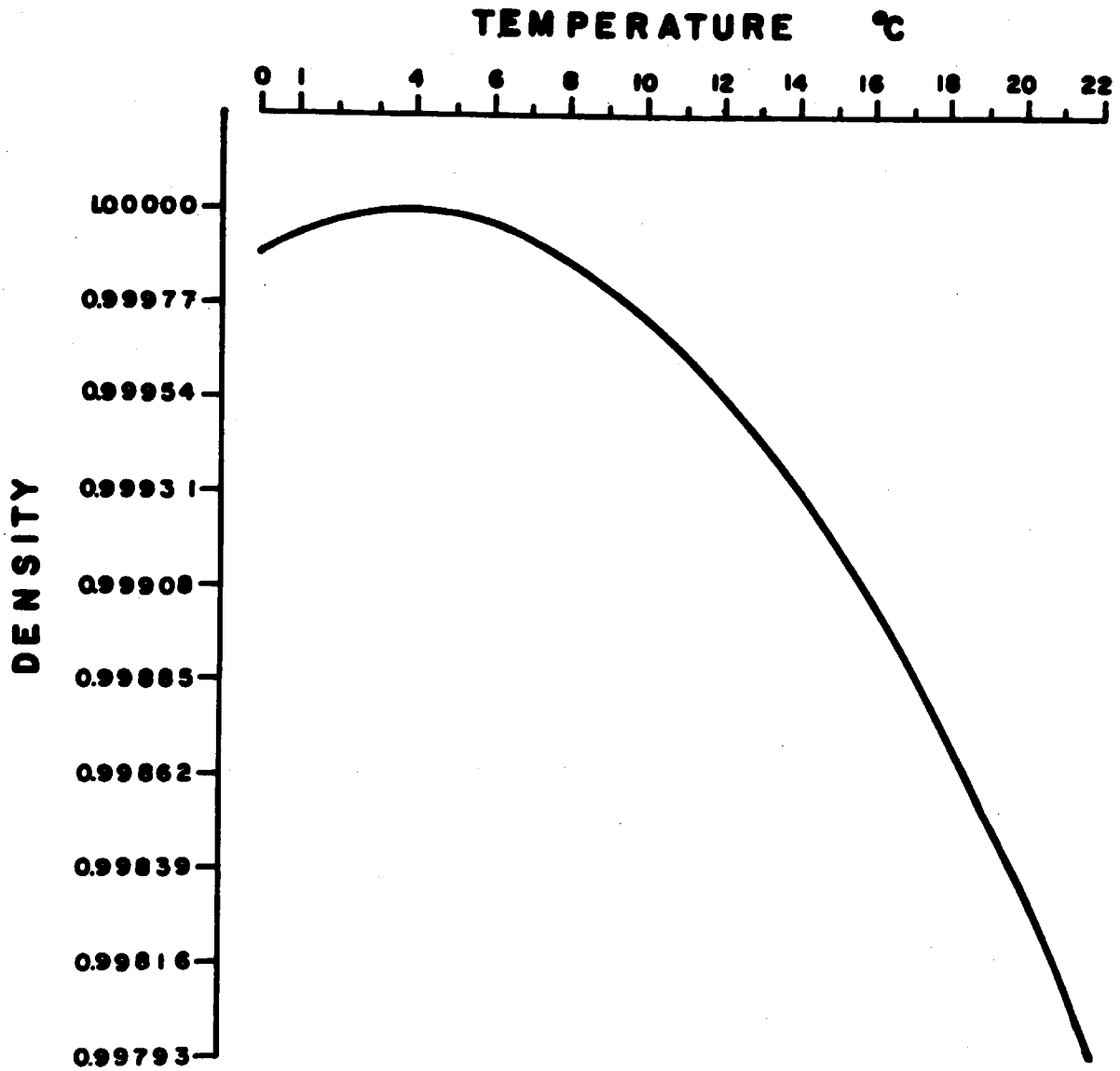


Figure 8. Relationship between freshwater density and temperature (after Welch, 1952).

mal bar temperature range (from 0°C to 12°C, for instance), the density variation with temperature change can be approximated as a cosine function. Let us define

$$\rho = \rho_o \cos A(T' - T_o) \tag{89}$$

where ρ is the density of water at any local temperature, T', ρ_o is the density

of water at reference temperature, $T_o = 4°C$, and A is a constant which adjusts the equation of state (89) to the nearest good approximation of the density variations within the temperature range ($0°C < T' < 12°C$). The appropriate constant A is, in general, a small number (10^{-2} to 10^{-3}). Thus the rate of change of density with respect to temperature is a function negatively correlated with the absolute value of the temperature difference between the local temperature and the temperature of maximum density. Then the thermal body force is

$$\frac{\Delta\rho}{\rho_o} = \cos A(T' - T) - 1 \quad , \tag{90}$$

which satisfies the special requirement that the water density decreases as temperature varies away from 4°C. This approximation is used in the type-C circulation.

NONDIMENSIONAL GOVERNING EQUATIONS

These follow closely the processes in Chapter III, using the same nondimensional variables as equation (9) and with the same basic assumptions as equations (11) and (12), the nondimensional governing equations of the thermal bar current, after introducing the nondimensional stream function, become,

$$\varepsilon\nabla^2\psi + \frac{\partial v}{\partial z} - \sin AT\,\frac{\partial T}{\partial x} = R\left[\frac{\partial\psi}{\partial z}\frac{\partial^3\psi}{\partial x\partial z^2} - \frac{\partial\psi}{\partial x}\frac{\partial^3\psi}{\partial z^3} + \gamma^2\left(\frac{\partial\psi}{\partial z}\frac{\partial^3\psi}{\partial x^3} - \frac{\partial\psi}{\partial x}\frac{\partial^3\psi}{\partial x^2\partial z}\right)\right] \quad , \tag{91}$$

$$\varepsilon\nabla^2 v - \frac{\partial\psi}{\partial z} = R\left(\frac{\partial\psi}{\partial z}\frac{\partial v}{\partial x} - \frac{\partial\psi}{\partial x}\frac{\partial v}{\partial z}\right) \quad , \tag{92}$$

$$\varepsilon\nabla^2 T = \sigma R\left(\frac{\partial\psi}{\partial z}\frac{\partial T}{\partial x} - \frac{\partial\psi}{\partial x}\frac{\partial T}{\partial z}\right) \quad , \tag{93}$$

where $\mathcal{L}$, ∇^2 are operators and γ, ε, σ are nondimensional parameters (Table 2). Note that the basic geostrophic thermal wind relationship is now a nonlinear equation,

$$2\Omega \frac{\partial v'}{\partial z'} = Ag \sin A(T' - T_o) \frac{\partial T'}{\partial x} \quad , \tag{94}$$

which after being nondimensionalized becomes

$$2\Omega \frac{V}{D} \frac{\partial v}{\partial z} = \frac{Ag\Delta T \sin A\Delta T}{L} \sin AT \frac{\partial T}{\partial x} \quad ,$$

where the sin AT has been normalized in order to make the two terms of the same order in the nondimensional equation. Thus the dimensional reference velocity becomes

$$V = \frac{AgD\Delta T \sin A\Delta T}{2\Omega L} \quad , \tag{95}$$

and the thermal Rossby number is now

$$R = \frac{V}{2\Omega L} = \frac{AgD\Delta T \sin A\Delta T}{(2\Omega L)^2} \quad . \tag{96}$$

Similarly, since $R \ll 1$, by observation, the regular perturbation method can be used to achieve approximate solutions. All dependent variables are expanded in powers of R as shown in equation (17). The same argument in Chapter III can be used here for the validity of expressing the temperature in powers of R. We also expand sin AT in a power series. Due to the smallness of A, terms higher than second order in the sine series have been neglected. Then, after equating each power of R in equations (91), (92), and (93), the zeroth R-order equations are:

$$\varepsilon\mathcal{L}\psi^{(0)} + \frac{\partial v^{(0)}}{\partial z} - AT^{(0)}\frac{\partial T^{(0)}}{\partial x} = 0 \quad , \tag{97}$$

$$\varepsilon\nabla^2 v^{(0)} - \frac{\partial \psi^{(0)}}{\partial z} = 0 \quad , \tag{98}$$

$$\nabla^2 T^{(0)} = 0 \quad . \tag{99}$$

We notice that from equation (99), the zeroth R-order temperature is still due to conduction only.

The first R-order equations are:

$$\varepsilon\mathcal{L}\psi^{(1)} + \frac{\partial v^{(1)}}{\partial z} - A\left(T^{(1)}\frac{\partial T^{(0)}}{\partial x} + T^{(0)}\frac{\partial T^{(1)}}{\partial x}\right) = \frac{\partial \psi^{(0)}}{\partial z}\frac{\partial^3 \psi^{(0)}}{\partial x \partial z^2} - \frac{\partial \psi^{(0)}}{\partial x}\frac{\partial^3 \psi^{(0)}}{\partial z^3}$$

$$+ \gamma^2\left(\frac{\partial \psi^{(0)}}{\partial z}\frac{\partial^3 \psi^{(0)}}{\partial x^3} - \frac{\partial \psi^{(0)}}{\partial x}\frac{\partial^3 \psi^{(0)}}{\partial x^2 \partial z}\right) , \tag{100}$$

$$\varepsilon\nabla^2 v^{(1)} - \frac{\partial \psi^{(1)}}{\partial z} = \frac{\partial \psi^{(0)}}{\partial z}\frac{\partial v^{(0)}}{\partial x} - \frac{\partial \psi^{(0)}}{\partial x}\frac{\partial v^{(0)}}{\partial z} \quad , \tag{101}$$

and

$$\varepsilon\nabla^2 T^{(1)} = \sigma\left(\frac{\partial \psi^{(0)}}{\partial z}\frac{\partial T^{(0)}}{\partial x} - \frac{\partial \psi^{(0)}}{\partial x}\frac{\partial T^{(0)}}{\partial z}\right) \quad . \tag{102}$$

The second R-order equations are:

$$\varepsilon\mathcal{L}\psi^{(2)} + \frac{\partial v^{(2)}}{\partial z} - A\left(T^{(0)}\frac{\partial T^{(2)}}{\partial x} + T^{(2)}\frac{\partial T^{(0)}}{\partial x} + T^{(1)}\frac{\partial T^{(1)}}{\partial x}\right) = \frac{\partial \psi^{(0)}}{\partial z}\frac{\partial^3 \psi^{(1)}}{\partial x \partial z^2}$$

$$- \frac{\partial \psi^{(0)}}{\partial x}\frac{\partial^3 \psi^{(1)}}{\partial z^3} + \frac{\partial \psi^{(1)}}{\partial z}\frac{\partial^3 \psi^{(0)}}{\partial x \partial z^2} - \frac{\partial \psi^{(1)}}{\partial x}\frac{\partial^3 \psi^{(0)}}{\partial z^3} + \gamma^2\left(\frac{\partial \psi^{(0)}}{\partial z}\frac{\partial^3 \psi^{(1)}}{\partial x^3}\right.$$

$$\left. - \frac{\partial \psi^{(0)}}{\partial x}\frac{\partial^3 \psi^{(1)}}{\partial x^2 \partial z} + \frac{\partial \psi^{(1)}}{\partial z}\frac{\partial^3 \psi^{(0)}}{\partial x^3} - \frac{\partial \psi^{(1)}}{\partial x}\frac{\partial^3 \psi^{(0)}}{\partial x^2 \partial z}\right) , \tag{103}$$

$$\varepsilon\nabla^2 v^{(2)} - \frac{\partial \psi^{(2)}}{\partial z} = \frac{\partial \psi^{(0)}}{\partial z}\frac{\partial v^{(1)}}{\partial x} - \frac{\partial \psi^{(0)}}{\partial x}\frac{\partial v^{(1)}}{\partial z} + \frac{\partial \psi^{(1)}}{\partial z}\frac{\partial v^{(0)}}{\partial x} - \frac{\partial \psi^{(1)}}{\partial x}\frac{\partial v^{(0)}}{\partial z} \quad , \tag{104}$$

$$\varepsilon\nabla^2 T^{(2)} = \sigma\left(\frac{\partial \psi^{(0)}}{\partial z}\frac{\partial T^{(1)}}{\partial x} - \frac{\partial \psi^{(0)}}{\partial x}\frac{\partial T^{(1)}}{\partial z} + \frac{\partial \psi^{(1)}}{\partial z}\frac{\partial T^{(0)}}{\partial x} - \frac{\partial \psi^{(1)}}{\partial x}\frac{\partial T^{(0)}}{\partial z}\right) \quad . \tag{105}$$

Boundary conditions, with reference to equations (4) and (6), are:

$$T^{(0)} = \frac{1}{3}(1 - 2\cos 2\pi x) \quad , \quad \psi^{(0)} = \frac{\partial^2 \psi^{(0)}}{\partial z^2} = \frac{\partial v^{(0)}}{\partial z} = 0 \quad \text{at} \quad z = 1 \quad ,$$

$$T^{(0)} = 0 \quad , \text{ and } \quad \psi^{(0)} = v^{(0)} = \frac{\partial \psi^{(0)}}{\partial z} = 0 \quad \text{at} \quad z = 0 \quad , \tag{106}$$

and $\vec{q}^{(0)} = 0$ on the slant boundaries and

$$\frac{\partial T^{(0)}}{\partial x} = 0 \quad \text{at} \quad x = \pm\frac{1}{2}$$

for the zeroth R-order equations;

and

$$T^{(i)} = 0 \quad , \quad \psi^{(i)} = \frac{\partial^2 \psi^{(i)}}{\partial z^2} = \frac{\partial v^{(i)}}{\partial z} = 0 \quad \text{at} \quad z = 1 \quad ,$$

$$T^{(i)} = 0 \quad , \quad \psi^{(i)} = \frac{\partial \psi^{(i)}}{\partial z} = v^{(i)} = 0 \quad \text{at} \quad z = 0 \tag{107}$$

$$\vec{q}^{(i)} = 0 \text{ on the slant boundaries and } \frac{\partial T^{(i)}}{\partial x} = 0 \text{ at } x = \pm\frac{1}{2}$$

for the ith R-order equations, i = 1,2,3,...

Equations (97), (100), and (103) are highly nonlinear in temperature, which produces the thermal body force in generating currents. Fortunately, by virtue of the energy equation, the temperature field of every ith R-order equa-

tion can be solved first and the nonlinearity in the ith R-order momentum equation is eliminated. In this way, the temperature and velocity fields can be found.

BOUNDARY LAYER SCALING

Equations (97), (98) with the Ekman number $\varepsilon \ll 1$, lead automatically to the method of matched asymptotic expansion as before. Using the same notation to indicate the ith R-order dependent variables in the interior as well as in the boundary regions (Figure 7) as shown in equation (31), equations (97), (98), and (99) result

$$\varepsilon^2\chi\nabla^2\psi^{(o)} + \frac{\partial^2\psi^{(o)}}{\partial z^2} = \varepsilon\frac{\partial}{\partial x}\left[\left(\frac{\partial T^{(o)}}{\partial x}\right)^2 + \frac{1}{\gamma}\left(\frac{\partial T^{(o)}}{\partial z}\right)^2\right] \quad . \tag{108}$$

Since $T^{(o)}$ has no boundary layer characteristics as we noticed from equation (99) which is simply the Laplace equation, the right-hand side of equation (108) is $O(\varepsilon)$ throughout the flow field, even in the boundary layer regions. After stretching the normal coordinate in each boundary region, the right-hand side of equation (108) is relatively only $O(\varepsilon^2)$ which can be easily neglected without causing much error. Then the characteristic equation for boundary layer scaling is exactly the same equation as (32). Following the same steps, we obtain the boundary layer thickness in region 1 and region 2 is $O(\varepsilon_1^{1/2})$ and in region 3 and region 4 is $O(\varepsilon_2^{1/2})$. All local coordinates are as shown in Table 2.

Analytical Approximate Solutions

THE ZEROTH R-ORDER SOLUTIONS

Temperature Distribution

The zeroth R-order temperature solution satisfying the Laplace equation and the boundary conditions (106) is:

$$T^{(o)} = \frac{1}{3}\left(z - \frac{2}{H} \sinh az \cos 2\pi x\right) \tag{109}$$

which has no boundary layer characteristics.

Velocity Field

Following closely the procedures of the last chapter, interior solutions can be obtained by neglecting the viscous effects. Equations (97) and (98) in the interior region, become

$$\frac{\partial_o v^{(o)}}{\partial z} = T^{(o)} \frac{\partial T^{(o)}}{\partial x} \quad , \tag{110}$$

and

$$\frac{\partial_o \psi^{(o)}}{\partial z} = 0 \quad . \tag{111}$$

Since $T^{(o)}$ is known, both equations (110) and (111) can be integrated. The integration constants will be determined after matching the interior solutions with the boundary layer solutions. As before, we are using the technique of additive type boundary layer analysis. In the boundary region, after stretching the normal coordinate, the governing equations in terms of the boundary local coordinates can be treated as ordinary differential equations. In each

boundary region, the stream function can be obtained first from the equation similar to equation (34) by satisfying the decay condition and the boundary conditions. Then the meridional velocity in the boundary region can be found from equation (98) after substitution of the boundary layer stream function and satisfaction of the meridional boundary condition on the boundary. Considering that the interior solution is dominant in the interior region and has no boundary layer characteristics and that the boundary layer solution is important only at its respective boundary, the zeroth R-order solutions have been obtained as: in the interior

$$ {}_{o}v^{(o)} = \frac{4\pi A}{9}\left[\left(\frac{z}{Ha}\cosh az - \frac{1}{Ha^2}\sinh az\right)\sin 2\pi x \right. $$

$$ \left. - \left(\frac{1}{4H^2 a}\sinh 2az - \frac{z}{2H^2}\right)\sin 4\pi x\right] - \varepsilon_1^{1/2}\sqrt{2}\, b_o(x) \quad , \qquad (112) $$

$$ {}_{o}\psi^{(o)} = \varepsilon_1 b_o(x) \quad , \qquad (113) $$

where

$$ b_o(x) = \frac{4\pi A}{9}(\sin 2\pi x - \sin 4\pi x) \quad ; \qquad (114) $$

in region 1,

$$ {}_{1}v^{(o)} = \varepsilon_1^{1/2}\frac{b_o(x)}{\sqrt{2}}\, e^{-\zeta_1/\sqrt{2}}\left(\sin\frac{\zeta_1}{\sqrt{2}} - \cos\frac{\zeta_1}{\sqrt{2}}\right) \quad , \qquad (115) $$

$$ {}_{1}\psi^{(o)} = -\varepsilon_1 b_o(x)\, e^{-\zeta_1/\sqrt{2}}\cos\frac{\zeta_1}{\sqrt{2}} \quad ; \qquad (116) $$

in region 2,

$$ {}_{2}v^{(o)} = \varepsilon_1^{1/2}\sqrt{2}\, b_o(x)\, e^{-\zeta_2/\sqrt{2}}\cos\frac{\zeta_2}{\sqrt{2}} \quad , \qquad (117) $$

$$ {}_2\psi^{(o)} = - \varepsilon_1 b_o(x)\, e^{-\zeta_2/\sqrt{2}} \left(\cos \frac{\zeta_2}{\sqrt{2}} + \sin \frac{\zeta_2}{\sqrt{2}}\right) \quad ; \tag{118} $$

in region 3,

$$ {}_3v^{(o)} = d_o(\eta_1) + \varepsilon^{1/2} \sqrt{2}\, b_o(\eta_1)\left[\frac{1}{\sqrt{\gamma}} + \frac{\lambda\sqrt{K}}{(1 + \lambda^2\gamma)}\left(e^{\xi_1/\sqrt{2}} \cos \frac{\xi_1}{\sqrt{2}} - 1\right)\right] \quad , \tag{119} $$

$$ {}_3\psi^{(o)} = \varepsilon_1 b_o(\eta_1) e^{\xi_1/\sqrt{2}} \left(\sin \frac{\xi_1}{\sqrt{2}} - \cos \frac{\xi_1}{\sqrt{2}}\right) \quad ; \tag{120} $$

where

$$ b_o(\eta) = \frac{4\pi A}{9}\left[\sin 4\pi\lambda\gamma(1 - \eta) + \sin 2\pi\lambda\gamma(1 - \eta)\right] \quad , \tag{121} $$

and

$$ d_o(\eta) = \frac{4\pi A}{9}\left[\left(\frac{\sinh a\eta}{Ha^2} - \frac{\eta \cosh a\eta}{Ha}\right) \sin 2\pi\lambda\gamma(1 - \eta)\right. $$

$$ \left. - \left(\frac{\sinh 2a\eta}{4H^2 a} - \frac{\eta}{2H^2}\right) \sin 4\pi\lambda\gamma(1 - \eta)\right] \quad ; \tag{122} $$

in region 4,

$$ {}_4v^{(o)} = - d_o(\eta_2) - \varepsilon^{1/2} \sqrt{2}\, b_o(\eta_2)\left[\frac{1}{\sqrt{\gamma}} + \frac{\lambda\sqrt{K}}{(1 + \lambda^2\gamma)}\left(e^{-\xi_2/\sqrt{2}} \cos \frac{\xi_2}{\sqrt{2}} - 1\right)\right] \quad , \tag{123} $$

$$ {}_4\psi^{(o)} = \varepsilon_1 b_o(\eta_2) e^{-\xi_2/\sqrt{2}} \left(\cos \frac{\xi_2}{\sqrt{2}} + \sin \frac{\xi_2}{\sqrt{2}}\right) \tag{124} $$

where $b_o(\eta_2)$ and $d_o(\eta_2)$ are direct substitutions of η_2 for η in equations (121), (122).

THE FIRST R-ORDER SOLUTIONS

Temperature Distribution

The governing equation and boundary conditions for the first R-order temperature are the same as for the general thermal currents. We notice from equation (102) that the first R-order temperature has boundary layer characteristics because of the forcing terms due to heat fluxes coupled with the boundary layer velocity components. As before, after stretching the normal coordinate and rewriting in terms of the local coordinates as shown in Table 2, the boundary layer part of the temperature can be obtained by integrating equation (102) with all the boundary layer effects included and by satisfying boundary conditions in (107) on its own boundary. Using the same notions as indicated in equation (31), the ${}_jT^{(1)}$'s are summarized as:

in region 1,

$$ {}_1T^{(1)} = \varepsilon_1^{1/2} \frac{2\sigma\pi}{3} b_o(x) \sin 2\pi x \left[1 - e^{-\zeta_1/\sqrt{2}} \left(\cos \frac{\zeta_1}{\sqrt{2}} - \sin \frac{\zeta_1}{\sqrt{2}} \right) \right] , \quad (125) $$

in region 2,

$$ {}_2T^{(1)} = 0 , \quad (126) $$

in region 3,

$$ {}_3T^{(1)} = \varepsilon_2^{1/2} \frac{\sqrt{2}\,\sigma b_o(\eta_1)}{3(1+\lambda^2\gamma)\gamma} \left[1 + \frac{2a}{H} \cosh a\eta_1 \cos 2\pi\lambda\gamma(1-\eta_1) + \frac{4\pi\lambda\gamma}{H} \sinh a\eta_1 \sin 2\pi\lambda\gamma(1-\eta_1) \right] \left(e^{\xi_1/\sqrt{2}} \cos \frac{\xi_1}{\sqrt{2}} - 1 \right) , \quad (127) $$

in region 4,

$$
{}_4T^{(1)} = \varepsilon_2^{1/2} \frac{2\sigma b_o(\eta_2)}{3(1+\lambda^2\gamma)\gamma} \left[1 + \frac{2a}{H} \cosh a\eta_2 \cos 2\pi\lambda\gamma(1-\eta_2) \right.
$$

$$
\left. - \frac{4\pi\lambda\gamma}{H} \sinh a\eta_2 \sin 2\pi\lambda\gamma(1-\eta_2) \right] \left(e^{-\xi_2/\sqrt{2}} \cos \frac{\xi_2}{\sqrt{2}} - 1\right) \quad , \tag{128}
$$

where $b_o(x)$ is shown in equation (114), $b_o(\eta)$, in equation (121). In the interior region, after substitutions of equations (109) and (114), equation (102) leads to:

$$
\nabla_o^2 T^{(1)} = \frac{8\pi^2 A\sigma}{27\gamma}\left(\frac{a}{H} \cosh az - \cos 2\pi x + 2\cos 4\pi x - \frac{2a}{H} \cosh az \cos 2\pi x \right.
$$

$$
\left. + \frac{a}{H} \cosh az \cos 4\pi x - \frac{2a}{H} \cosh az \cos 6\pi x \right) \quad . \tag{129}
$$

The boundary conditions are still as expressed in equation (107). Since the homogeneous solution of equation (129) has terms like

$$
\cosh naz \cos 2n\pi x \quad , \; n = 1,2,3,\ldots,
$$

the particular solution, knowing that equation (129) is an even function, is

$$
{}_oT_p^{(1)} = C_1 \cos 2\pi x + C_2 \cos 4\pi x + C_3 \cosh az + C_4 \sinh az \cos 2\pi x
$$

$$
+ C_5 \cosh az \cos 4\pi x + C_6 \cosh az \cos 6\pi x \quad . \tag{130}
$$

Substituting equation (130) into (129), we obtain

$$
C_1 = \frac{2A\sigma}{27\gamma} \quad , \qquad C_2 = \frac{-A\sigma}{27\gamma} \quad , \qquad C_3 = \frac{4A\pi\sigma}{27\sqrt{\gamma}} \quad ,
$$

$$
C_4 = \frac{-8\pi^2 A\sigma}{27H} \quad , \quad C_5 = \frac{-4\pi A\sigma}{81\sqrt{\gamma}H} \quad , \quad C_6 = \frac{\pi A\sigma}{27\sqrt{\gamma}H} \tag{131}
$$

For convenience, all the C_i's are listed in Table 3 as abbreviated constants for later use.

After the transfer of the particular solution as new boundary conditions for the homogeneous solution, we obtain:

$$
\begin{aligned}
{}_oT_h^{(1)} &= C_3(1 - G)z - C_3 - C_1 \cosh az \cos 2\pi x - (C_2 + C_5) \cosh 2az \cos 4\pi x \\
&\quad - C_6 \cosh 3az \cos 6\pi x + \left(\frac{C_1 G - C_1}{H} - C_4\right) \sinh az \cos 2\pi x \\
&\quad + \frac{(C_2 + C_5)G - C_2 - C_5 G}{H_2} \sinh 2az \cos 4\pi x + \frac{C_6(1 - G)}{H_3} \sinh 3az \cos 6\pi x \quad .
\end{aligned}
\tag{132}
$$

Therefore, the overall part of the first R-order temperature without boundary layer characteristics is,

$$
\begin{aligned}
{}_oT^{(1)} &= C_3(1 - G)z + C_3(\cosh az - 1) + \{C_1(1 - \cosh az) - [C_4(1 - z) \\
&\quad - \frac{C_1(G - 1)}{H}] \sinh az\} \cos 2\pi x + [C_2 + C_5 \cosh az - (C_2 + C_5) \cosh 2az \\
&\quad + \frac{(C_2 + C_5)G_2 - C_2 - C_5 G}{H_2} \sinh 2az] \cos 4\pi x + [C_6(\cosh az - \cosh 3az) \\
&\quad + \frac{C_6(G_3 - G)}{H_3} \sinh 3az] \cos 6\pi x
\end{aligned}
\tag{133}
$$

and has $O(\varepsilon^{1/2})$ modifications on the boundary regions.

Velocity Field

In the interior region, since $\partial_o \psi^{(o)}/\partial z = 0$, equations (100) and (101) lead to

$$\frac{\partial_o v^{(1)}}{\partial z} = A\left({}_oT^{(1)} \frac{\partial T^{(o)}}{\partial x} + T^{(o)} \frac{\partial T^{(1)}}{\partial x}\right) \quad , \tag{134}$$

and

$$\frac{\partial_o \psi^{(1)}}{\partial z} = \frac{\partial_o \psi^{(o)}}{\partial x} \frac{\partial_o v^{(o)}}{\partial z} \quad . \tag{135}$$

The values of $T^{(o)}$, ${}_ov^{(o)}$, ${}_o\psi^{(o)}$, and ${}_oT^{(1)}$ are known as shown in equations (27), (38), (39), and (133). Therefore the solutions for ${}_ov^{(1)}$ and ${}_o\psi^{(1)}$ can be obtained by integration. As before, the integration constants will be determined after matching the boundary solutions and the interior solutions.

In the boundary regions, equations (100), (101), and (102) lead to the boundary layer characteristic equation:

$$\begin{aligned}
\varepsilon^2 \nabla^2 \psi^{(1)} + \frac{\partial^2 \psi^{(1)}}{\partial z^2} = {} & \frac{\partial}{\partial z}\left(\frac{\partial \psi^{(o)}}{\partial x} \frac{\partial v^{(o)}}{\partial z} - \frac{\partial \psi^{(o)}}{\partial z} \frac{\partial v^{(o)}}{\partial x}\right) + A\sigma \frac{\partial T^{(o)}}{\partial x}\left(\frac{\partial \psi^{(o)}}{\partial z} \frac{\partial T^{(o)}}{\partial x}\right. \\
& \left. - \frac{\partial \psi^{(o)}}{\partial x} \frac{\partial T^{(o)}}{\partial z}\right) + A\sigma T^{(o)} \frac{\partial}{\partial x}\left(\frac{\partial \psi^{(o)}}{\partial z} \frac{\partial T^{(o)}}{\partial x} - \frac{\partial \psi^{(o)}}{\partial x} \frac{\partial T^{(o)}}{\partial z}\right) \\
& + \varepsilon 2A\left[\frac{\partial T^{(1)}}{\partial x} \frac{\partial^2 T^{(o)}}{\partial x^2} + \frac{\partial T^{(o)}}{\partial x} \frac{\partial^2 T^{(1)}}{\partial x^2} + \frac{1}{\gamma}\left(\frac{\partial T^{(1)}}{\partial z} \frac{\partial^2 T^{(o)}}{\partial z \partial x}\right.\right. \\
& \left.\left. + \frac{\partial T^{(o)}}{\partial z} \frac{\partial^2 T^{(1)}}{\partial z \partial x}\right)\right] + \varepsilon \nabla^2 \left[\frac{\partial \psi^{(o)}}{\partial z} \frac{\partial^3 \psi^{(o)}}{\partial x \partial z^2} - \frac{\partial \psi^{(o)}}{\partial x} \frac{\partial^3 \psi^{(o)}}{\partial z^3}\right. \\
& \left. + \gamma^2\left(\frac{\partial \psi^{(o)}}{\partial z} \frac{\partial^3 \psi^{(o)}}{\partial x^3} - \frac{\partial \psi^{(o)}}{\partial x} \frac{\partial^3 \psi^{(o)}}{\partial x^2 \partial z}\right)\right] \quad .
\end{aligned} \tag{136}$$

The right-hand side of equation (136) is separately denoted as I, II, III, IV, and V for each successive part for convenience. It is easy to check from so-

lutions obtained above that I is $O(\varepsilon^{1/2})$, II is $O(\varepsilon^{1/2})$, III is $O(\varepsilon^{1/2})$, IV is $O(\varepsilon)$, and V is $O(\varepsilon^{1/2})$ in regions 1 and 2. In regions 3 and 4, note that the contributions normal to the slant boundary of each individual term in the different parts, except part III, cancel each other and what is left is a portion, $O(\varepsilon^{1/2})$ lower than the normally differentiated portion. It is also noticed that the portion of order of unity of the zeroth R-order boundary meridional velocity, ${}_1v^{(o)}$, is a function of η alone. Thus every part on the right-hand side of the equation (136) is estimated to be $O(\varepsilon^{1/2})$. Hence, to the $O(\varepsilon^{3/2})$ on the boundaries, equation (136) leads to the same boundary layer thickness and same governing equations as before.

Following closely the procedures in the zeroth R-order solutions, after having matched the boundary solutions to the interior solutions and satisfied all boundary conditions, the first R-order solutions for the velocity field are:

in the interior region,

$$
\begin{aligned}
{}_ov^{(1)} = {} & \frac{2\pi A}{3}\Big\{\frac{C_1}{a^2} + \frac{2C_4}{a^3} + \frac{18C_3 + 56C_2 + 17C_5}{12Ha} - C_1z^2 - \Big[\frac{2C_3(1-G) - C_1(G-1) + C_4H}{Ha^2} \\
& + \frac{(C_2 + C_5)G_2 - C_2 + C_5G}{HH_2a}\Big] \sinh az + \frac{(C_2 + C_5)G_2 - C_2 - C_5G}{6H_2Ha} \sinh 3az \\
& - \Big(\frac{C_1}{a^2} + \frac{2C_4}{a^3} + \frac{4C_3 + 9C_2 + 3C_5}{2Ha}\Big) \cosh az + \frac{2C_3 + C_5}{4Ha} \cosh 2az \\
& - \frac{(C_2 + C_5)}{6Ha} \cosh 3az + \Big(\frac{4C_4}{a^2} + \frac{2C_1}{a}\Big) z \sinh az + \frac{2C_3(1-G) - C_1(G-1) + C_4H}{Ha} \\
& \cdot z \cosh az + \frac{C_4}{a} z^2 \cosh az\Big\} \sin 2\pi x - \frac{\pi A}{3}\Big\{\frac{3C_5 - C_2}{a^2} - \frac{C_4}{4Ha^2} \\
& + \frac{24C_1 - 5C_8}{8Ha} + \frac{2C_1(G-1) - 2C_4H}{H^2} z + \Big(\frac{C_4}{H} + \frac{C_4}{4} + 4C_2\Big)z^2 \\
& - \Big[\frac{C_2 + C_5G - (C_2 + C_5)G_2}{H_2a^2} - \frac{C_4}{4Ha^2} + \frac{C_1(G-1) - C_4H}{H^2a.} - \frac{C_8(G_3 - G)}{4HH_3a}\Big] \sinh 2az
\end{aligned}
$$

$$- \frac{C_6(G_3 - G)}{8HH_3a} \sinh 4az - \left(\frac{4C_1}{Ha} + \frac{4C_5}{a^2}\right) \cosh az + \left(\frac{C_4}{4Ha} + \frac{C_2 + C_5}{a^2}\right.$$

$$\left. + \frac{2C_1 + C_6}{2Ha}\right) \cosh 2az + \frac{C_6}{8Ha} \cosh 4az + \frac{4C_5}{a} z \sinh az - \left(\frac{C_4}{2Ha}\right.$$

$$\left. + \frac{2(C_2 + C_5)}{a}\right) z \sinh 2az + \left[\frac{2C_2(G_2 - 1) + 2C_5(G_2 - G)}{H_2a} - \frac{C_4}{2Ha}\right] z \cosh 2az\}$$

$$\cdot \sin 4\pi x - \frac{2\pi A}{3H}\left(\frac{8HC_6}{3a^2} + \frac{16C_2 + 7C_5}{4a} + \frac{3(C_2 + C_5)G_2 - 3C_2 - 3C_5G}{2H_2a} \sinh az\right.$$

$$- \left[\frac{(C_2 + C_5)G_2 - C_2 - C_5G}{2H_2a} + \frac{HC_6(G_3 - G)}{3H_3a^2}\right] \sinh 3az - \left(\frac{3HC_6}{a^2} + \frac{9C_2 + 3C_5}{2a}\right)$$

$$\cdot \cosh az - \frac{3C_5}{4a} \cosh 2az + \left(\frac{C_2 + C_5}{2a} + \frac{HC_6}{3a^2}\right) \cosh 3az + \frac{3HC_6}{a} z \sinh az$$

$$- \frac{HC_6}{a} z \sinh 3az + \frac{HC_6(G_3 - G)}{H_3a} z \cosh 3az\} \sin 6\pi x - \frac{\pi A}{2H}\left[\frac{C_6(G - G_3)}{6H_3a} \sinh 2az\right.$$

$$\left. + \frac{C_6(G_3 - G)}{12H_3a} \sinh 4az + \frac{C_6}{3a} \cosh 2az - \frac{C_6}{12a} \cosh 4az - \frac{C_6}{4a}\right] \sin 8\pi x$$

$$- \varepsilon_1^{1/2} \sqrt{2}\, b_1(x) \quad , \tag{137}$$

where

$$b_1(x) = \frac{16\pi^3A^2}{81}\left[\left(\frac{2G}{Ha} - \frac{2}{a^2} - \frac{H_2}{4H^2a} + \frac{1}{2H^2}\right) \sin 2\pi x + \left(\frac{G}{Ha} - \frac{1}{a^2}\right) \sin 4\pi x - \left(\frac{2G}{Ha} - \frac{2}{a^2}\right.\right.$$

$$\left.\left. + \frac{G - 1}{2H^2a} - \frac{1}{2H^2}\right) \sin 6\pi x + \left(\frac{H_2}{2H^2a} - 1\right) \sin 8\pi x\right] \quad ; \tag{138}$$

and

$$\overset{(1)}{\psi}_o = \varepsilon_1 \frac{16\pi^3A^2}{81}\left[\left[\frac{2}{H}\left(\frac{G - z \cosh az}{a} + \frac{\sinh az - H}{a^2}\right) + \frac{\sinh 2az - H_2}{4H^2a} + \frac{1 - z}{2H^2}\right]\right.$$

$$\cdot \sin 2\pi x - \left(\frac{z \cosh az - G}{Ha} - \frac{\sinh az - H}{Ha^2}\right) \sin 4\pi x + \left[\frac{2}{H}\left(\frac{z \cosh az - G}{a}\right.\right.$$

$$\left.\left. - \frac{\sinh az - H}{a^2}\right) + \frac{\cosh az - G}{2H^2a} - \frac{z - 1}{2H^2}\right] \sin 6\pi x - \left(\frac{\sinh 2az - H_2}{2H^2a} - z + 1\right)$$

$$\left.\cdot \sin 8x\right) \quad ; \tag{139}$$

in region 1,

$$ {}_1v^{(1)} = 0 \quad , \tag{140} $$

$$ {}_1\psi^{(1)} = 0 \quad ; \tag{141} $$

in region 2,

$$ {}_2v^{(1)} = \sqrt{2}\ \varepsilon_1^{1/2}\ b_1(x)\ e^{-\zeta_2/\sqrt{2}}\ (\cos\frac{\zeta_2}{\sqrt{2}} + \sin\frac{\zeta_2}{\sqrt{2}}) \quad , \tag{142} $$

$$ {}_2\psi^{(1)} = -\varepsilon_1 b_1(x)\ e^{-\zeta_2/\sqrt{2}}\ \cos\frac{\zeta_2}{\sqrt{2}} \quad ; $$

in region 3,

$$ {}_3v^{(1)} = \varepsilon_2^{1/2}\ \frac{\sqrt{2}\ \lambda}{(1+\lambda^2\gamma)}\ b_3(\eta_1)(e^{\xi_1/\sqrt{2}}\ \cos\frac{\xi_1}{\sqrt{2}} - 1) + d_3(\eta_1) \quad , \tag{144} $$

$$ {}_3\psi^{(1)} = \varepsilon_1 b_3(\eta_1)\ e^{\xi_1/\sqrt{2}}\ (\cos\frac{\xi_1}{\sqrt{2}} - \sin\frac{\xi_1}{\sqrt{2}}) \quad ; \tag{145} $$

where

$$ b_3(\eta) = \frac{-16\pi^3A^2}{81}\{[\frac{2}{H}(\frac{\sinh a\eta - H}{a^2} - \frac{\eta\cosh a\eta - G}{a}) + \frac{\sinh 2a\eta - H_2}{4H^2a} + \frac{1-\eta}{2H^2}] $$

$$ \cdot \sin 2\pi\lambda\gamma(1-\eta) + (\frac{\sinh a\eta - H}{Ha^2} - \frac{\eta\cosh a\eta - G}{Ha})\sin 4\pi\lambda\gamma(1-\eta) $$

$$ + [\frac{2}{H}(\frac{\sinh a\eta - H}{a^2} - \frac{\eta\cosh a\eta - G}{a}) + \frac{G - \cosh a\eta}{2H^2a} + \frac{\eta - 1}{2H^2}]\sin 6\pi\lambda\gamma(1-\eta) $$

$$ + (\frac{\sinh 2a\eta - H_2}{2H^2a} - \eta + 1)\sin 8\pi\lambda\gamma(1-\eta) \quad , \tag{146} $$

$$ d_3(\eta) = \frac{2\pi A}{3}\{C_1\eta^2 + [\frac{2C_3(1-G) - C_1(G-1) + C_4H}{Ha^2} + \frac{(C_2+C_5)G_2 - C_2 - C_5G}{HH_2a}] $$

$$ \cdot \sinh a\eta - \frac{(C_2+C_5)G_2 - C_2 - C_5G}{6HH_2a}\sinh 3a\eta + (\frac{C_1}{a^2} + \frac{4C_3 + 9C_2 + 3C_5}{2Ha} + \frac{2C_4}{a^3}) $$

$$\cdot (\cosh a\eta - 1) - \frac{2C_3 + C_5}{4Ha}(\cosh 2a\eta - 1) - \frac{C_2 + C_5}{6Ha}(\cosh 3a\eta - 1) - (\frac{2C_4}{a^2}$$

$$+ \frac{2C_1}{a})\eta \sinh a\eta - \frac{2C_3(1 - G) - C_1(G - 1) + C_4H}{Ha} \eta \cosh a\eta + \frac{C_4}{a} \eta^2 \cosh a\eta\}$$

$$\cdot \sin 2\pi\lambda\gamma(1 - \eta) - \frac{\pi A}{3}\{\frac{2C_1(G - 1) - 2C_4H}{H^2} \eta + (\frac{C_4}{H} + \frac{C_4}{4} + 4C_2)\eta^2$$

$$- [\frac{G_2(C_2 + C_5) - C_2 - C_5G}{H_2a^2} - \frac{C_4}{4Ha^2} + \frac{C_1(G - 1) - C_4H}{H^2a} + \frac{C_6(G_3 - G)}{4HH_3a}] \sinh 2a\eta$$

$$- \frac{C_6(G_3 - G)}{8HH_3a} \sinh 4a\eta - (\frac{4C_1}{Ha} + \frac{4C_5}{a^2})(\cosh a\eta - 1) + (\frac{C_4}{4Ha^2} + \frac{C_2 + C_5}{a^2} + \frac{2C_1 + C_6}{2Ha})$$

$$\cdot (\cosh 2a\eta - 1) + \frac{C_6}{8Ha}(\cosh 4a\eta - 1) + \frac{4C_5}{a} \eta \sinh a\eta - [\frac{C_4}{2Ha} + \frac{2(C_2 + C_5)}{a}]\eta$$

$$\cdot \sinh 2a\eta + [\frac{2C_2(G_2 - 1) + 2C_5(G_2 - G)}{H_2a} - \frac{C_4}{2Ha}] \eta \cosh 2a\eta\} \sin 4\pi\lambda\gamma(1 - \eta)$$

$$- \frac{2\pi A}{3H}\{\frac{3C_2 + 3C_5G - 3(C_2 + C_5)G_2}{2H_2a} \sinh a\eta + [\frac{(C_2 + C_5)G_2 - C_2 - C_5G}{2H_2a}$$

$$+ \frac{HC_6(G_3 - G)}{3H_3a^2}] \sinh 3a\eta + (\frac{3HC_6}{a^2} + \frac{9C_2 + 3C_5}{2a})(\cosh a\eta - 1) + \frac{3C_5}{4a}(\cosh 2a\eta - 1)$$

$$- (\frac{C_2 + C_5}{2a} + \frac{HC_6}{3a^2})(\cosh 3a\eta - 1) - \frac{3HC_6}{a} \sinh a\eta + \frac{HC_6}{a} \sinh 3a\eta$$

$$- \frac{HC_6(G_3 - G)}{H_3a} \eta \cosh 3a\eta\} \sin 6\pi\lambda\gamma(1 - \eta) - \frac{\pi A}{2H}\{\frac{C_6(G - G_3)}{6H_3a} \sinh 2a\eta$$

$$+ \frac{C_6(G_3 - G)}{12H_3a} \sinh 4a\eta + \frac{C_6}{3a}(\cosh 2a\eta - 1) - \frac{C_6}{12a}(\cosh 4a\eta - 1)\}$$

$$\cdot \sin 8\pi\lambda\gamma(1 - \eta) + \varepsilon_1^{1/2} \frac{16\sqrt{2}\pi^3A^2}{81}\{(\frac{2G}{Ha} - \frac{2}{a^2} - \frac{H_2}{4H^2a} + \frac{1}{2H^2}) \sin 2\pi\lambda\gamma(1 - \eta)$$

$$- (\frac{G}{Ha} - \frac{1}{a^2}) \sin 4\pi\lambda\gamma(1 - \eta) - (\frac{2G}{Ha} - \frac{2}{a^2} + \frac{G - 1}{2H^2a} - \frac{1}{2H^2}) \sin 6\pi\lambda\gamma(1 - \eta)$$

$$- (\frac{H_2}{2H^2a} - 1) \sin 8\pi\lambda\gamma(1 - \eta)] \quad ; \qquad (147)$$

and in region 4,

$$ {}_4v^{(1)} = \varepsilon_2^{1/2} \frac{2\lambda}{(1+\lambda^2\gamma)} b_3(\eta_2)\left(1 - e^{-\xi_2/\sqrt{2}} \cos\frac{\xi_2}{\sqrt{2}} - d_3(\eta_2)\right) \qquad (148) $$

$$ {}_4\psi^{(1)} = -\varepsilon_1 b_3(\eta_2)\, e^{-\xi_2/\sqrt{2}} \left(\cos\frac{\xi_2}{\sqrt{2}} + \sin\frac{\xi_2}{\sqrt{2}}\right) \qquad (149) $$

all $b_3(\eta_{1,2})$, $d_3(\eta_{1,2})$ are direct substitutions of $\eta_{1,2}$ for η in equations (145) and (143).

The magnitudes of approximation errors for the higher order terms neglected in the power series expansion in terms of R can be estimated from the second R-order equations (103), (104), and (105). They are $O(\sigma^2R^2)$ for the temperature and $O(R^2)$ for the velocity field.

V. EDDY VISCOSITY AND EDDY DIFFUSIVITY IN LAKE MICHIGAN

Introduction to the Characteristics of Eddy Viscosity and Eddy Diffusivity

Theoretically, a flow field of incompressible Newtonian fluid can be found by solving the equation of conservation of mass and the Navier-Stokes equations of motion, and satisfying its respective boundary and/or initial conditions. In the event that a transformation of energy is important, the energy equation must also be used. When the flow is viscous and laminar, there appears in the equations of motion a term related to shear stress which, according to Stokes' law of viscosity, is

$$\tau_1 = \mu \frac{du}{dz}$$

where the subscript 1 denotes "laminar," z is normal to the direction of the flow velocity u, and μ is the molecular viscosity which is a property of the fluid depending only on temperature under ordinary conditions. In compressible laminar flow, when temperature variations are involved, the heat flux following Fourier's law of thermal conduction is

$$Q_1 = -k \frac{dT}{dz}$$

where k is the molecular thermal conductivity which is also a property of the fluid and usually depends only on temperature.

On the other hand, if the flow is turbulent a kind of motion with random irregular fluctuations is superimposed on the main flow. Since its fluctua-

tions are irregular, it is impossible to describe the motion in all details as a function of time and space. However, one can study its average behavior using the statistical methods which have been pointed out by Hinze (1959): "Turbulent fluid motion is an irregular condition of flow in which the various quantities show a random variation with time and space coordinates, so that statistically distinct average values can be discerned." Therefore, in describing a turbulent flow in mathematical terms, it is convenient to separate it into a mean motion and a fluctuation, such as

$$\begin{aligned} \vec{q} &= \bar{\vec{q}} + \vec{q}' \ , \\ T &= \bar{T} + T' \end{aligned} \tag{150}$$

where the "bar" indicates mean quantities and the "prime" indicates the fluctuation from the mean.

The presence of random irregular fluctuations often manifest themselves as an apparent increase of viscosity and diffusivity (Defant, 1961). In turbulent flow, therefore, additional Reynolds stresses must be considered in the general governing equations of the motion.

Analogous to the coefficient of molecular viscosity, Boussinesq (1877) introduced a mixing coefficient, A_t, for the Reynolds stress in turbulence to express it in terms of the mean velocity gradients in the flow field

$$\tau_t = -\rho \, \overline{u' \, w'} = A_t \frac{d\bar{u}}{dz}$$

where the subscript t denotes turbulent flow. In a similar definition to that for molecular diffusivity, Schlichting (1968) postulated that the turbulent heat flux is

$$Q_t = -C_p A_q \frac{dT}{dz} \quad .$$

The exchange coefficients of turbulent momentum and turbulent heat flux, A_t and A_q, both have the dimension of a viscosity, μ, (g/cm/sec.).

If the turbulence is isotropic (i.e., the relation between stresses and strains is independent of choice of axis) then A_t corresponds to the molecular viscosity μ, A_q corresponds to the molecular heat diffusivity $\frac{k}{Cp}$; and $\nu_t = \frac{A_t}{\rho}$, the eddy kinematic viscosity, corresponds to the molecular kinematic viscosity $\nu_l = \frac{\mu}{\rho}$. Then the turbulent shear stress is

$$\tau_t = \rho \nu_t \frac{d\bar{u}}{dz} \quad .$$

The eddy kinematic viscosity, ν_t, can be expected to occur as a constant only if the turbulence field is homogeneous. Generally speaking, since the eddy viscosity is 10^2 to 10^9 greater in magnitude than molecular viscosity, the latter may be neglected in many cases. As pointed out by Lamb (1932) in illustrating the wind producing current, in reality μ is replaced by A_t.

Using the analogies mentioned above, it is possible to attack geophysical fluid problems which are turbulent in nature. In this way we can probably predict or evaluate the time-mean value of the entities of these complicated turbulences whose complete theoretical formulations have so far proved impossible (Lamb, 1932).

Nevertheless, not all the turbulence is homogeneous and isotropic. The eddy viscosity usually does have directional preference. Eddy viscosity becomes effective only if there is some flow in the fluid and its value depends on the velocity distributions and on the characteristic length of the flow

field as shown in Boussinesq's hypothesis and von Kármán's similarity theory that

$$A_t = \rho\, \ell^2 \left|\frac{d\bar{u}}{dz}\right| , \quad \text{or} \quad \nu_t = \ell^2 \left|\frac{d\bar{u}}{dz}\right|$$

where ℓ is the Prandtl's mixing length. Therefore, A_t or ν_t is not a property of the fluid itself, whereas the molecular viscosity, μ, is. However, it is still extremely useful to introduce the eddy viscosity in relating the Reynolds stress to the mean velocity gradients of the flow. As A_t or ν_t is not a physical constant, but varies from one part of the flow to another, estimating the magnitude of the average eddy viscosity is the key factor to the success of geophysical fluid modeling. In Lake Michigan, though the mean velocity is in general less than 1/2 m/s (Ayers, et al., 1958), the flows are turbulent in nature. Therefore, it is important to estimate the order of magnitude of the eddy viscosity and eddy diffusivity.

Theoretical Background of the Formulae

In order to evaluate the magnitude of the eddy viscosity and eddy diffusivity, different approaches have been used for the easier management of appropriate field data.

REYNOLDS STRESS AND VELOCITY GRADIENT

Analogous to the kinematic molecular viscosity formally introduced by Boussinesq (1877), Reynolds stresses are written, in the conventional Cartesian tensor notations,

$$\tau_{ij} = -\rho \overline{u_i u_j} = \rho \nu_t \left(\frac{\partial \bar{u}_j}{\partial x_i} + \frac{\partial \bar{u}_i}{\partial x_j}\right) \quad . \tag{151}$$

For example, if the mean flow is unidirectional, then the Reynolds stress is

$$\tau_{zx} = -\rho \overline{u' w'} = \rho \nu_z \frac{\partial \bar{u}}{\partial z}$$

where τ_{zx} is the stress on a surface perpendicular to Z-axis in the direction of X-axis. The Reynolds stress component $\tau_{zx} = -\rho \overline{u'w'}$ represents the mean rate of turbulent transport of u' - momentum by the w' component of the flow, where u', v', w', are the turbulent fluctuations of velocity components upon the mean flow as mentioned in equation (150). At the ocean or lake surface, the very top layer may be considered as Edman's "sensitive wind-driven layer." Theoretically, the stress on the air-water interface should be approximately the same whether the measurement is made from air or from water. If the magnitude of surface shear stress is known and if the vertical velocity gradient can be measured near the interface, then the vertical eddy viscosity can be evaluated by using equation (151).

A characteristic velocity of the turbulent fluctuating motion called the friction velocity is defined as

$$U_* = \left(\frac{\tau_t}{\rho}\right)^{1/2} \tag{152}$$

which is a measure of the intensity of turbulence, where ρ is the density of the fluid. It can be written in terms of drag coefficient and the wind speed at 10 m height,

$$C_{10} = \left(\frac{U_*}{U_{10}}\right)^2 \tag{153}$$

where C_{10} is the drag coefficient with reference to the 10 m height wind, U_{10}. The values of C_{10} as a function of the wind speed in m/s at 10 m level have been given in many empirical equations, such as (Pierson, 1964):

$$C_{10} = 0.009\ U_{10}^{-1/2} \quad \text{(By Neumann)},$$

$$C_{10} = (1.00 + 0.007\ U_{10})\ 10^{-3} \quad \text{(by Deason and Webb)},$$

$$C_{10} = (0.80 + 0.114\ U_{10})\ 10^{-3} \quad \text{(by Sheppard)}.$$

In the case of a wind-driven lake current a friction velocity may be found, according to Deacon (1962), as

$$U_* = (0.0012 \frac{\rho_a}{\rho_w})^{1/2}\ U_{10}\ , \tag{154}$$

where ρ_a and ρ_w are densities of air and water, respectively.

Elder and Soo (1967) have analyzed wind profile data from The University of Michigan research tower one mile from shore in Lake Michigan and came up with a best fit exponential relation of friction velocity and U_{10} under neutral conditions as shown,

$$U_* = 0.066\ \exp\ (0.163\ U_{10})\ . \tag{155}$$

Following the evaluation of friction velocity, if the vertical velocity gradient is measured or estimated, the vertical magnitude of eddy viscosity can be calculated.

MIXING LENGTH AND LOGARITHMIC VELOCITY DISTRIBUTION

By analogy to the mean free path in the kinetic theory of gases, Prandtl introduced the "mixing length" of the fluid and von Kármán related it to the property of the mean motion. Near a solid boundary such as the lake bottom,

the theory of Prandtl and von Kármán leads to the logarithmic law of velocity distribution,

$$\bar{U} = \frac{U*}{k_o} \ln \frac{z + z_o}{z_o} \tag{156}$$

where $U*$ is the friction velocity near a solid boundary, and z_o is the "roughness length," k_o is the von Kármán constant. The logarithmic law has been used widely in all branches of fluid mechanics, especially in meteorology. In the region of neutral stability, the vertical eddy viscosity is shown (Bowden, 1964) as,

$$A_z = k_o U* (z + z_o) \approx k_o U* z \quad , \tag{157}$$

since z_o is usually small.

Bowles et al., (1958) and Charnock (1959) used this method to investigate the velocity profile in the English Channel and Irish Sea and confirmed the approximate form of the logarithmic velocity distribution up to 2 m from the bottom. The value of z_o was from 1 to 3 mm. Lesser (1951) measured the current at a different level near the bottom in homogenous water and found the logarithmic law was valid and the roughness length for gravel-sand bottom to be 1.3 mm, and for mud-sand, 1.6 mm.

Assuming the logarithmic mean velocity profile is valid in Lake Michigan near the bottom, then the friction velocity can be deduced from a point current measurement near the bottom and the vertical eddy viscosity can be calculated.

EMPIRICAL FORMULA FOR ESTIMATING VERTICAL EDDY VISCOSITY FROM WIND

The vertical eddy viscosity can at least be approximated by the surface wind in a homogenous sea by (Sverdrup et al., 1942),

$$A_z = 1.02\ W^3 \quad \text{for } W < 6 \text{ m/s} \quad \text{(Thorade)} \tag{158}$$

$$A_z = 4.3\ W^2 \quad \text{for } W > 6 \text{ m/s} \quad \text{(Ekman)} \tag{159}$$

where W is measured in m/s.

EDDY DIFFUSIVITY BASED ON STATISTICAL THEORY OF TURBULENCE

In a real geophysical fluid, though pure isotropic turbulence rarely exists, the local isotropy as introduced by the similarity theory of Kolmogoroff (1941) has been proved valid. The hypothesis assumes that there exists a continuous spectrum of fluctuations in the turbulence. The small-scale components of the turbulence are approximately in statistical equilibrium. They owe their existence to the nonlinear interchange of energy between different wave-number components. Apart from the effects of the variation of the viscosity and another parameter which is determined by the large-scale components of the turbulence, this equilibrium is universal. The continuous spectrum of fluctuations is considered as different scales of eddies. The intermediate scale eddies receive energy from large eddies (which are supposed to receive their energy from mean flow) and the intermediate eddies pass the energy to the small eddies, which finally dissipate it. Obviously, large eddies are anisotropic and small eddies are isotropic. Intermediate eddies can be thought of as quasi-isotropic.

In recent years, investigations of turbulent diffusion using "marked" particles have become very prevalent. By introducing into the turbulent water such "marked" particles as Rhodamine B solution or other similar markers which do not affect the dynamics of the fluid and which have almost the same density as the fluid, the behavior of the marked particles will show only the turbulent characteristics of diffusion of the fluid. In this way the effect of molecular diffusion, which might be important as suggested by Batchelor and Townsend (1956), is separated out from the turbulent diffusion due to their extreme difference in scales. In turbulent diffusion analyses both Eulerian and Lagrangian descriptions are used. If the scale of turbulence is small as compared to the size of the configuration of the patch of marked-particles, an Eulerian type of analysis is used. If the turbulent scale is much larger than the dimension of the patch, a Lagrangian type of analysis is preferred. For continuous source experiments the diffusion measurements are made relative to fixed positions, and the Eulerian analysis is appropriate.

In a homogenous flow field, the turbulent dispersal of marked particles is the phenomenon of relative diffusion. For simplest illustration, let $\vec{X}_j(t)$ and $\vec{q}_j(t)$ be the position vector and the velocity vector of the j-particle in the marked particles patch at time t after release. Then let

$$\vec{D}_j(t) = \vec{X}_j(t) - \vec{X}_c(t) \tag{160}$$

$$\vec{\phi}_j(t) = \vec{q}_j(t) - \vec{q}_c(t)$$

where $\vec{D}_j(t)$ and $\vec{\phi}_j(t)$ are the relative displacement and velocity of the j^{th} particle with respect to the center of the mass of the patch, $\vec{X}_c(t)$, at time t.

If all particles are identical as assumed, then the mean relative distance is zero at the center of the patch. According to the central limit theorem the distribution of marked particles will be Gaussian after a long period of time. Then the average value of $\vec{D}_j(t)$ is the standard deviation of the patch at time t, and $\vec{q}_c(t)$ is the mean velocity.

Considering a stationary process, the auto-correlation function at two points can be converted to a correlation function of the time difference between the velocities, as

$$f(\tau) = \frac{\overline{\vec{\phi}(t_1)\ \vec{\phi}(t_2)}}{\phi^2(t)} \tag{161}$$

where $\overline{(\quad)}$ indicates ensemble average and $\tau = t_1 - t_2$.

If, at $t = 0$, the particle is at the original position, then after sufficiently large diffusion time has elapsed, due to continuous independent movement of the marked particle, the mean variance is

$$\overline{D^2(t)} = 2\ \overline{\phi^2} \int_0^t \int_0^{t'} f(\tau)\ d\ t'\ d\ \tau. \tag{162}$$

For small t, $f(\tau) \approx 1$. Therefore,

$$\overline{D^2(t)} = \overline{\phi^2}\ t^2 + \overline{D^2(0)} \tag{163}$$

where $\overline{\vec{D}(0)}$ is the initial separation. For large t, $f(\tau) \to 0$ and

$$\Lambda = \int_0^\infty f(\tau)\ d\ \tau, \tag{164}$$

will approach a limiting value which is considered as the scale of turbulence. Hence for large t,

$$\overline{D^2(t)} = 2\,\overline{\phi^2}\,\Lambda\,t \quad . \tag{165}$$

Bachelor (1953) has proposed a development based on a similarity hypothesis of turbulence for discussing the relative diffusion. Its application is limited by the dependence of the relative diffusion on the turbulence only through the parameters as viscosity, ν, energy dissipation, E, diffusion interval time, t, and the initial separation, $\vec{D}(0)$. Dimensional arguments, then show that (Okubo, 1962)

$$\overline{\frac{d\,D^2(t)}{dt}} = p_1(E\,D(0))^{2/3}\,t \quad , \quad \text{for small } t, \tag{166}$$

$$\overline{\frac{d\,D^2(t)}{dt}} = p_2\,E\,t^2 \quad , \quad \text{for intermediate } t \tag{167}$$

and

$$\overline{\frac{d\,D^2(t)}{dt}} = p_3\,\overline{\phi^2}\,\Lambda \quad \text{asymptotically}, \tag{168}$$

where p_1, p_2, p_3 are constants.

By analogy to the development of the molecular diffusion when the scale of dispersion becomes large as compared with the largest eddy present, the equivalent eddy diffusivity may be shown as

$$K_e = \frac{1}{2}\,\overline{\frac{d\,D^2(t)}{dt}} \quad \text{as } t \to \infty \quad , \tag{169}$$

or

$$K_e = \frac{1}{2}\,\frac{\overline{D^2(t)}}{t} \quad . \tag{170}$$

RICHARDSON'S NEIGHBOR SEPARATION

Richardson (1926) and Richardson and Stommel (1948) have considered "neighbor separation." Instead of the diffusivity K, they use $F(\ell)$, the "diffusivity for neighbors." The ordinary Fick's diffusion equation is replaced by

$$\frac{\partial q}{\partial t} = \frac{\partial}{\partial \ell} \left[F(\ell) \frac{\partial q}{\partial \ell} \right] ,$$

where $q(\ell)$ is the neighbor concentration function, which is the number of neighbors per unit projected length ℓ. From observed atmospheric data, Richardson deduced the well known 4/3 power law of relative diffusion,

$$F(\ell) = C \ \ell^{4/3} , \tag{171}$$

where C is a constant.

In the ocean as well as in the Great Lakes, a thermocline usually exists and migrates up and down seasonally. The induced vertical gradient in density, mostly in stable situations, causes a reduction of vertical turbulent velocity by converting a portion of kinetic energy to increase the potential energy. Thus, in a stable vertical density gradient, the intensity of turbulence is reduced, hence the eddy viscosity, A_z, and eddy diffusivity, K_z, are also reduced. The latter will decrease more than the former (Hill, 1962). In the sea as well as in the Great Lakes, the horizontal components of turbulence are usually much greater than the vertical component, not only because of the vast difference in dimensions but because of the effects of the vertical density gradients. Hence the horizontal eddy viscosity and the eddy diffusivity are expected to be much greater, though the horizontal and vertical mixing transport of the fluid property may be still of the same order due to much larger

vertical gradient of the fluid property (Defant, 1961). Csanady (1963) has shown that the vertical eddy diffusivity of the Great Lakes is only one or two orders of magnitude greater than molecular viscosity (about 0.1 - 0.5 cm^2/sec) while horizontal diffusivity is 10^4 to 10^5 times greater. Moreover, the longitudinal horizontal diffusivity is 4 to 5 times greater than the lateral diffusivity. Bowden (1965) has shown K_x (longitudinal diffusivity) is about 10 times greater than K_y (lateral diffusivity), and the mixing produced by a shearing current becomes important if a moderate degree of stability is present. In the Great Lakes, a shearing current has been observed to increase the effective horizontal diffusivity by a factor of 5 or so (Csanady, 1966). Foxworthy and Barsom (1967) have come to the same conclusion as Csanady that increasing stability results in a lower vertical diffusivity, K_z, causing a more complex current pattern. This in turn increases the horizontal viscosity, K_y, and the net result is that the product of $K_z K_y$ is nearly constant.

The Magnitudes

Eddy viscosity and eddy diffusivity are essential parameters for the theoretical thermal current model study of Lake Michigan. Therefore, a series of experiments were carried out to evaluate the representative order-of-magnitude values for the eddy viscosity and eddy diffusivity to be used in the modeling investigation.

AN ESTIMATE OF EDDY VISCOSITY BY REYNOLDS STRESS AND VERTICAL VELOCITY GRADIENTS

In August 1967 a pair of current meter buoy stations were set 8 miles off-

shore from Sheboygan, Wisconsin. During the period of the current measurement, the research vessel R/V INLAND SEAS was operating around the stations (during the daytime) whenever weather permitted. Winds, as well as other weather data, were automatically recorded on a digital meteorological tape recorder. The anemometer and vane that fed into the recorder were on the mast of the INLAND SEAS 14 m above the water surface. The Captain's log and hourly meteorological observations recorded wind from a lower vane and anemometer at about 11 m above the surface. Using the analyzed recorded mean wind versus height, plotted on a log scale with the mean velocity zero at about 1 cm height, (Floyd C. Elder, personal communication) the 10-m level wind was interpolated with reference to the Captain's log. The 10-m daily winds are shown in Table 4. The vertical velocity gradients in the direction of the surface current were deduced from two current meters separated vertically by 10 m. According to equation (154), the Reynolds stress is

$$\tau_t = \rho_w U_*^2 = 0.012 \rho_a U_{10}^2 .$$

Then using $\rho_w = 1$ g/cm^3 and $\rho_a = 1.23 \times 10^{-3}$ g/cm^3 the eddy viscosity can be calculated. The data, wind, wave conditions, absolute vertical velocity gradient, shear stress, and calculated eddy viscosity are shown in Table 4. The values of Reynolds stresses obtained here by using Deacon's formula are in good agreement with the mean value of stress obtained by Elder and Soo (1967) at The University of Michigan Research Tower on the east side of the lake.

TABLE 4

Eddy Viscosity on Two Current-Meter Buoy Stations
(17-24 August 1967 at 8 miles off Sheboygan)

Date	Wind		Condition of lake	u_{10} (m/s)	τ^* (dyne/cm^2)	$\left\|\frac{du}{dz}\right\|$ (sec^{-1})	Eddy viscosity Az (cm^2/sec)
	Direction	Speed (kt)					
17 Aug	SW	19	$\frac{1}{2}$'-1' waves	9.3	1.21	1.96×10^{-3}	620
18 Aug	NNE	22	3'-5' waves	9.8	1.42	1.52×10^{-2}	93
20 Aug	WSW	12	1'-3' waves	5.7	0.47	1.16×10^{-2}	41
21 Aug	S	7	calm	3.4	0.17	5.8×10^{-3}	29
23 Aug	ESE	13	3'-5' waves	6.2	0.56	4.8×10^{-2}	12
24 Aug	SE	9	1'-2' waves	4.6	0.32	7.1×10^{-3}	45
						average value	1.4×10^2 cm^2/sec

*Shear stress is estimated by Deacon's formula and $\rho_a = 1.23 \times 10^{-3}$ g/cc.

AN ESTIMATE OF THE UPPER LIMIT VALUE OF EDDY VISCOSITY AND EDDY DIFFUSIVITY BY STATISTICAL THEORY

It is quite well known (e.g., Ayers, et al., 1958) that a large clockwise eddy exists in southern Lake Michigan between Grand Haven and Michigan City. This large eddy has the length of scale of a little less than half the dimension of the width of the lake. Bowden (1964) has shown the effective eddy viscosity is proportional to the 4/3 power of the length scale L, of the particular eddy under consideration, similar to the Richardson's formula equation (171). In Lake Michigan, let this largest eddy have an average length scale of L = 40 km or L = 4 x 10^6 cm. Then, according to Richardson's formula, the eddy viscosity will be of the order 10^7 cm^2/sec which is the upper limit of the numerical values of the eddy viscosity and eddy diffusivity in Lake Michigan.

AN ESTIMATION OF VERTICAL EDDY VISCOSITY FROM CURRENT MEASUREMENT NEAR THE BOTTOM

From 11 May to 11 October 1967, a tripod-supported pendulum current meter was installed under the direction of Dr. Ayers, about 230 m off shore, 7-1/2 miles south of Benton Harbor at a depth of 5 m. The pendulum was suspended only 20.3 cm above the sandy bottom. The monthly mean current is shown in Table 5. Using Lesser's (1951) roughness length for sand bottom, z_o = .15 cm, the friction velocity near the bottom can be determined through equation (156),

$$U_* = k_o \bar{U} \ln \left(\frac{z_o}{z + z_o}\right)$$

where $\bar{U}$ is the mean velocity, z is the height from the bottom during measurement, and k_o = 0.41. The monthly mean friction velocity for z = 20.0 cm is shown in Table 5. The neutral stability condition generally persists near the bottom. Then the vertical eddy viscosity can be estimated by equation (157) as shown in Table 5.

TABLE 5

Estimated Vertical Eddy Viscosity from Current Measurement Near Bottom

Month	Mean current (cm/sec)	Friction velocity (cm/sec)	Vertical eddy viscosity ($Az = k_o u_* z$ cm^2/sec)
May	59.5	4.64	40.0
June	31.7	2.47	20.7
July	47.2	3.68	30.9
August	58.5	4.56	38.3
September	56.1	4.38	36.0
October	69.8	5.44	45.7
Average value			35 cm^2/sec

AN APPROXIMATION OF THE VERTICAL EDDY VISCOSITY BY SURFACE WIND

Wind data from both the two-current-meter-buoy operation off Sheboygan and the wind and current station outside of the Benton Harbor beach are used for approximating the vertical eddy viscosity in Lake Michigan. In the two-current-meter-buoy operation off Sheboygan, wind data were measured aboard the R/V INLAND SEAS. At the current meter station outside of the Benton Harbor beach, the wind was measured just above the water. From Sverdrup et al., (1942), depending on whether the magnitude of wind was greater or less than 6 m/s, the vertical eddy viscosity was approximated by equations (158), (159)

as shown in Table 6. Notice that the vertical eddy viscosity is smaller when the wind is averaged for a longer period of time.

TABLE 6

Estimated Vertical Eddy Viscosity from Wind Speed

Time	Wind (m/s)	Vertical eddy viscosity, A_z cm^2/sec	Remarks
17 Aug. 1967	9.3	381	Wind averaged over 6 hours
18 Aug. 1967	9.8	413	
20 Aug. 1967	5.7	140	
21 Aug. 1967	3.4	40	
23 Aug. 1967	6.2	165	
24 Aug. 1967	4.6	100	
	Average value	206 cm^2/sec	
May 1967	3.5	44	Monthly mean wind
June 1967	2.5	16	
July 1967	3.1	30	
Aug. 1967	3.2	33	
Sept. 1967	2.8	22	
Oct. 1967	4.1	70	
Nov. 1967	4.4	87	
	Average value	43 cm^2/sec	

MEASUREMENTS OF THE EDDY DIFFUSIVITY BY THE DISPERSION OF MARKED PARTICLES

In a series of experiments conducted in Lake Michigan, the fluorescent dye rhodamine B was used as a tracer for diffusivity measurements. Rhodamine B has a peak fluorescence wavelength of 580 mμ. In May 1968, a fluorometer with only one sample cell was used. At this season the phytoplankton was abundant, and since they have an ultraviolet fluorescence frequency just a little lower than that of rhodamine B, the fluorescence of the peak concentration of rhodamine B dye was not distinguishable from the background after

an hour or so. In all subsequent experiments, a comparative measuring fluorometer with two cells was used. The rhodamine B mixed with natural lake water flowed through the dye sample cell, while the standard cell contained natural lake water. The relative difference in fluorescence between two cells was measured to obtain reliable data in the possible presence of any intensity variation of the ultraviolet light lamp, systematic changes in the characteristics of photocell, and differences in the amount of naturally occurring fluorescent substances in the water (Noble and Ayers, 1961). Both instantaneous source and continuous source measurements were made in 1968.

Instantaneous Sources

Three runs of instantaneous sources of marked particles for diffusivity studies were conducted. These were 1 and 8 miles off Grand Haven in May, and 5 miles off Milwaukee in June. Rhodamine B dye was diluted with methanol to have a specific gravity very close to the lake water. Generally, one part of stock solution of rhodamine B in 40% acetic acid solution was mixed with 5-1/2 parts of methanol. The dye mixture was gently poured out on the surface lake water at the upwind side of the boat in order to allow the boat to drift away with least interference to the dye patch. The first and second runs were investigated aboard the R/V MYSIS and the third run aboard the R/V INLAND SEAS. During the first 20 min after the source had been instantaneously released, the diameters of the expanding dye patch were estimated by eye with the ship's length at reference. At 20-min intervals, the boat was used to coast through the dye patch longitudinally and laterally at the lowest possible speed. For

each transect, fixes were obtained from shore objects when entering and leaving the patch, along with the time required to traverse through the patch. Running back and forth across the dye patch, the concentration of the dye patch was continuously recorded from the fluorometer on an AZAR recorder. The concentration distribution of a typical pass through the patch is shown in Figure 9.

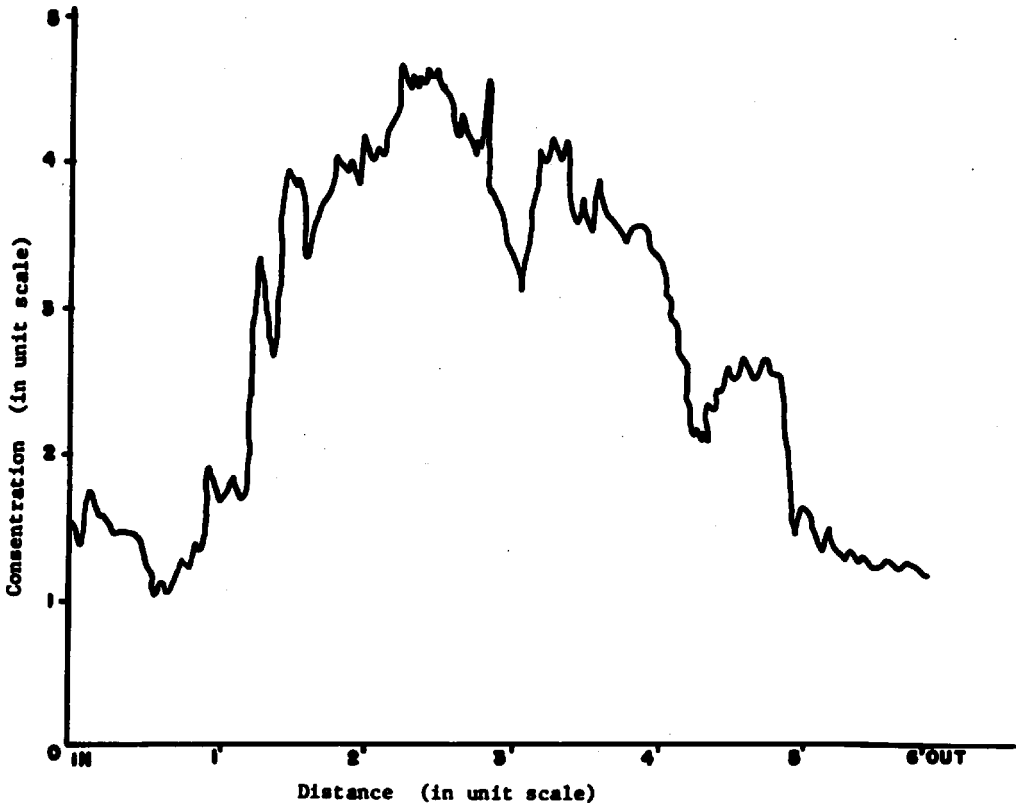


Figure 9. A typical distribution of dye concentration across a dye patch.

Most generally, the dye concentration distribution showed a form of Gaussian distribution. The diameter of the patch, longitudinally or laterally, is properly approximated as 4 times the standard deviation of the patch from its mean position. Batchelor (1953) shows that (assuming the velocity field is uniform, homogeneous, and steady) at the initial stage of a diffusion process, the effective diffusivity (which is proportional to the rate of change of the square

of standard deviation with time) is proportional to the first power of the elapsed time; in the intermediate phase, it grows as a 4/3 power of the patch size; and at the final stage, as the standard deviation grows as 1/2 power of the elapsed time, the diffusivity should symptotically approach a constant. The eddy diffusivities have been evaluated according to equations (169) or (170). The growth of dye patch versus time is shown in Figures 10 and 11. General information and values of diffusivities are shown in Table 7.

TABLE 7

General Information and Effective Eddy Diffusivity of Dye Patch Studies

	Run 1	Run 2	Run 3
Date	1 May 1968	2 May 1968	27 June 1968
Location	1 mile off shore near Grand Haven	8 miles off shore near Grand Haven	4 miles off shore near Milwaukee
Depth	20 ft	40 ft	65 ft
Duration of run	1130 - 1210 EST	1300 - 1450 EST	0910 - 1240 EST
Current velocity (cm/sec)	11.6	5.5	7.6
Wind			
Direction	NW	SW	SSW
Speed (kt)	13	15-20	5
Lake Condition	2-3 ft waves	1 ft wave	2 ft waves
Effective eddy diffusivity (cm^2/sec)			
Lateral	Not available	1140	743
Longitudinal	Not available	4731	4019
Remark	Very poor visibility		

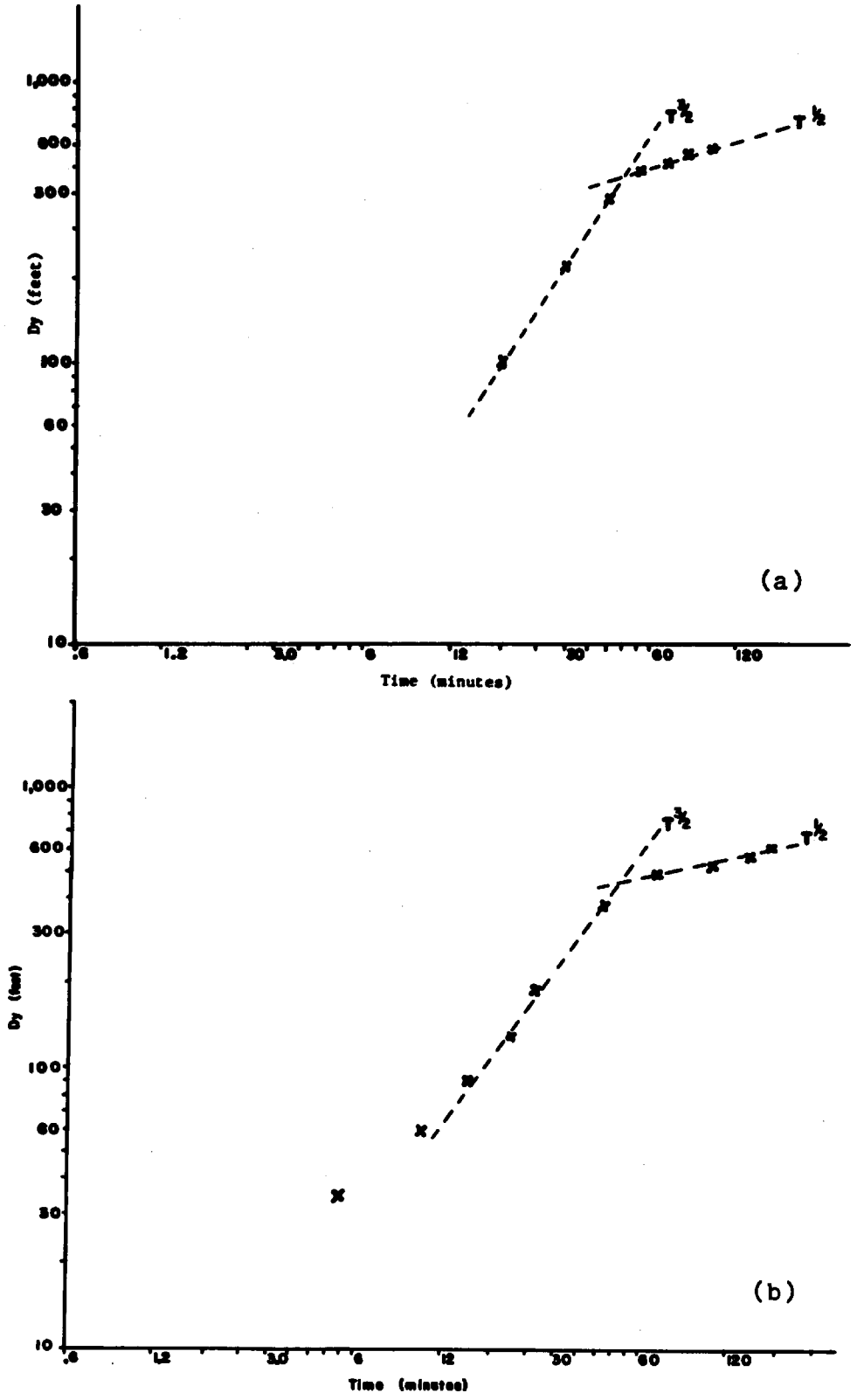


Figure 10. Lateral growth of the dye patch with time. (a) 2 May 1968. (b) 27 June 1968.

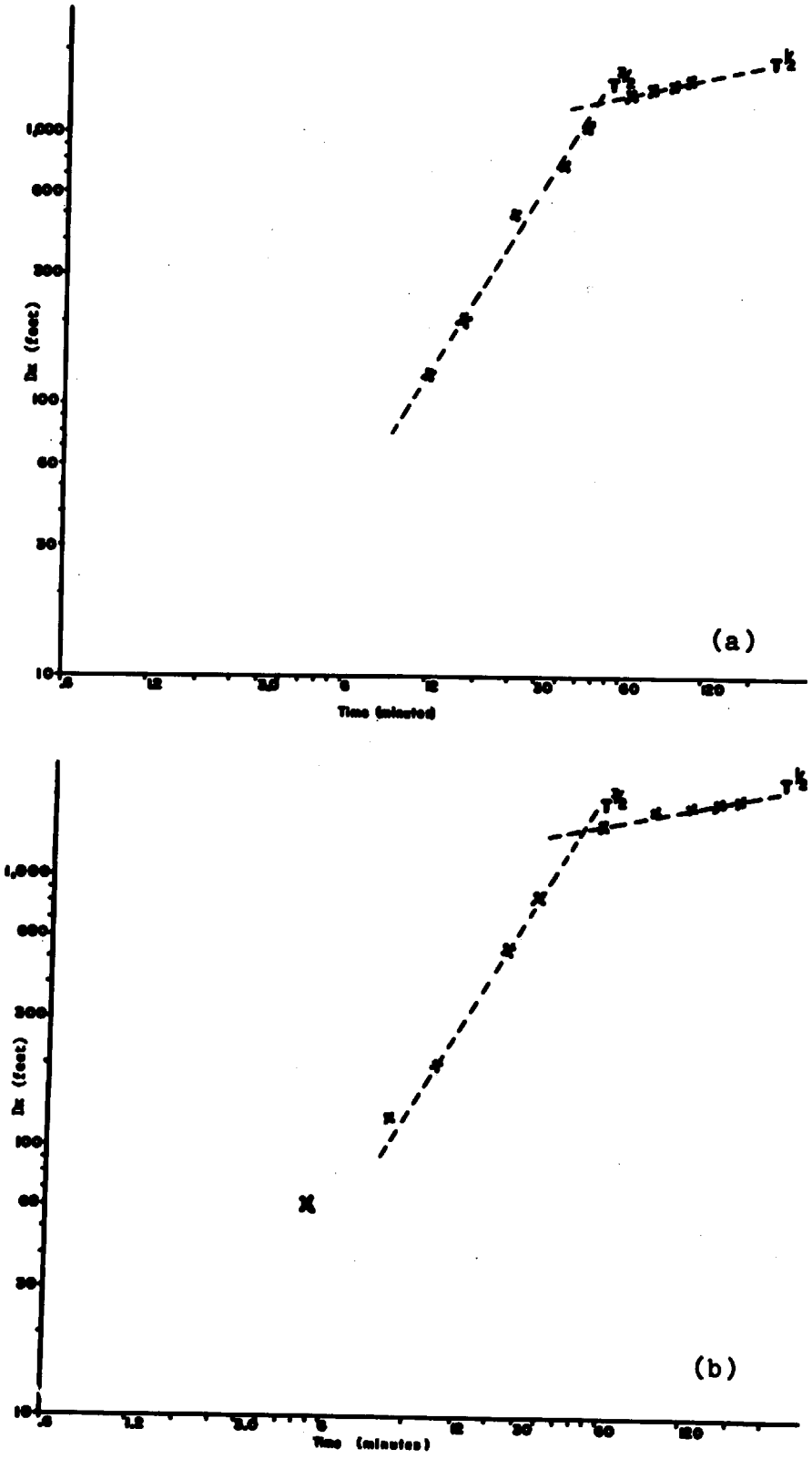


Figure 11. Longitudinal growth of the dye patch with time. (a) 2 May 1968. (b) 27 June 1968.

Continuous Source

Four runs of continuous (in time) point sources of marked particles were conducted near the meteorological research tower 1 mile off the east shore in Lake Michigan. Ten gallons of rhodamine B and methanol mixture were contained in two 5-gal carboys connected together by plastic tubing as shown in Figure 12.

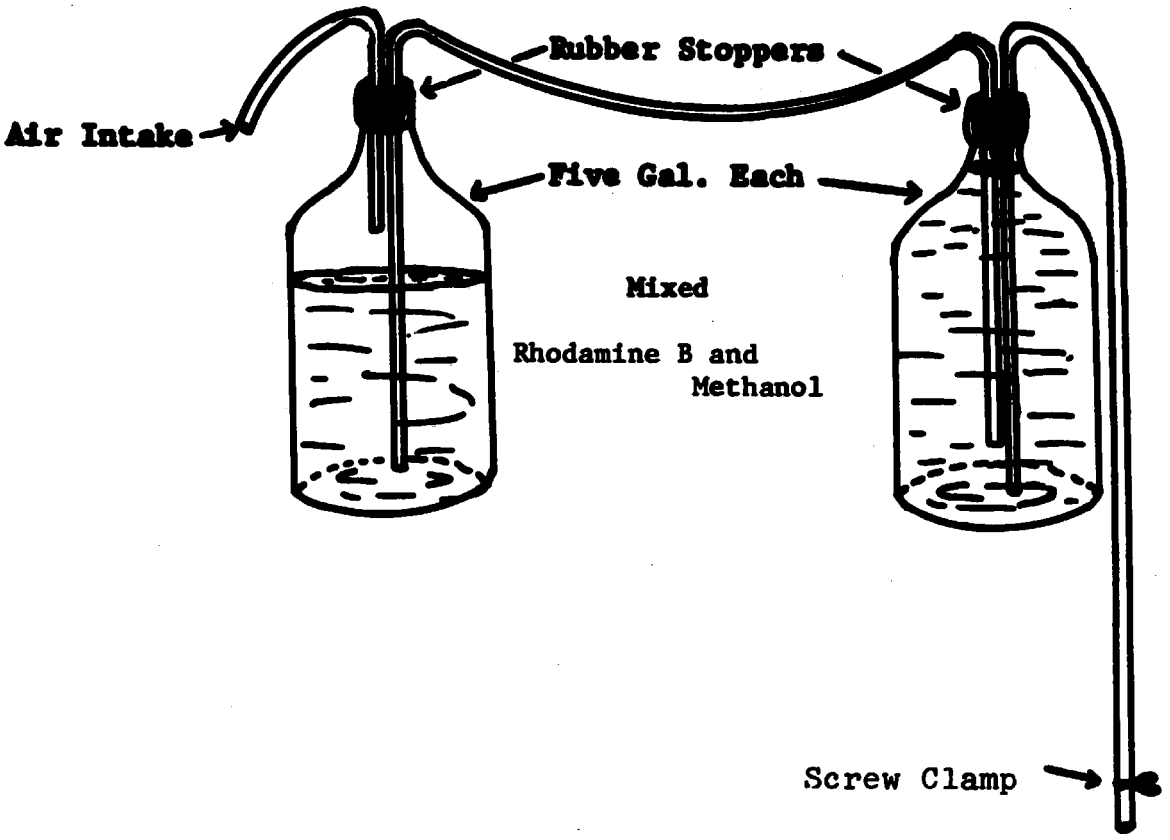


Figure 12. Continuous source apparatus.

The continuous point source was released from the apparatus through a rubber tube which had its outlet about 20 cm above the water surface. The rate of discharge of the dye was controlled by a screw clamp on the tubing, and was usually allowed to flow at a rate of 3 gal/hr, or approximately 4 gm/sec. In a homogeneous fluid with a steady uniform current, the continuous dye source produced a slender plume extending downstream.

The direction of the dye plume was reported by the observer using a theodolite mounted on the meteorological research tower 37 feet above the water surface. Buoys were dropped as markers on the edges of the dye plume at right angles to the direction of flow. The approximate distance of the marker from the source depended on the mean velocity of the current which was estimated from drogues set earlier.

The R/V MYSIS crossed the dye plume back and forth at 10-min intervals at the lowest speed she could make (about 4.5 mph). As soon as the dye plume passed through the markers, samples of water were taken through a constant-flow fluorometer that fed into an AZAR recorder. Communication between the tower and the boat was maintained through a VHF transceiver. Whenever the boat entered and left the dye plume a "MARK" signal was transmitted to the theodolite observer. The observer obtained the azimuths of both edges of the plume and the angular elevation from the tower to the boat.

The horizontal distance between the boat and the tower was obtained from the elevation angle as well as by fixes from land objects. The angle subtended by the edges of the plume is the difference of the two azimuths. The arc length of the plume at this distance from the tower was arbitrarily taken as four times the lateral standard deviation unit. At each return crossing, the vertical diffusion was measured by lowering the fluorometer intake at half-meter intervals until there was no indication of the dye. Half of the maximum vertical displacement was taken as the vertical standard deviation unit.

In the last few minutes before the exhaustion of the point source, continuous crossings were conducted at various distances along the plume from the

tower to approximately 1-1/2 miles downstream. These crossings measured the asymptotically steady diffusion of the plume.

These continuous point source diffusion studies were carried out on 30 July and 1-2 August 1967. On 30 July, sampling was discontinued about 2 hr after the experiment was initiated, because of high seas. The dye plume was continuously sampled for 3 hr on 1 August, and during the sampling period the current shifted its direction of flow about 15°. Two sampling runs were conducted on 2 August under a very steady current condition. The general information for each run and the values of diffusivity obtained are shown in Table 8. The lateral growth of the dye plume versus time at a constant distance from source is shown in Figure 13. The lateral growth versus distance under asymptotically steady condition is shown in Figure 14.

A MEASUREMENT OF THE HORIZONTAL DIFFUSION BY DROGUE STUDIES

A drogue is made of 4 pieces of light sheet metal (e.g., aluminum alloy) approximately 1 x 2 m in dimension, linked together in the shape of a cross and suspended by chains in the water by a float which supports a radar reflection above the water surface (similar to Farlow, 1965). It is frequently used for measuring the mean current of the flowing layer at the drogue depth. The equivalent radius of the drogue is about 1 m and, based on its geometry and the corresponding Reynolds numbers (10^4 to 10^5 in the Great Lakes), its time constant is estimated to be 100 sec (Okubo and Farlow, 1967). Though the small-scale turbulence may be averaged out, the drogue is adequate for measurement of large-scale turbulent diffusion for eddies larger than 10 m in scale

TABLE 8

General Information and Effective Eddy Diffusivity
of Continuous Source Dye Plume Studies

	Run 1	Run 2	Run 3	Run 4
Date	30 July 1968	1 Aug. 1968	2 Aug. 1968	2 Aug. 1968
Location	1 mile off shore near Mona Lake, Muskegon, in Lake Michigan	1 mile off shore near Mona Lake, Muskegon, in Lake Michigan	1 mile off shore near Mona Lake, Muskegon, in Lake Michigan	1 mile off shore near Mona Lake, Muskegon, in Lake Michigan
Depth	50 ft	50 ft	50 ft	50 ft
Duration of run	1120 - 1220 EST	0915 - 1337 EST	0800 - 0945 EST	1210 - 1540 EST
Current velocity (cm/sec)	12.7	6.8	28.0	28.0
Wind				
Direction	SE	ENE	WNW	WNW
Speed, kts	10	15	8	8
Lake Condition	3-5 ft waves	1/2-1 ft wave	1-2 ft waves	1-2 ft waves
Effective eddy diffusivity (cm^2/sec)	Not available	583	1371	1231
Remark	Measuring time not long enough			

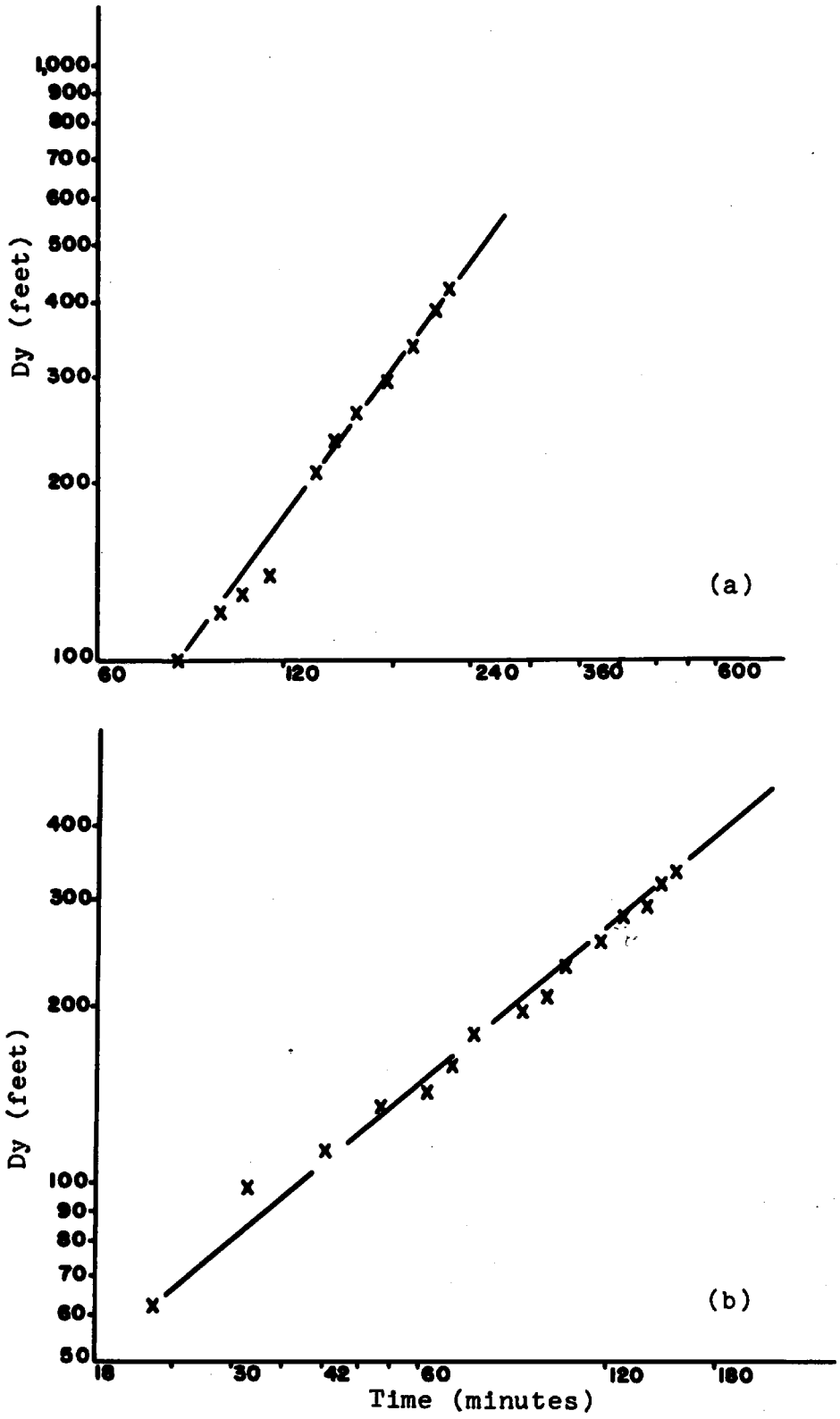


Figure 13. Lateral growth of dye plume at a constant distance from the source (between two marker buoys transverse to the current). (a) 1 August 1968 (distance 650 ft). (b) 2 August 1968 (distance 770 ft).

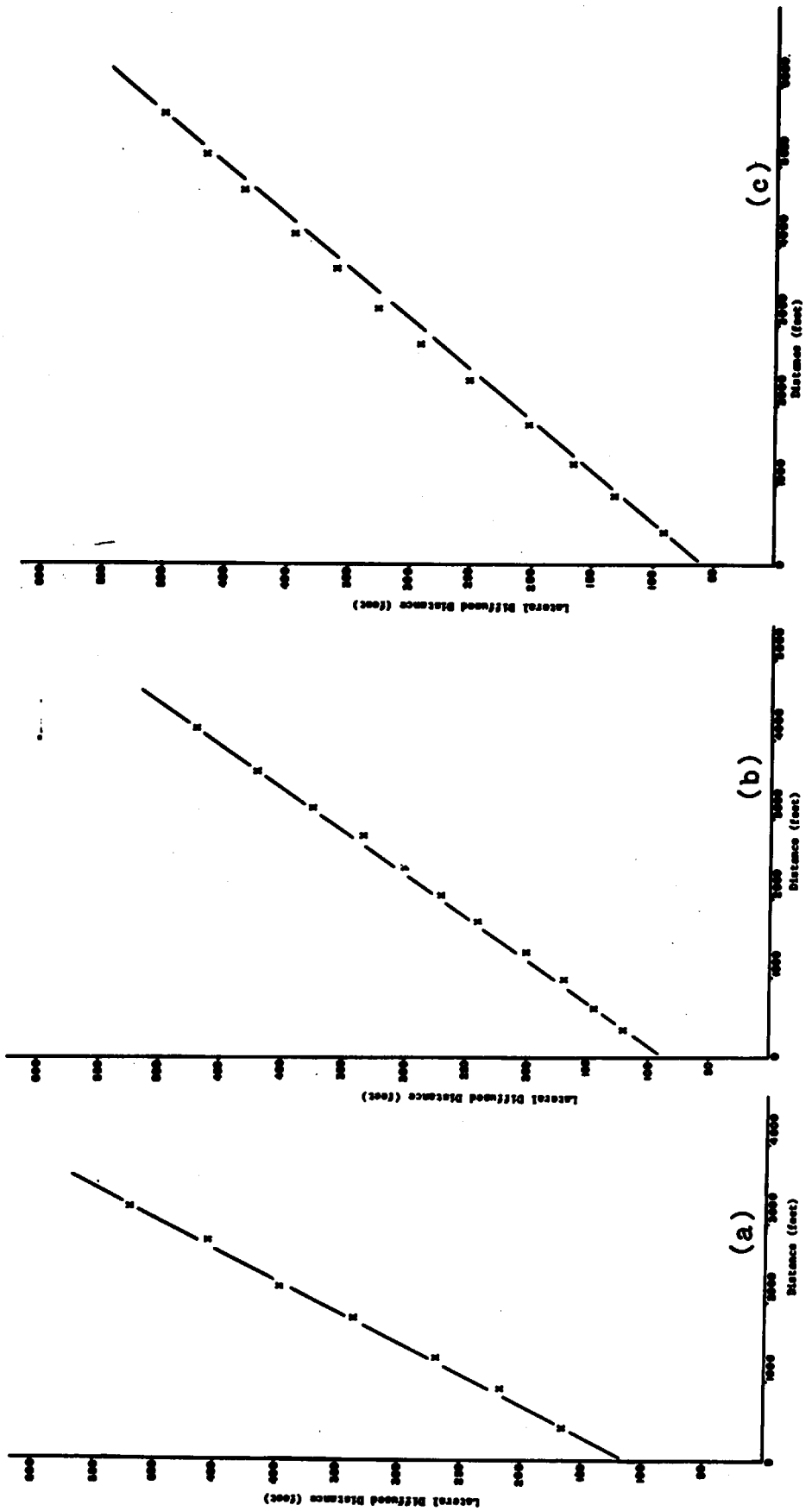


Figure 14. Lateral growth of dye plume with distance from source. (a) 1 August 1968. (b,c) 2 August 1968.

which represent the energy-containing eddy scales in the Great Lakes (Csanady, 1963; Okubo and Farlow 1967).

On 27 June 1968 a hexagonal pattern of surface drogues, with the central one very close to a fixed buoy, was set about 5 miles off shore near Milwaukee in Lake Michigan. The original distance between each pair of drogues was 1/2 mile. After setting the pattern, the R/V INLAND SEAS continuously fixed each drogue for the following 6-1/2 hr. Similar to the result mentioned by Okubo and Farlow (1967), the growth of the pattern size with time was not clearly noticed. The diffusion constant was deduced from the second moments about the mean of the hexagonal pattern. At any particular time, the instantaneous positions of all drogues were interpolated from their respective previous fixes. The general information on the experimental run and the value of eddy diffusivity are shown in Table 9.

TABLE 9

General Information and Eddy Diffusivity
of Drogue Study in Lake Michigan

Date	27 June 1968
Location	5 miles off Milwaukee
Depth of water	65 ft
Depth of drogues	5 ft
Duration of run	1207 - 1830 EST
Current velocity	7.6 cm/sec
Wind	
Direction	N
Speed	6 kts
Lake Condition	1/2 - 1 ft waves
Mean initial separation	2378 ft
Final deviation from mean	3400 ft
Effective eddy diffusivity	3.4×10^4 cm^2/sec

Comparisons of Values with Other Studies

In Lake Michigan, there is little data about eddy viscosity or eddy diffusivity. Some figures from the ocean or other lakes are available as reference. In modeling the Gulf Stream, Munk (1950) estimated the lateral eddy viscosity as 5×10^7 cm^2/sec. Stommel (1955) estimated the eddy viscosity of the Gulf Stream near the Florida Straits to be 2×10^5 cm^2/sec. Defant (1961) determined the exchange coefficient of lateral large-scale turbulence in ocean phenomena as 5×10^7 cm^2/sec.

In general, the vertical turbulence scale is much smaller in dimensions than that of the horizontal. Therefore, the magnitude of vertical eddy viscosity is much smaller. According to Defant (1961), Sverdrup obtained a value for the vertical eddy viscosity of 75-260 cm^2/sec in the North Siberian Shelf region; Fjeldstad estimated the vertical eddy viscosity in the Caspian Sea as 0-224 cm^2/sec, and Suda measured the values 680-7500 cm^2/sec for the Kuroshio and 150-1460 cm^2/sec in the Japan Sea.

For vertical eddy diffusivity, some typical values have been summarized by Defant (1961) as: Mediterranean, 42 cm^2/sec; California current, 30-40 cm^2/sec; Caspian Sea, 2-16 cm^2/sec; Equatorial Atlantic Ocean, 320 cm^2/sec. Csanady (1963, 1964, 1966) has measured the eddy diffusivity in Lake Huron and Lake Erie, and found horizontal diffusivity of the order of 500-2500 cm^2/sec in Lake Huron and 1000-5000 cm^2/sec in Lake Erie. These values are much greater than vertical eddy diffusivity, which is only of the order 0.1-10 cm^2/sec. Okubo and Farlow (1967) measured the horizontal diffusivity for large eddies

in Lake Michigan and Lake Erie using drogues and found the eddy diffusivity to be 3×10^4 to 6×10^4 cm^2/sec.

According to our estimation, the vertical eddy viscosity is on the order of 1.2×10 to 2×10^2 cm^2/sec in Lake Michigan. The lateral eddy diffusivity we found using marked particles is 750-1200 cm^2/sec for small eddies and 3.4×10^4 cm^2/sec for larger eddies. The effective longitudinal eddy diffusivity for small eddies is in the order of 4×10^4 cm^2/sec. All the data we used appear quite consistent and in good agreement with that of others.

As Csanady (1966) has pointed out, shearing flow and unsteady currents or any kind of complex circulation patterns accelerate the diffusion very repidly. Therefore, the above estimations may still be in the lower range of eddy viscosity or diffusivity in Lake Michigan.

Reasonable Values for Model Study

In modeling a geofluid problem, the eddy viscosity and the eddy diffusivity are of critical importance in order to predict the natural current or wave phenomena. In Lake Michigan, though the mean current velocity is small in general, the flow field is turbulent in nature. In solving or explaining the flow pattern of the mean lake current, it is possible to use the governing equations of laminar flow with eddy viscosity and eddy diffusivity in place of the molecular viscosity and the molecular diffusivity. A series of experiments have been conducted in order to estimate these two values. The data presented are quite consistent and in good agreement with the data reported by other in-

vestigators. The vertical eddy viscosity in Lake Michigan is in the range of 1 to 10^2 with a mean 30 cm^2/sec. The horizontal viscosity is in the range of 10^2 to 10^5 with a mean value of 10^4 cm^2/sec. The eddy diffusivity may reach the same magnitude as the viscosity but it is in general smaller. A typical mean value for vertical eddy diffusivity is 10 cm^2/sec, and for the horizontal eddy diffusivity 10^3 cm^2/sec. Though the few experiments are far from enough to state the characteristic values of turbulent phenomena, the data presented together with values reported by others can be used as good reference values for Lake Michigan.

VI. REPRESENTATIVE VALUES OF PARAMETERS IN THE LAKE MICHIGAN MODEL

General Physical Data

General features of Lake Michigan have been discussed in detail in Chapter I and II.

All physical parameters used for our theoretical model study in similitude to the real phenomena in Lake Michigan are summarized in Table 10. Note that all notations have been specified in Table 2. The magnitudes of ε, ε_1, ε_2 should also be noted.

TABLE 10

General Physical Data Used in the Lake Michigan Model

Parameter Notation	Value	Unit
L	1.22×10^7	cm
D	1.22×10^4	cm
2Ω	10^{-4}	rad/sec
ν_V	30	cm/sec
ν_H	3×10^4	cm/sec
λ	10^2	
ε	2×10^{-6}	
γ	10^{-3}	
σ	1	
K	11	
ε_1	4×10^{-3}	
ε_2	4.4×10^{-5}	
g	980	cm/sec

Parameters as Functions of Seasonal Temperatures

The horizontal temperature difference ΔT as well as the thermal Rossby number, R, are functions of seasonal temperatures. The reference velocity V, satisfying the geostrophic thermal wind relationship, varies as the seasonal temperature changes.

GENERAL THERMAL CURRENT

In the type-A or type-B circulations the equation of state is approximated as equation (7). The coefficient of thermal expansion of freshwater density, α, is a special function of local temperature. Since the whole lake is above 4°C, during the summer-heating period in the type-A circulation and autumn-cooling period in the type-B circulation, α is positive in equation (7), that is, as the local temperature T' increases away from the temperature of maximum density, the density of water decreases. The horizontal temperature difference, ΔT, ranges from 0° to 10°C. Hence, the coefficient of thermal expansion of fresh water near 11°C is taken as a representative value. All values of special parameters connected with seasonal temperature changes used for general thermal current are listed in Table 11.

During the winter-cooling and spring-heating periods the temperature in the lake is all below 4°C. The horizontal temperature differences during these periods are smaller due to the occurrence of icing. The coefficient of thermal expansion, α, is negative in the equation (7) as the local temperature, T', is less than T_o, but the density of water is still decreasing as T' deviates away from 4°C. The approximate general thermal-current circulations during these

TABLE 11

Values of Parameters Connected With Temperature for the General Thermal Currents

Parameter notation	Value: Spring-heating and autumn-cooling periods	Value: Winter-cooling and autumn-heating periods	Unit
α	2×10^{-4}	2×10^{-5}	$^{o}C^{-1}$
ΔT	10	4	^{o}C
V	20	1	cm/sec
R	1.65×10^{-2}	10^{-3}	

periods are deduced from the circulation pattern during the summer-heating and autumn-cooling periods. It can easily be checked out either physically or mathematically that the winter-cooling period and the summer-heating period possess the same circulation pattern due to the combined effects of the special character of the α above or below the temperature of maximum fresh water density and the opposite imposed horizontal temperature gradients. For similar reason, the period of autumn-cooling and the period of spring-heating have the same circulation pattern. Therefore, with the circulation pattern of the summer-heating period as reference, we can still take α as positive, but treat the horizontal temperature difference in the negative sense during winter-cooling and spring-heating periods. The coefficient of thermal expansion at 3°C is used as representative for these two periods.

All values of special parameters connected with seasonal temperature changes used for general thermal current are listed in Table 11. The magnitude of R should be noted.

THERMAL BAR CURRENT

With the same reasoning, either the spring thermal bar or the autumn thermal bar periods have the same circulation pattern except the latter is much weaker. The equation of state during thermal bar periods is approximated by equation (89). All values of parameters connected with temperature during thermal bar periods are listed in Table 12. The magnitude of R should be noted.

TABLE 12

Values of Parameters Connected with Temperature for the Thermal Bar Currents

Parameter Notation	Values	Unit
A	4×10^{-3}	$^{o}C^{-1}$
ΔT	8	^{o}C
V	12	cm/sec
R	10^{-2}	

VII. THERMAL CURRENT CIRCULATION PATTERNS AND TEMPERATURE DISTRIBUTIONS FROM SOLUTIONS OF THE BAROCLINIC DYNAMIC MODEL OF LAKE MICHIGAN

In our simple categorization for thermal current circulation as functions of seasonal temperature differences as introduced in Chapter I, the type-A circulation pattern induced during the winter-cooling period and the summer-heating period, and the type-B circulation pattern induced during the spring-heating period and the autumn-cooling period, belong to the general thermal currents. The thermal bar circulation pattern induced during both spring and autumn thermal bar periods is the type-C circulation in our terms. The surface temperature profiles in different periods have been mentioned in the above chapters. Note also that the strong thermal stratification period is not included in our quasi-homogeneous model study.

The general thermal current circulation pattern and temperature distribution have been mathematically investigated in detail in Chapter III, using the summer-heating features as representative. The special thermal circulation pattern during the thermal bar period has been demonstrated theoretically in Chapter IV. Following the double perturbation procedures, with regular perturbation expansion in powers of the thermal Rossby number R, and then singular perturbation analysis with respect to the Ekman number ε for each power of R, analytic approximate solutions of the whole flow field have been obtained, except in the small corners of the cross-section. Representative values of parameters closely in similitude to the real field phenomena in Lake Michigan have been put into the solutions obtained in Chapters III and IV by computer.

The results shall be discussed in more detail below.

Temperature Distribution

GENERAL THERMAL CURRENT PERIODS

The zeroth R-order temperature is shown in equation (37) which has no boundary layer effect, and the first R-order temperature is shown in equation (71) with boundary layer modifications in each individual boundary region as shown in equations (73), (74), (75), and (76). According to the double perturbation method (equations (17) and (31)), the total temperature, is

$$T = T^{(o)} + R\sigma[{}_oT^{(1)} + \varepsilon_1{}^{1/2}({}_1T^{(1)} + {}_2T^{(1)})$$

$$+ \varepsilon_2{}^{1/2}({}_3T^{(1)} + {}_4T^{(1)})] + O(\sigma^2R^2). \qquad (172)$$

Remember the boundary solutions are only of local importance at their respective boundaries. We notice from the above equation that the boundary layer effect of temperature is not very important.

Using representative values of parameters given in Chapter VI, the nondimensional temperature distribution is shown in Figure 15. During the summer-heating period, the surface temperature is concave cosine profile and the horizontal temperature is much higher on the edges than in the middle portion of the lake. We consider this kind of temperature difference with higher temperature near the shore as a positive gradient. With data given in Table 11, each isotherm in Figure 15 is about 1°C in difference. Though the middle portion of the lake may still be at 4°C, the two edges of water near shore may have

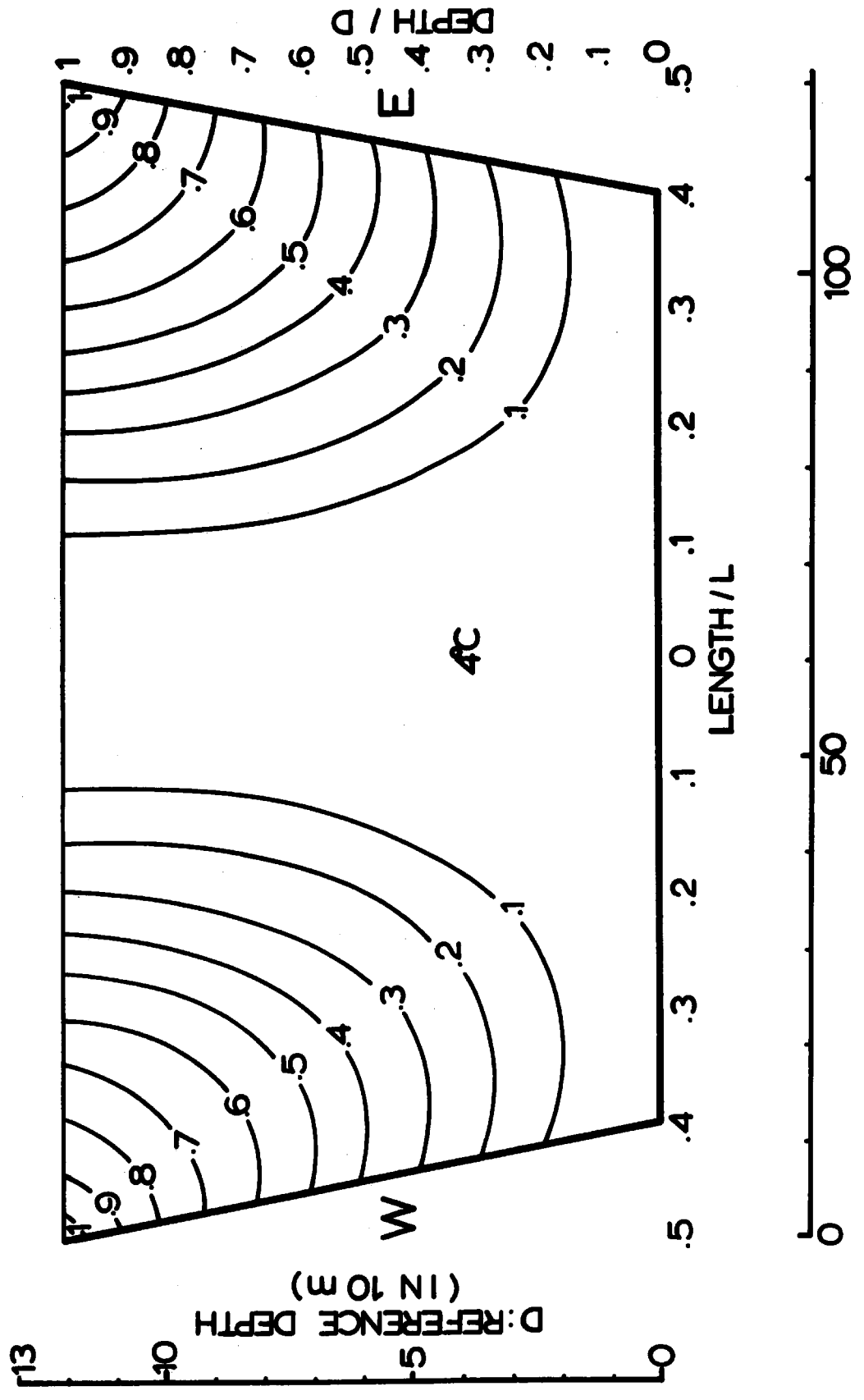


Figure 15. Nondimensional temperature distribution in Lake Michigan model for general thermal current periods. For explanation see text.

been warmed up to 14°C.

During the autumn-cooling period, since the atmospheric temperature is colder, the surface temperature of the lake has a cosine profile with the two edges at nearly the reference temperature, T_o. The horizontal temperature difference is in the negative sense because the edges of water are colder. The temperature profile has exactly the same form in isotherm distribution, but with a reversed direction of temperature difference as compared with that of the summer-heating period, that is, the temperature gradient is in the negative sense with maximum temperature at the middle during this period.

For the other two periods of time under general thermal currents the temperature isotherms have the same form except that the magnitudes of temperature differences are smaller. During the winter-cooling period, the maximum surface temperature is nearly the temperature of maximum density in the middle of the lake while the edges may well be frozen. The temperature distribution is of exactly the same form as that of the autumn-cooling period except the temperature difference is only 4°C. The spring-heating period is exactly the same as the summer-heating period except the horizontal difference is smaller.

THERMAL BAR PERIODS

The zeroth R-order temperature of the thermal bar period is shown in equation (109) and its first R-order overall part of temperature is shown in equation (133) with $O(\varepsilon^{1/2})$ boundary parts respectively shown in equations (125), (126), (127), and (128). The total nondimensional temperature, with values of parameters shown in Tables 10 and 12, is shown in Figure 16. During the

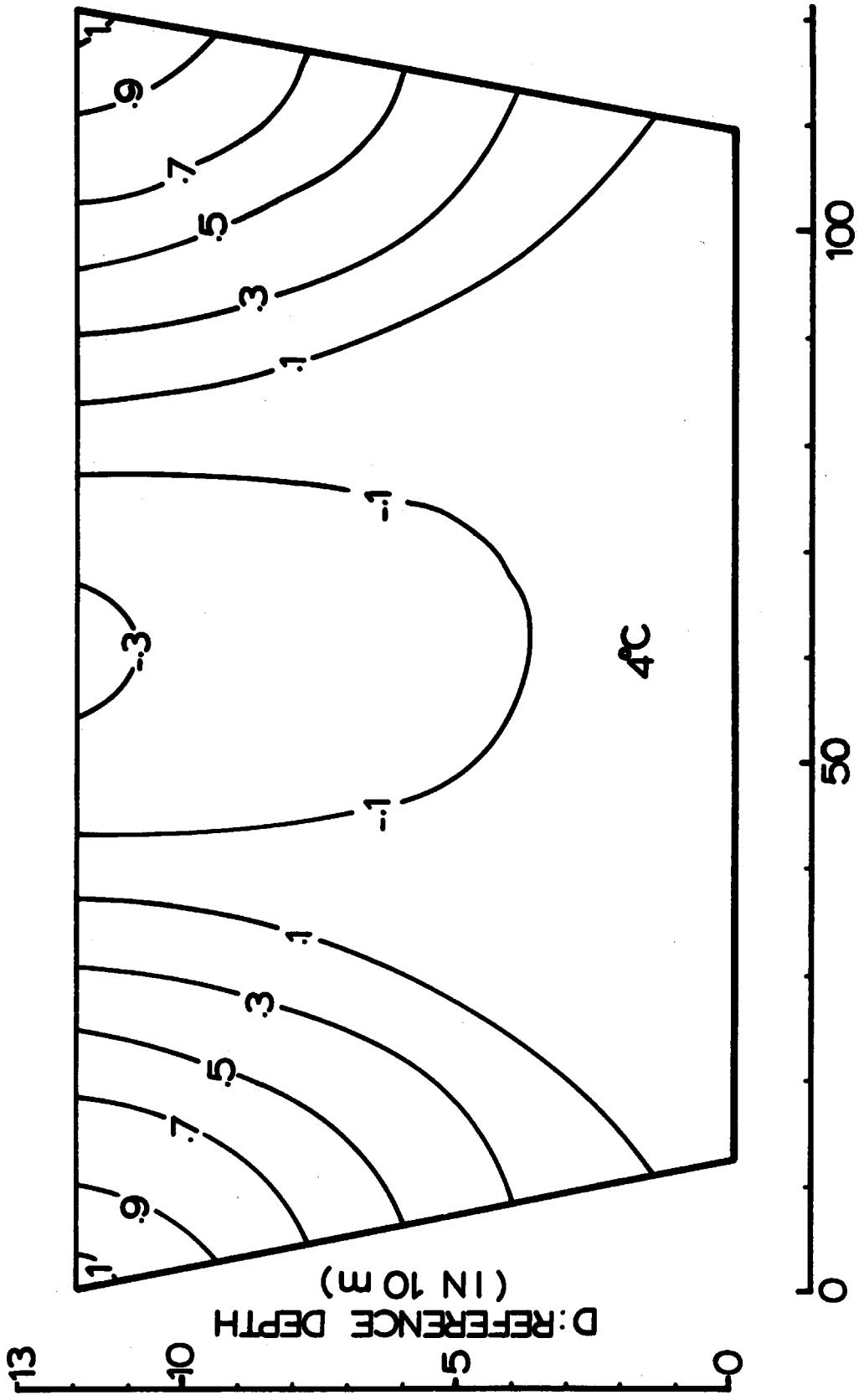


Figure 16. Nondimensional temperature distribution during thermal bar periods. For explanation see text.

spring thermal bar period, the surface temperature in the middle of the lake is at 2°C to 3°C but the edges near shore have already warmed up to a temperature far above 4°C. The thermal bar exists near the zone of temperature of maximum density. The maximum horizontal temperature difference between the thermal bar and the shallowest edges may be as large as 10°C.

The autumn thermal bar has the reverse distribution with the temperature in the middle of the lake slightly above 4°C and two edges of the lake much colder at nearly 2°C. The temperature isotherms have the same form but temperatures decrease shoreward and the horizontal temperature difference is only 2 to 3°C.

Velocity Field

GENERAL THERMAL CURRENTS

Meridional Velocity

Under the basic assumption that the geostrophic and thermal gradient forces are in equilibrium in the flow field, the meridional velocity dominates the circulation pattern. The zeroth R-order meridional velocities of the type-A circulation pattern, the circulation pattern occurring during the winter-cooling and summer-heating periods, are shown in equation (38) for the interior region and equations (49), (53), (57), (59) for the respective boundary regions. The first R-order meridional velocities are shown in equation (78) and equations (80), (82), (84), (88). The total meridional velocity, in form similar to equation (172) for temperature, is then,

$$v = {}_0v^{(0)} + \varepsilon_1^{1/2}({}_1v^{(0)} + {}_2v^{(0)}) + \varepsilon_2^{1/2}({}_3v^{(0)} + {}_4v^{(0)})$$

$$+ R\,[{}_0v^{(1)} + \varepsilon_1^{1/2}({}_1v^{(1)} + {}_2v^{(1)}) + \varepsilon_2^{1/2}({}_3v^{(1)} + {}_4v^{(1)})]$$

$$+ O(R^2). \qquad (173)$$

The nondimensional total meridional velocity of the type-A circulation has been plotted as shown in Figure 17. In the upper half of the fluid in the Lake Michigan model, there is a northbound flow on the eastern part of the lake and a southbound flow on the western part of the lake. In the middle portion of the lake, the meridional velocity is very weak. It beomces stronger away from the center and reaches a maximum at places around one-fourth of the lake width from shores. Then it decreases toward the shore but becomes strong again within the eastern and western boundary regions due to the reinforcement of the boundary layer currents near the side slant boundaries. In general, the magnitude of meridional velocity first increases then decreases as depth increases. The meridional velocity has only a slight change in the upper Ekman layer due to the effect of the boundary layer current. The maximum meridional velocity in the vertical section occurs at few meters below the free surface and its magnitude may reach as high as 17 cm/sec during the summer-heating period. In the deeper part of the lake, the meridional velocity is much smaller. Below two-thirds of the lake depth, the current direction may reverse with southbound flow in the east and northbound flow near the west shore.

Meridional current during the winter-cooling period possesses the same circulation pattern as shown in Figure 17 except the magnitude is smaller.

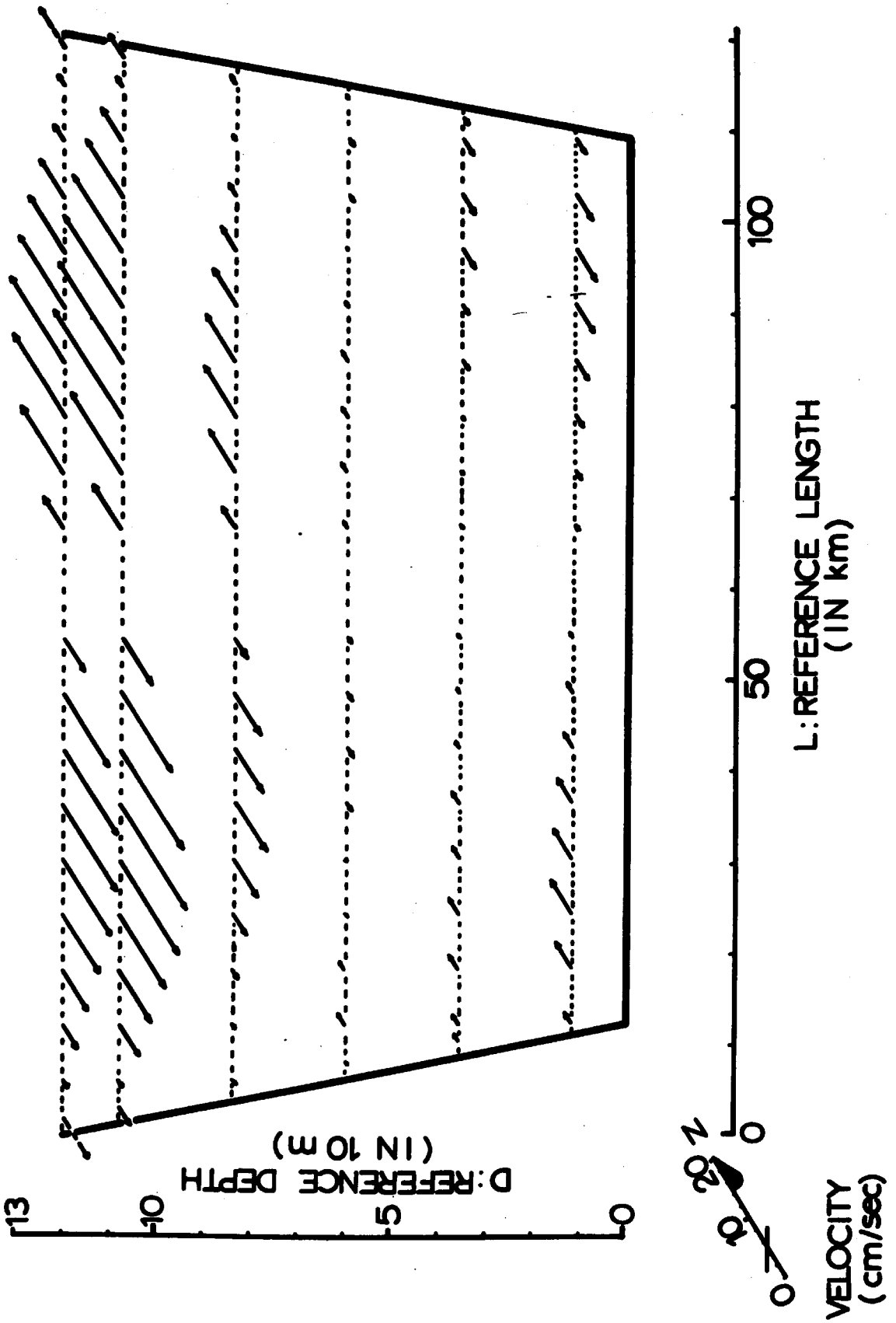


Figure 17. Nondimensional meridional velocity of type-A circulation.

The maximum magnitude may reach 1 cm/sec in winter.

The type-B circulation has exactly the reverse circulation pattern from that of the type-A circulation.

Zonal and Vertical Velocities

During the summer-heating period, the stream function for zonal and vertical velocity components is $O(\varepsilon)$. The zeroth R-order stream function in the interior region is independent of the vertical coordinate as shown in equation (39). According to the velocity definition in equation (13), the zonal velocity component is

$$u = \frac{\partial \psi}{\partial z} \quad , \tag{174}$$

and the vertical component is

$$w = - \frac{\partial \psi}{\partial x} \quad . \tag{175}$$

Therefore, there is no zeroth R-order zonal velocity in the interior. The zeroth R-order boundary stream functions are shown in equations (50), (53), (58), (60). The first R-order stream functions are shown in equation (79) for the interior region and in equations (81), (83), (85), (88) for the respective boundary regions. According to equation (174), the total zonal velocity can be written as:

$$u = R\varepsilon_1 \frac{\pi^2}{2\sqrt{\gamma H}} (\cosh az - G) \sin 4\pi x + \varepsilon_1^{1/2} \{ [\sqrt{2}\, e^{-\zeta_2/\sqrt{2}} \sin \frac{\zeta_2}{\sqrt{2}} - \frac{1}{\sqrt{2}} e^{-\zeta_1/\sqrt{2}}$$

$$\cdot (\cos \frac{\zeta_1}{\sqrt{2}} + \sin \frac{\zeta_1}{\sqrt{2}})] \pi \sin 2\pi x + \frac{R\pi^2(1 - G)}{\sqrt{2}\, \gamma H} e^{-\zeta_2/\sqrt{2}} \sin \frac{\zeta_2}{\sqrt{2}} \sin 4\pi x \} + \varepsilon^{1/2}$$

$$\cdot \left[\frac{\sqrt{2\pi\lambda}}{\sqrt{K}} \left[\sin 2\pi\lambda\gamma(1 - \eta_2)\, e^{-\xi_2/\sqrt{2}} \sin\frac{\xi_2}{\sqrt{2}} - \sin 2\pi\lambda\gamma(1 - \eta_1) e^{\xi_1/\sqrt{2}} \sin\frac{\xi_1}{\sqrt{2}}\right]\right.$$

$$+ R\frac{\pi^2\lambda}{\sqrt{2K\gamma H}} \left[(\cosh a\eta_1 - G) \sin 4\pi\lambda\gamma(1 - \eta_1) e^{\xi_1/\sqrt{2}} \sin\frac{\xi_1}{\sqrt{2}} + (\cosh a\eta_2 - G)\right.$$

$$\left.\left.\cdot \sin 4\pi\lambda\gamma(1 - \eta_2) e^{-\xi_2/\sqrt{2}} \sin\frac{\xi_2}{\sqrt{2}}\right]\right] + O(R^2\varepsilon^{1/2}). \qquad (176)$$

The total vertical velocity, referring to equation (175), can be written as

$$w = \varepsilon_1 2\pi^2\left\{\left[\frac{R\pi}{\sqrt{\gamma H}} (\cosh az - G) \cos 4\pi x - \cos 2\pi x\right] + \left[e^{-\zeta_1/\sqrt{2}} \cos\frac{\zeta_1}{\sqrt{2}} + e^{-\zeta_2/\sqrt{2}}\right.\right.$$

$$\left.\cdot \left(\cos\frac{\zeta_2}{\sqrt{2}} + \sin\frac{\zeta_2}{\sqrt{2}}\right)\right]\cos 2\pi x + \frac{R\pi(1 - G)}{H\sqrt{\gamma}} e^{-\zeta_2/\sqrt{2}} \left(\cos\frac{\zeta_2}{\sqrt{2}} + \sin\frac{\zeta_2}{\sqrt{2}}\right) \cos 4\pi x\right\}$$

$$- \varepsilon_1{}^1{}^2\frac{\sqrt{2\pi}}{\sqrt{K\gamma}} \left\{\left[e^{\xi_1/\sqrt{2}} \sin\frac{\xi_1}{\sqrt{2}} \sin 2\pi\lambda\gamma\,(1 - \eta_1) + \sin 2\pi\lambda\gamma(1 - \eta_2)\, e^{-\xi_2/\sqrt{2}}\right.\right.$$

$$\left.\cdot \sin\frac{\xi_2}{\sqrt{2}}\right] - \frac{R\pi}{2\gamma H} \left[(\cosh a\eta_1 - G)\, e^{\xi/\sqrt{2}} \sin\frac{\xi_1}{\sqrt{2}} \sin 4\pi\lambda\gamma(1 - \eta_1) - (\cosh a\eta_2 - G)\right.$$

$$\left.\left.\cdot \sin 4\pi\lambda\gamma(1 - \eta_2)\, e^{-\xi_2/\sqrt{2}} \sin\frac{\xi_2}{\sqrt{2}}\right]\right\} + O(R^2\varepsilon^{1/2}). \qquad (177)$$

With data from Tables 10 and 11, equations (176) and (177) have been calculated by computer and the results are shown in Figure 18. There are two relatively extensive cells which meet at the middle of the lake. The convergence of cells results in a broad sinking motion in the central portion of the lake and upwellings at both east and west sides of the lake. The velocity components in the interior region are mostly vertical with only an $O(R\varepsilon)$ part zonally. In the upper and lower Ekman layers, zonal components are dominant but they are

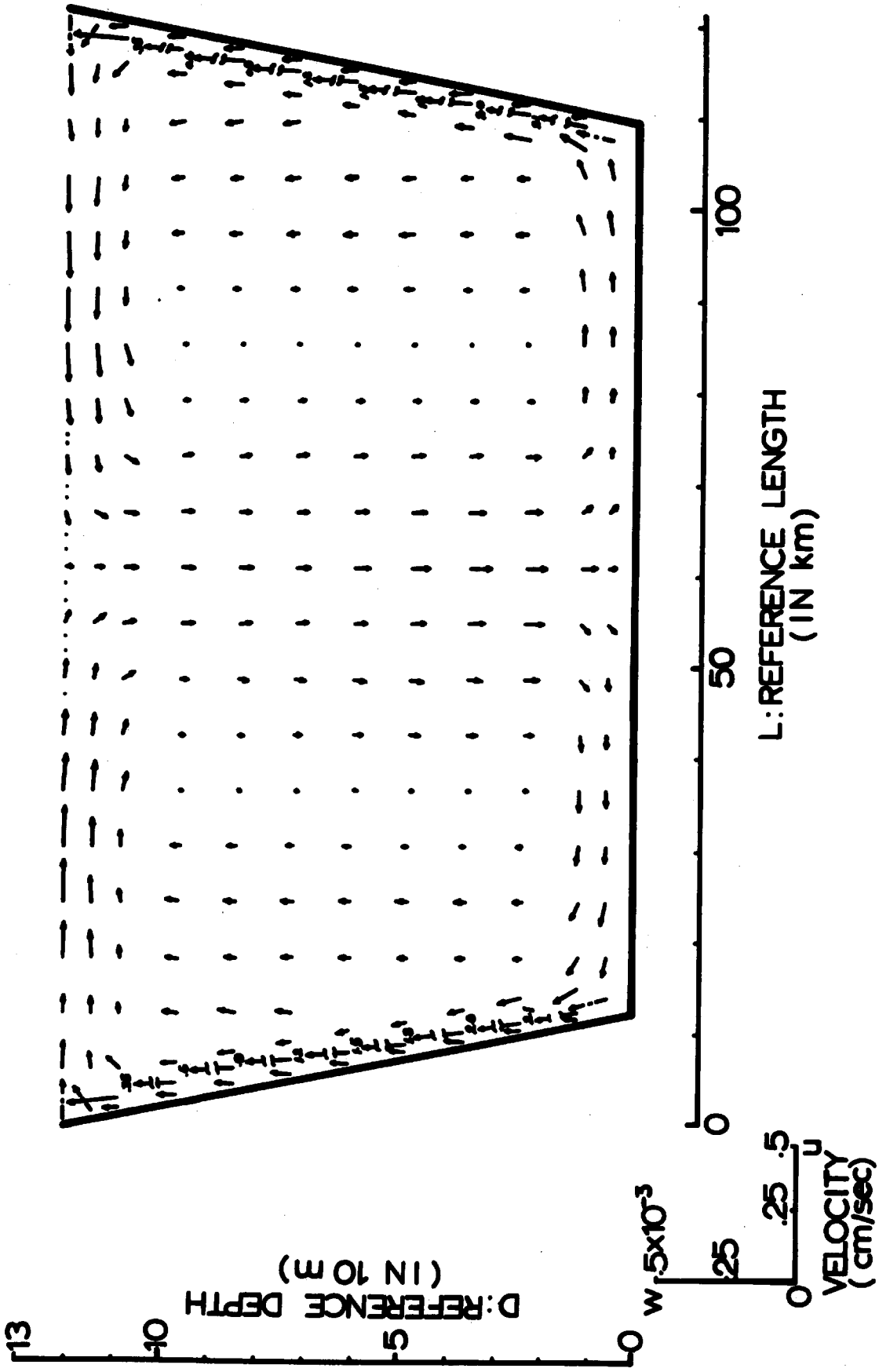


Figure 18. Nondimensional zonal and vertical velocity components of type-A circulation.

entirely within the surface and bottom boundary regions. On the slant side boundaries, the zonal and vertical velocities are much stronger than in any other place in the flow field. Generally, the magnitude of the mean zonal velocity is less than 1 cm/sec with a maximum near this value at the side slant boundaries. The mean vertical velocity is, in general, in the range of 10^{-5} to 10^{-3} cm/sec and may reach a maximum mean value of 2×10^{-3} cm/sec near the side boundaries.

As mentioned before, the zonal and vertical velocity components of the winter-cooling period have the same circulation pattern as shown in Figure 18 but the magnitude is about a factor of ten smaller.

The type-B circulation is just the reverse of the pattern as shown in Figure 18.

THERMAL BAR CURRENT

Meridional Velocity

The zeroth R-order meridional velocities of the type-C circulation are shown in equation (112) as the interior solution and equations (115), (117), (119), (123) as respective boundary layer solutions. The first R-order meridional velocities are shown in equation (137) and equations (140), (142), (144), (148). The result has been plotted in Figure 19. As we expected, the circulation pattern is more complicated. There are broad shearing flows along each thermal bar on each side of the lake near shore. The meridional flows in the main body of the lake between the two thermal bars, southward flow near the eastern thermal bar and northward flow near the western bar, form a clockwise

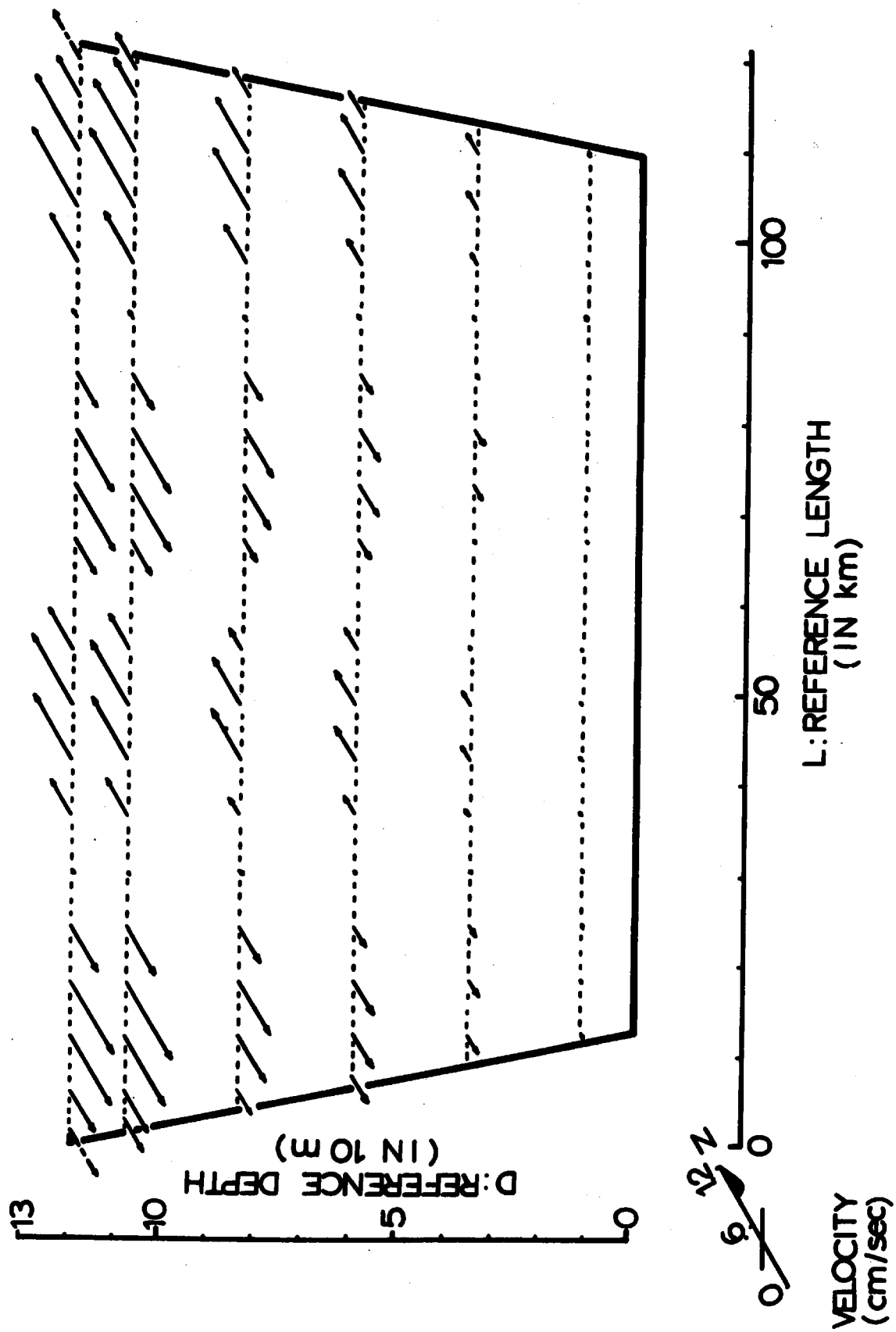


Figure 19. Nondimensional meridional velocity of thermal bar currents (type-C circulation).

couple while the middle portion of the lake is a nodal point. The meridional velocity at the thermal bar is very weak. Meridional flows between each thermal bar and its nearest shore are northbound on the eastern side and southbound on the western side of the lake. The magnitude of the meridional velocity, in general, decreases as the depth increases.

On the upper Ekman layer, the magnitude of the meridional velocity is almost uniform. The meridional flow is very weak near the bottom. The direction of flow is the same through the whole depth. Probably maximum meridional velocity in spring time is about 12 cm/sec.

The spring thermal bar current is stronger than the autumn thermal bar current which has a probable maximum meridional velocity of less than 1 cm/sec.

Zonal and Vertical Velocities

According to the stream functions given in equation (113), (116), (118), (120), (124) for the zeroth R-order and in equations (139), (141), (143), (146), (149) for the first R-order, the total zonal velocity during the thermal bar period is

$$u = R\varepsilon_1 \frac{16\pi^3 A^2}{81} \left[\left(\frac{1}{2H^2} \cosh 2az - \frac{2}{H} z \sinh az - \frac{1}{2H^2} \right) \sin 2\pi x - \frac{z \sinh az}{H} \sin 4\pi x \right.$$

$$\left. + \left(\frac{2}{H} z \sinh az + \frac{\cosh az - 1}{2H^2} \right) \sin 6\pi x + \left(1 - \frac{\cosh 2az}{H^2} \right) \sin 8\pi x \right] + \varepsilon_1^{1/2}$$

$$\cdot \left[b_o(x) \sqrt{2}\, e^{-\zeta_2/\sqrt{2}} \sin \frac{\zeta_2}{\sqrt{2}} - \frac{b_o(x)}{e^{\zeta_1/\sqrt{2}}} \left(\cos \frac{\zeta_1}{\sqrt{2}} + \sin \frac{\zeta_1}{\sqrt{2}} \right) - R\sqrt{2} b_1(x) e^{-\zeta_2/\sqrt{2}} \right.$$

$$\left. \cdot \sin \frac{2}{\sqrt{2}} \right] - \varepsilon^{1/2} \left[\frac{\sqrt{2\lambda}}{\sqrt{K}} \left(b_o(\eta_1) e^{\xi_1/\sqrt{2}} \sin \frac{\xi_1}{\sqrt{2}} + b_o(\eta_2) e^{-\xi_2/\sqrt{2}} \sin \frac{\xi_2}{\sqrt{2}} \right) \right.$$

$$- R\frac{\sqrt{2\lambda}}{\sqrt{K}}\left(b_3(\eta_1)e^{\xi_1/\sqrt{2}}\sin\frac{\xi_1}{\sqrt{2}} - b_3(\eta_2)e^{-\xi_2/\sqrt{2}}\sin\frac{\xi_2}{\sqrt{2}}\right] + O(R^2\varepsilon^{1/2}) \qquad (178)$$

where $b_o(x)$, $b_1(x)$, $b_o(\eta)$, $b_3(\eta)$ have shown in equations (114), (138), (121), (147). The total vertical velocity is,

$$w = \varepsilon_1\{ \frac{R32\pi^4A^2}{81}\left[\left(\frac{2(z\cosh az - G)}{Ha} - \frac{2(\sinh az - H)}{Ha^2} - \frac{\sinh az - H_2}{4H^2a} + \frac{z-1}{2H^2}\right)\right.$$

$$\cdot \cos 2\pi x + \left(\frac{z\cosh az - G}{Ha} - \frac{\sinh az - H}{Ha^2}\right) 2\cos 4\pi x - \left(\frac{2(z\cosh az - G)}{Ha}\right.$$

$$\left. - \frac{2(\text{shin } az - H)}{Ha^2} + \frac{\cosh az - G}{2H^2a} - \frac{z-1}{2H^2}\right) 3\cos 6\pi x + \left(\frac{\sinh 2az - H_2}{2H^2a} - z + 1\right)$$

$$\left. \cdot 4\cos 8\pi x\right] + b_o'(x)\left[e^{-\zeta_1/\sqrt{2}}\cos\frac{\zeta_1}{\sqrt{2}} - 1 + e^{-\zeta_2/\sqrt{2}}\left(\cos\frac{\zeta_2}{\sqrt{2}} + \sin\frac{\zeta_2}{\sqrt{2}}\right)\right]$$

$$- Rb_1'(x)\, e^{-\zeta_2/\sqrt{2}}\left(\cos\frac{\zeta_2}{\sqrt{2}} + \sin\frac{\zeta_2}{\sqrt{2}}\right)\} - \varepsilon^{1/2}\frac{\sqrt{2}}{\sqrt{K\gamma}}\left[\left(b_o(\eta_1)e^{\xi_1/\sqrt{2}}\sin\frac{\xi_1}{\sqrt{2}}\right.\right.$$

$$\left. + b_o(\eta_2)e^{-\xi_2/\sqrt{2}}\sin\frac{\xi_2}{\sqrt{2}}\right) - R\left(b_3(\eta_1)e^{\xi_1/\sqrt{2}}\sin\frac{\xi_1}{\sqrt{2}} - b_3(\eta_2)\, e^{-\xi_2/\sqrt{2}}\sin\frac{\xi_2}{\sqrt{2}}\right)\Big]$$

$$+ O(R^2\varepsilon^{1/2}) \qquad (179)$$

where

$$b_o'(x) = \frac{8\pi^2A}{9}(\cos 2\pi x - 2\cos 4\pi x) \qquad (180)$$

and

$$b_1'(x) = \frac{32\pi^4A^2}{81}\left[\left(\frac{2G}{Ha} - \frac{2}{a^2} - \frac{H_2}{4H^2a} + \frac{1}{2H^2}\right)\cos 2\pi x + 2\left(\frac{G}{Ha} - \frac{1}{a^2}\right)\cos 4\pi x\right.$$

$$\left. - \left(\frac{2G}{Ha} - \frac{2}{a^2} + \frac{G-1}{2H^2a} - \frac{1}{2H^2}\right) 3\cos 6\pi x + \left(\frac{H_2}{2H^2a} - 1\right) 4\cos 8\pi x\right] . \qquad (181)$$

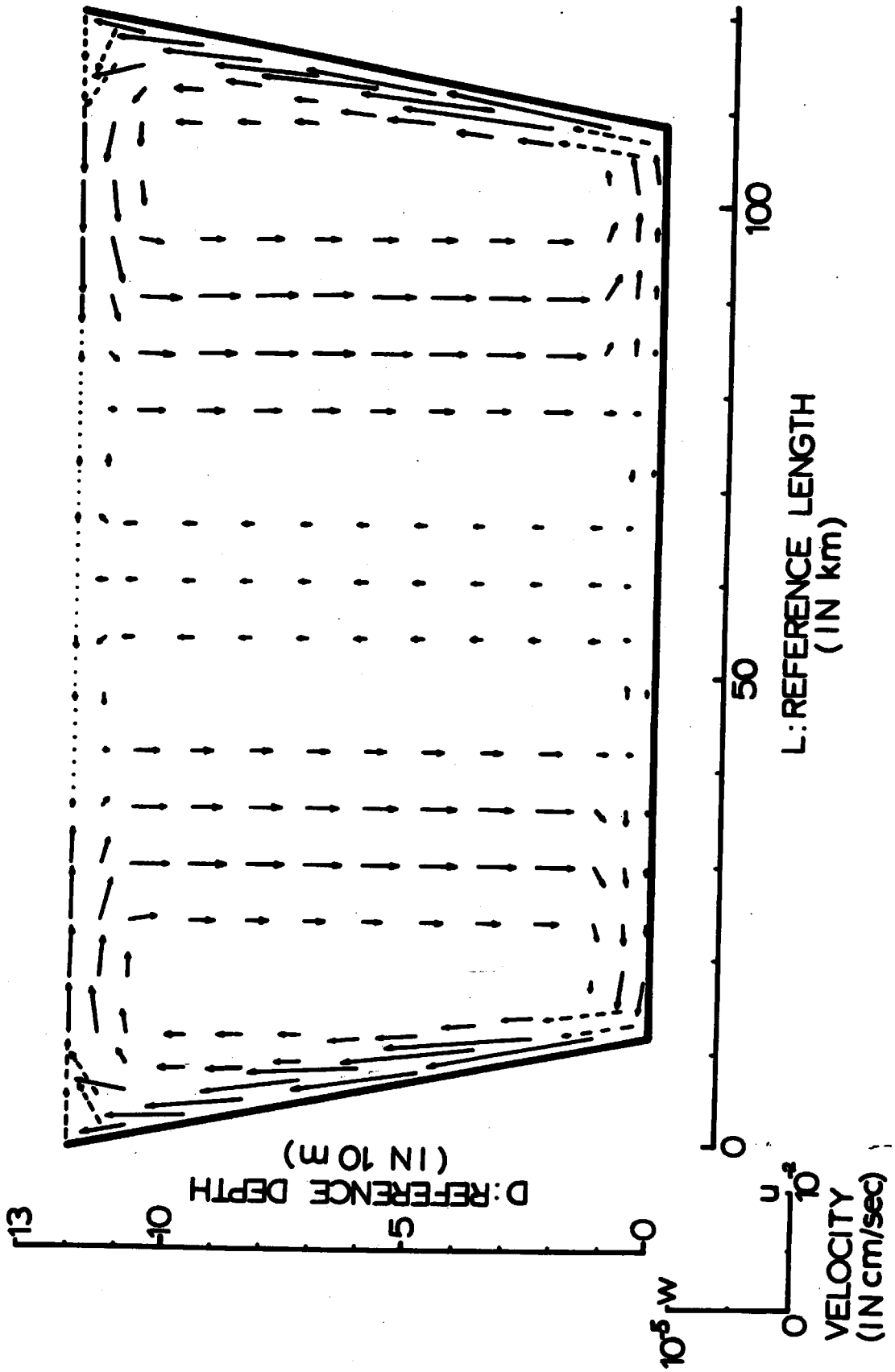


Figure 20. Nondimensional zonal and vertical thermal bar current circulation.

The total nondimensional zonal and vertical velocities are plotted in Figure 20. There are four cells circulating in the cross-section of the lake. Two large circulation cells between the thermal bars show a general broad upwelling in the middle portion of the lake and divergent flow from the center of the lake toward the thermal bar on each side of the lake. Two other smaller circulation cells are located between the thermal bars and their nearest shores. The four cells circulate clockwise and counterclockwise in such a way that sinking motions occur along the isotherms at the thermal bars and upwellings are present in the middle portion of the lake as well as at the both eastern and western shores. The zonal flows are almost entirely in the boundary regions. The flows along the slant-side-boundaries are more intense. The magnitude of zonal flow in the free surface Ekman layer is slightly stronger than that of the bottom layer. The vertical velocity apparently shows little change with depth. The maximum zonal velocity may reach 1 cm/sec and the maximum vertical velocity is in general two orders smaller.

VIII. COMPARISON OF THE RESULTS FROM THE THEORETICAL MODEL STUDY WITH FIELD OBSERVATIONS

As mentioned in the Introduction, Lake Michigan is one of the well surveyed large lakes in the world. Beginning at the end of the last century, a great many scientists have devoted themselves to the understanding of limnological phenomena and physical dynamics in the lake. Both current studies and temperature measurements in Lake Michigan are quite well documented. However, due to the complexity of the hydrodynamics in the lake and the multi-variability of the surrounding environment, detailed knowledge of the current circulation in Lake Michigan is still far from satisfactory. Since the thermal structure in the lake is more stable and the method for temperature measurement is simpler, much detailed and reliable field data of Lake Michigan are available.

Theoretical Results

In our theoretical study three types of temperature distributions and circulation patterns have been found at different periods of time around the year. During the winter-cooling period, the lake has already been cooled down to a temperature less than 4°C and both edges of the lake are still colder than the middle which is around the temperature of maximum density. The temperature distribution of this period has a profile shown in Figure 15, but the horizontal temperature difference is in the negative sense. This means that the isotherms are distributed as shown in Figure 15, but the temperature of each isotherm is successively decreasing from 4°C at the middle to the lowest temperature at the

edges. The meridional velocity circulation of this period is the type-A circulation as shown in Figure 17 with northbound flow on the east side and southbound flow on the west side of the lake. The zonal and the vertical velocity components as plotted as in Figure 18 which shows that two circulation cells converge at the middle of the lake. The winter-cooling period may last for quite a long period of time, from January to late March.

As the season progresses, the atmospheric temperature on the land has become much warmer than that of the lake in late March or early April. The spring-heating period has the temperature distribution shown in Figure 15. The meridional current during this period should be the type-B circulation with southbound flow on the east side and northbound flow on the west side of the lake as opposed to that shown in Figure 17. Since the middle portion of the lake is colder, being at temperatures less than 4°C, than the temperatures of edges at nearly 4°C, the zonal and vertical circulation is just opposite in direction to that shown in Figure 18. Note that the magnitudes of all current components are small.

The spring thermal bar period may start in late April or May. The temperature distribution is shown in Figure 16 with the middle portion of the lake at a temperature still below 4°C. The meridional current is more complicated as shown in Figure 19. The four-celled zonal and vertical circulation pattern unique to the thermal bar period is shown in Figure 20.

As soon as the thermal bar disappears, the summer-heating period exists before the lake becomes strongly stratified. The temperature of the summer-heating period is shown in Figure 15 and the currents belong to the type-A circulation.

Not until the long (nearly five months) strong-stratification period is over will the lake return to almost homogeneous conditions. The autumn-cooling period may start in late November or early December. The temperature distribution of the autumn-cooling period is exactly the same as in the winter-cooling period except the temperature of the whole lake is still at a temperature above 4°C and the maximum temperature at the middle is much higher than 4°C. The currents are typical type-B circulation.

The autumn thermal bar current, before the starting of the next cycle, is usually very weak and may possibly be hardly detected.

Closing the South End of the Lake Michigan Model

In our modeling considerations, since Lake Michigan is connected to Lake Huron, the length of the model is considered much longer than the width and the flow is treated as meridionally independent. Actually the south end of the lake is closed and the Straits of Mackinac also imposes some restrictions on the flow at the north end of the lake. However, we will notice that the dominant meridional current is anti-symmetrical to the center line of the lake. The meridional currents on each side of the lake are always flowing in opposite directions. Once the ends are closed or restricted, the theoretical flows on each side of the lake can be smoothly connected together at the ends by the continuity requirements, while the meridional currents become cyclonic or anti-cyclonic flows in the lake. We also notice in Figure 2 the existence of an everywhere positive north-south meridional temperature gradient. From the re-

sults obtained above, we deduce that the cyclonic flow in the lake is strengthened by this meridional temperature gradient, and the anticyclonic flow is weakened.

Comparison of Temperatures

Church (1942a,b) made a comprehensive study of the annual temperature cycle of Lake Michigan in many cross-sections of the lake during 1941-42. His temperature data, to my knowledge, are still the most complete for Lake Michigan. Some of his published figures are reproduced here for comparison with our results obtained from the theoretical study during the corresponding periods of the year. Figure 21 is the reproduction of Church's January temperature data across the Milwaukee-Muskegon section near the central part of Lake Michigan. As we noticed from Figure 21, the maximum surface temperature in the cross-section is at 4°C in the middle of the lake, while curved and concave isotherms decrease toward the shores. This is exactly the temperature distribution obtained in our theoretical study during the winter-cooling period discussed above, except that the former has sharper temperature gradient near the shores. Qualitatively, Figure 21 agrees very well with Figure 15. Figures 22 and 23 are the reproductions of Church's February and March temperature. They are all of the same distribution pattern as given by the theoretical study.

In late March or early April, the edges of the lake have already been warmed up to a temperature nearly 4°C or slightly above as shown in Figure 24, which is Church's observed temperature distribution of middle April. Figure 24 shows the characteristic temperature distribution of the spring-heating period

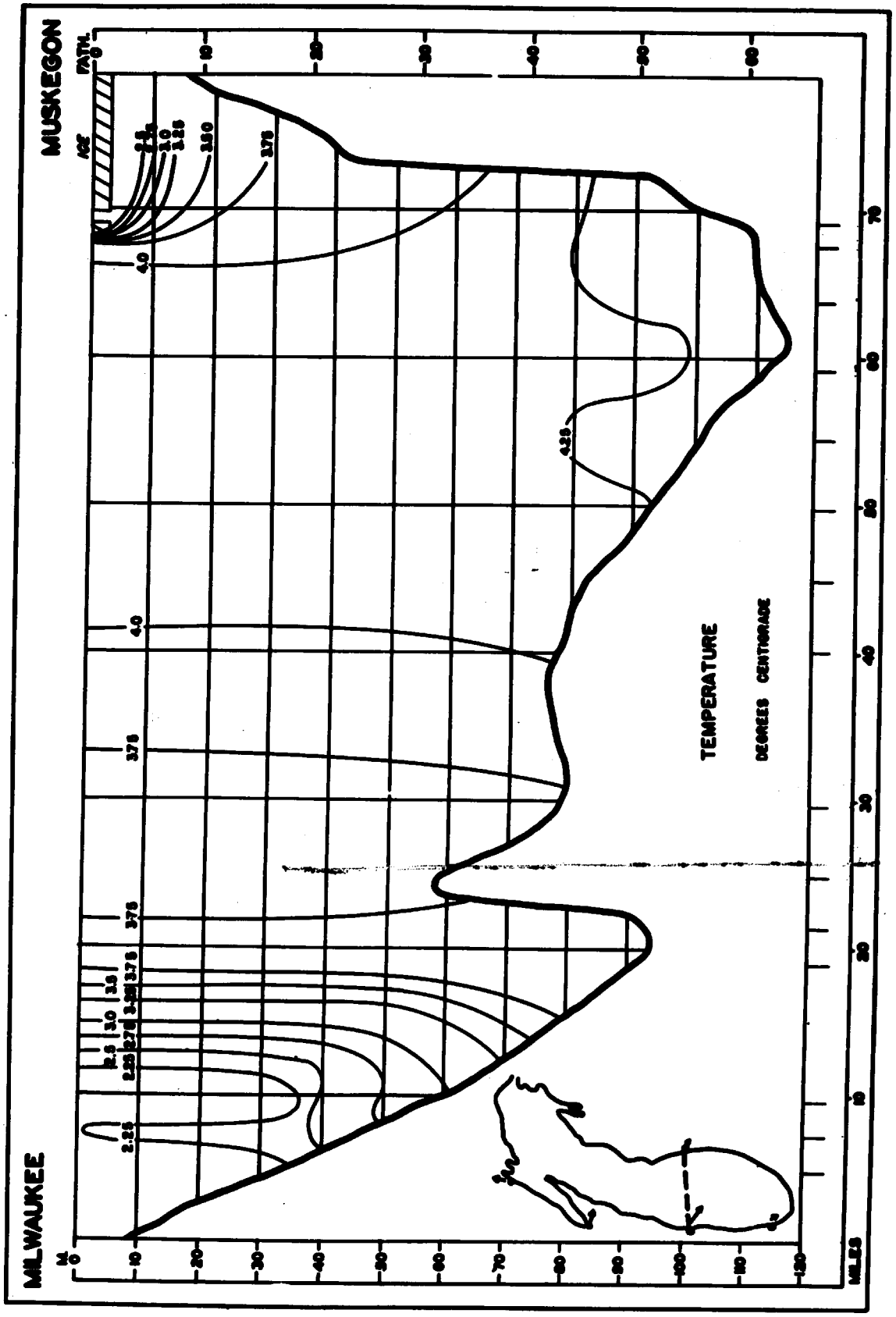


Figure 21. January temperature distribution across the Milwaukee-Muskegon section in Lake Michigan (from Church, 1942a,b).

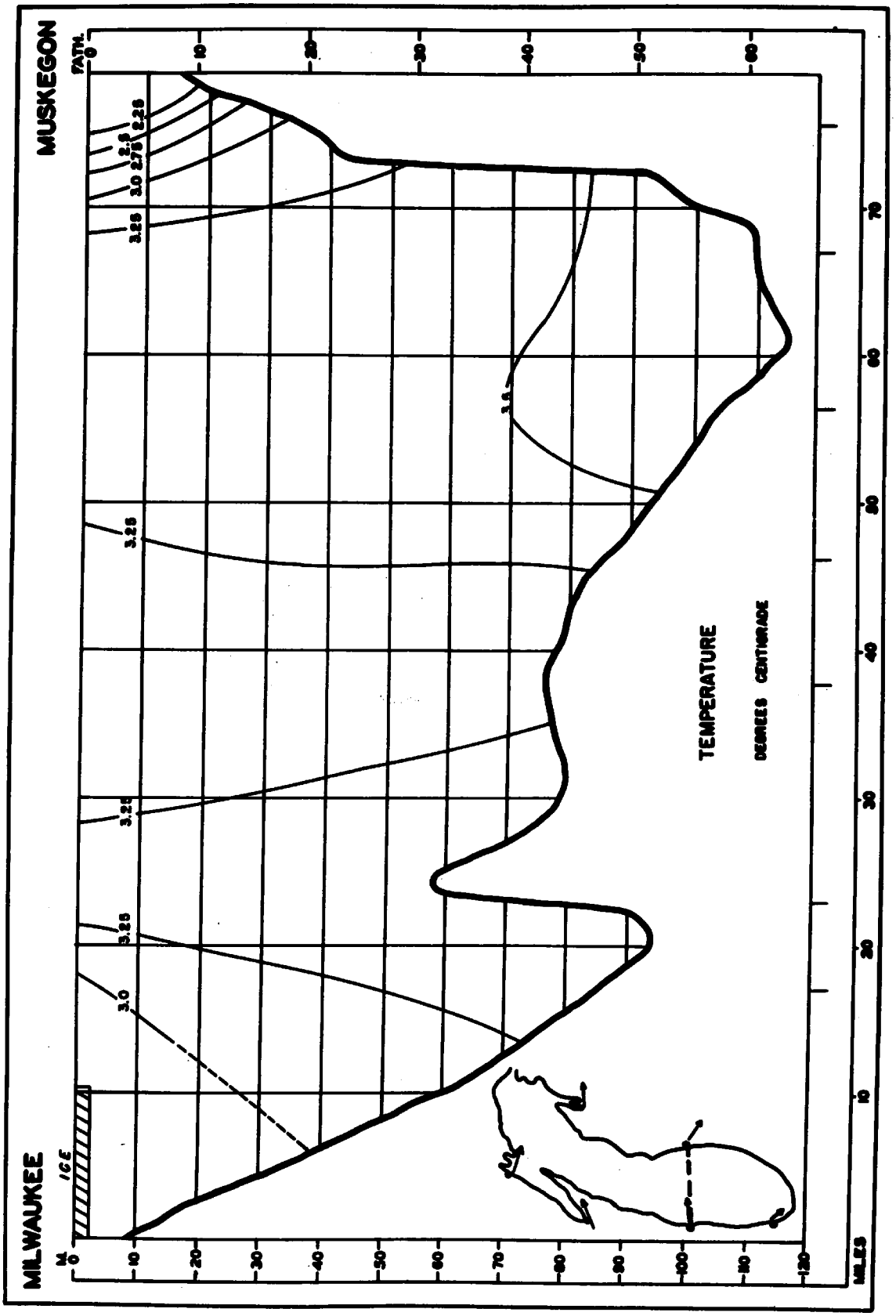


Figure 22. February temperature distribution across the Milwaukee-Muskegon section in Lake Michigan (from Church, 1942a,b).

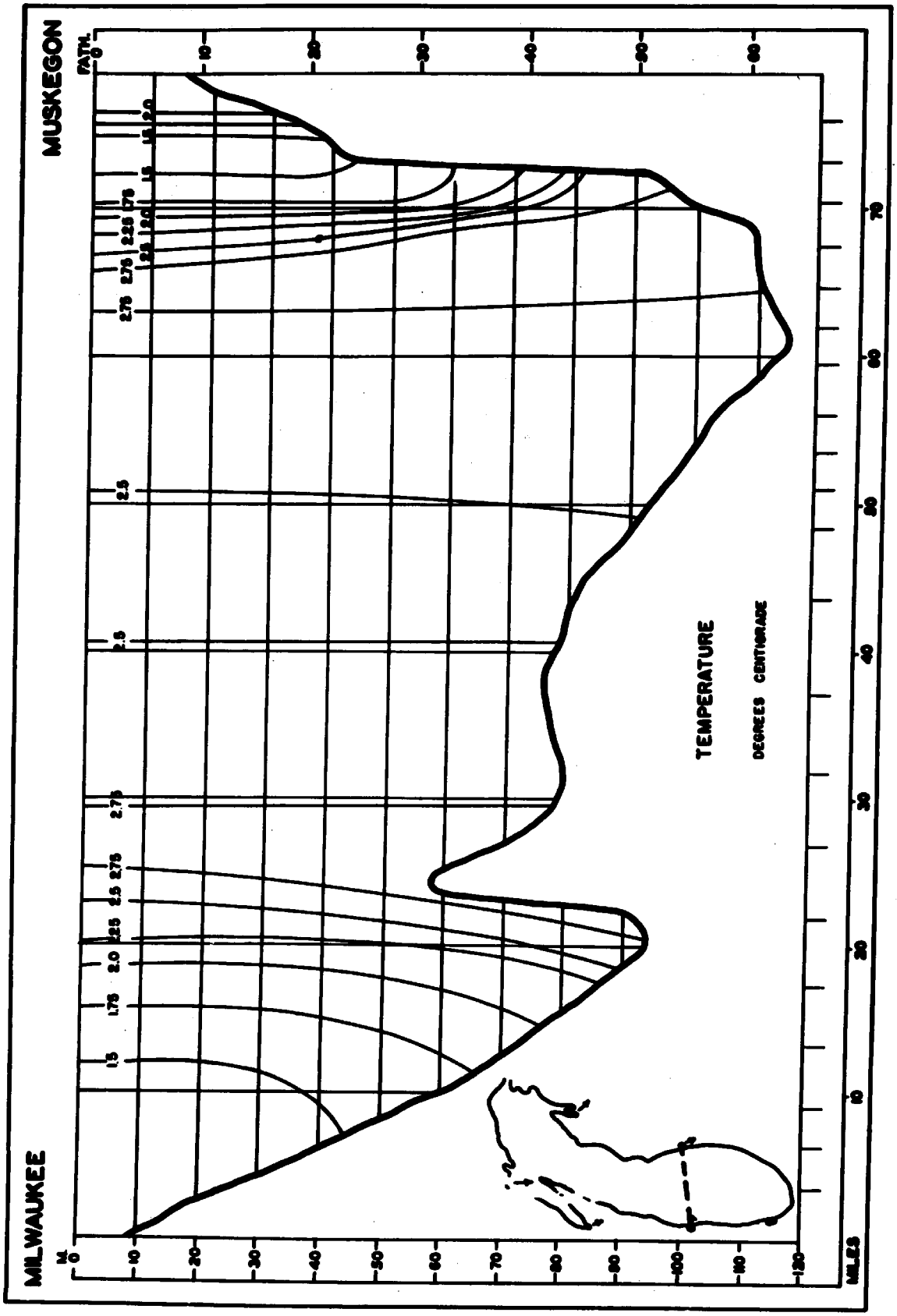


Figure 23. March temperature distribution across the Milwaukee-Muskegon section in Lake Michigan (from Church, 1942a,b).

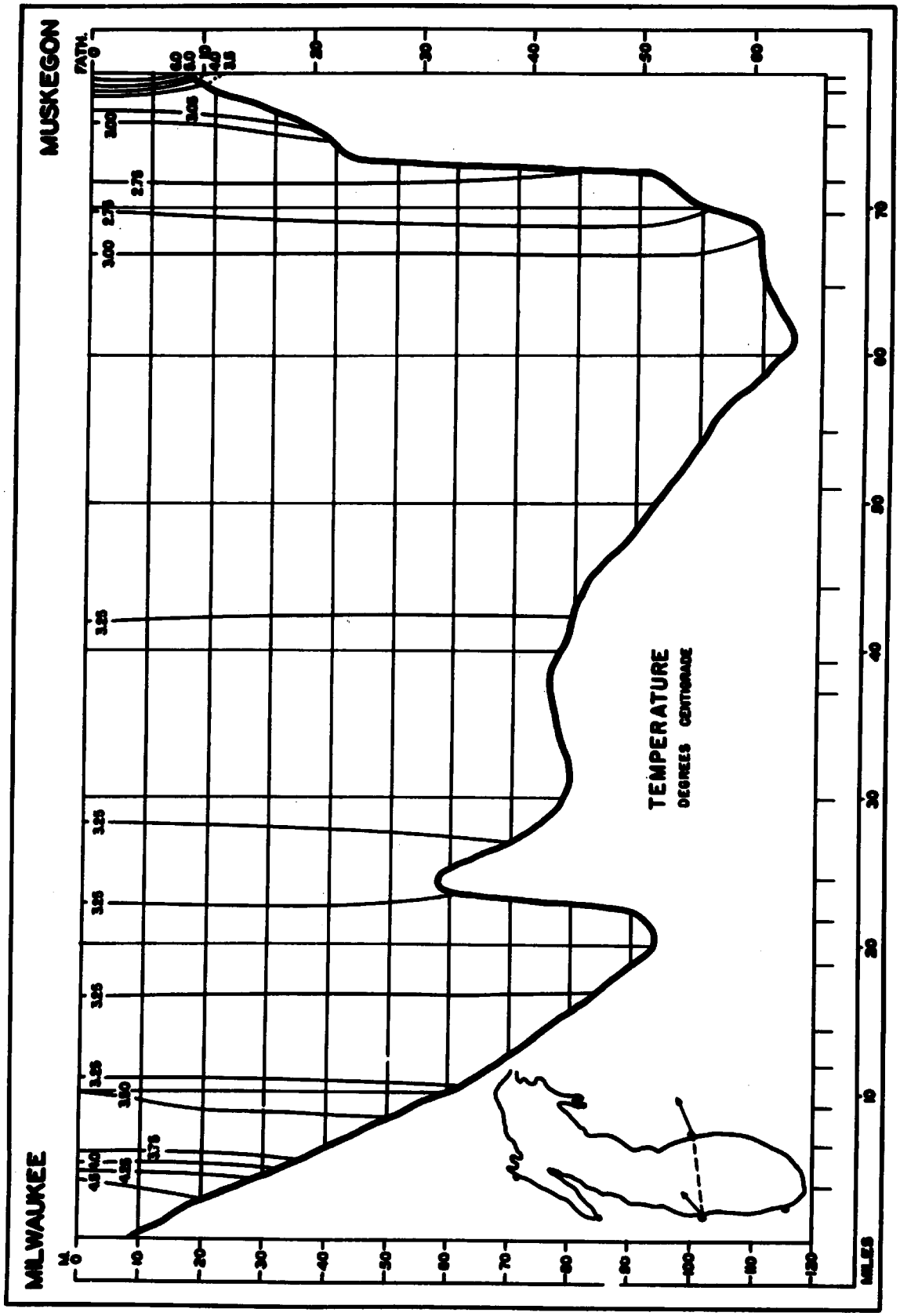


Figure 24. April temperature distribution across the Milwaukee-Muskegon section in Lake Michigan (from Church, 1942a,b).

which has two edges at nearly 4°C and the middle of the lake at slightly lower temperature. Qualitatively the theoretical prediction agrees well with the field data.

As the atmospheric temperature gets higher and higher, the thermal bar period immediately follows. Figure 24 already shows some of the beginning phenomenon of a thermal bar at each edge. Detailed temperature distribution across a thermal bar is not available from Church's temperature figures.

Rodgers (1965, 1966) has investigated the thermal bar in the Great Lakes and has measured the temperature across the thermal bar in great detail. His temperature section across the thermal bar is reproduced here as shown in Figure 25. Notice from Figure 25 the temperature near the east shore is above

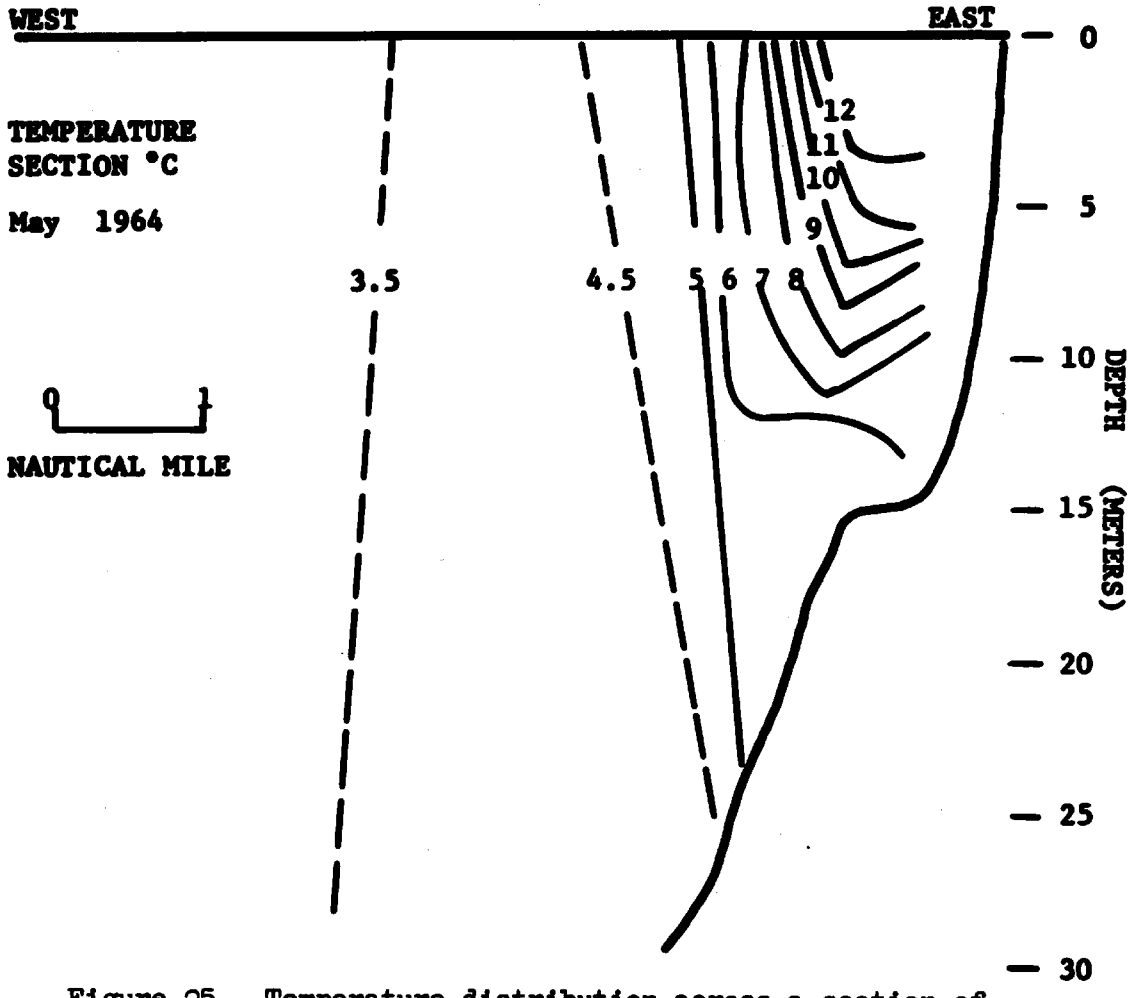


Figure 25. Temperature distribution across a section of the thermal bar (after Rodgers, 1965).

12°C and the temperature of the open lake indicated by the "west" end in the figure is less than the temperature of maximum density. The temperature between two broken isotherms shown in the figure is the band of fluid of nearly 4°C called the thermal bar. There is a strong horizontal temperature gradient toward the shore and a weak one toward the center of the lake. Isotherms between the thermal bar and the shore are concave up and shoreward. Noble and Anderson (1968) found the same temperature pattern across a thermal bar off Grand Haven in Lake Michigan as that of Rodgers in Lake Huron. The temperature distribution across a thermal bar shows exactly the features of our theoretical temperature solution during the thermal bar period obtained from the model study as shown in Figure 16.

The thermal bar period usually lasts four to six weeks. After the disappearance of the thermal bar the summer-heating period starts. The surface temperature of the lake is above 4°C everywhere at this stage with the minimum temperature near 4°C at the middle of the lake. Figure 26 is the reproduction of Church's May temperature data which shows the general feature of the summer-heating period and qualitatively agrees well with the theoretical temperature distribution of this period as shown in Figure 15. Figure 27 is the June temperature distribution of a cross section farther north of Lake Michigan, which still shows the basic temperature structure of the summer-heating period indicated in Figure 15.

The thermocline in Lake Michigan usually starts to form not long after the disappearance of the thermal bar and gets stronger in June as indicated in Figure 27. At the beginning, the thermocline may be very weak. The lake may

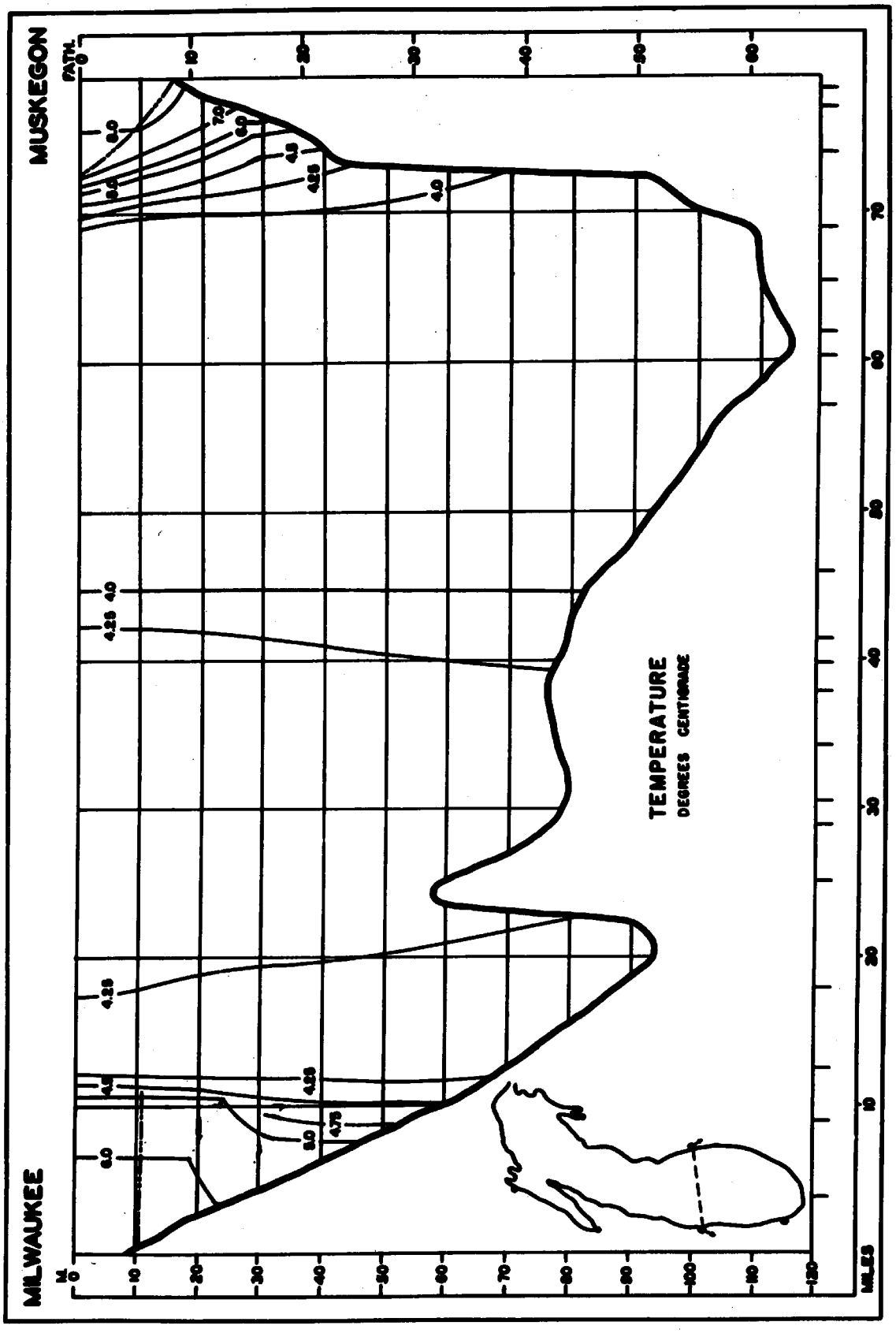


Figure 26. May temperature distribution across the Milwaukee-Muskegon section in Lake Michigan (from Church, 1942a,b).

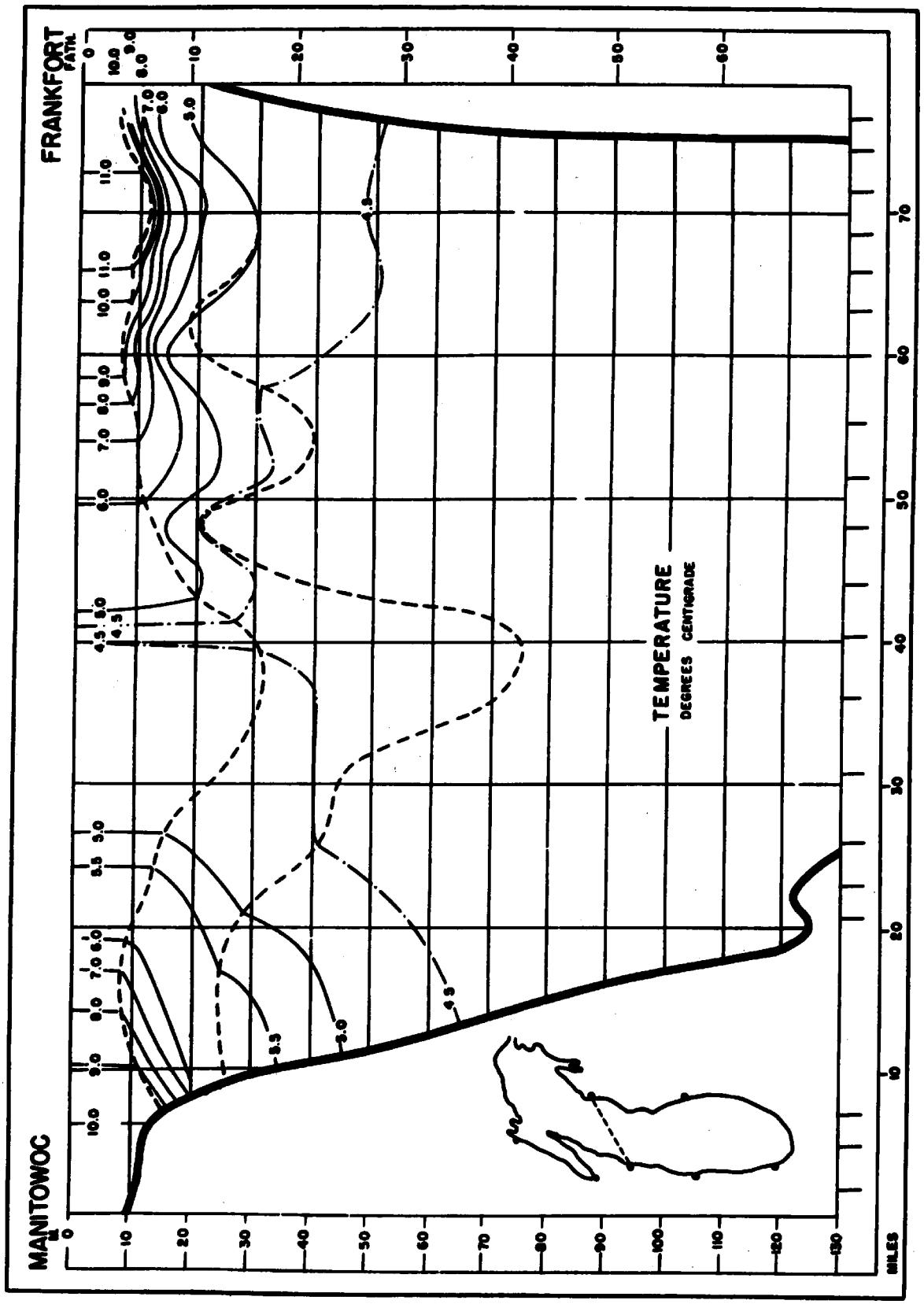


Figure 27. June temperature distribution across the Manitowoc-Frankfort section in Lake Michigan (from Church, 1942a,b).

form a shallow thermocline during the hot day which disappears at night. As the temperature gets higher and higher, the thermocline gets stronger and stronger after June. Not until the thermocline is very deep and weak in late November as indicated in Figure 28 can the lake be considered in a homogeneous state again. At that time the atmospheric temperature has already become colder than the temperature of the lake.

After the disappearance of the thermocline, the autumn-cooling period begins. The temperature at the middle portion of the lake is higher than that of the edges as shown in Figure 29. Qualitatively, Figure 29 also shows the predicted temperature feature indicated in Figure 15 with temperature decreasing toward shores.

There are no data available to compare the temperature distribution during autumn thermal bar period. It will happen theoretically after the autumn-cooling period when the edge temperature of the lake is already below 4°C. As we have mentioned, due to the smallness of the horizontal temperature differences and to the instability of the air mass above the lake the autumn thermal bar may be hardly observed.

In general, the predicted temperature distributions of our model study agree qualitatively very well with the observed field data. But the isotherms of the theoretical temperature solution are more widely spread and evenly distributed than the real data. The location of the thermal bar is also farther from shore than observed. This is because of the smoothed surface temperature profile we used as a boundary condition in solving the energy equation.

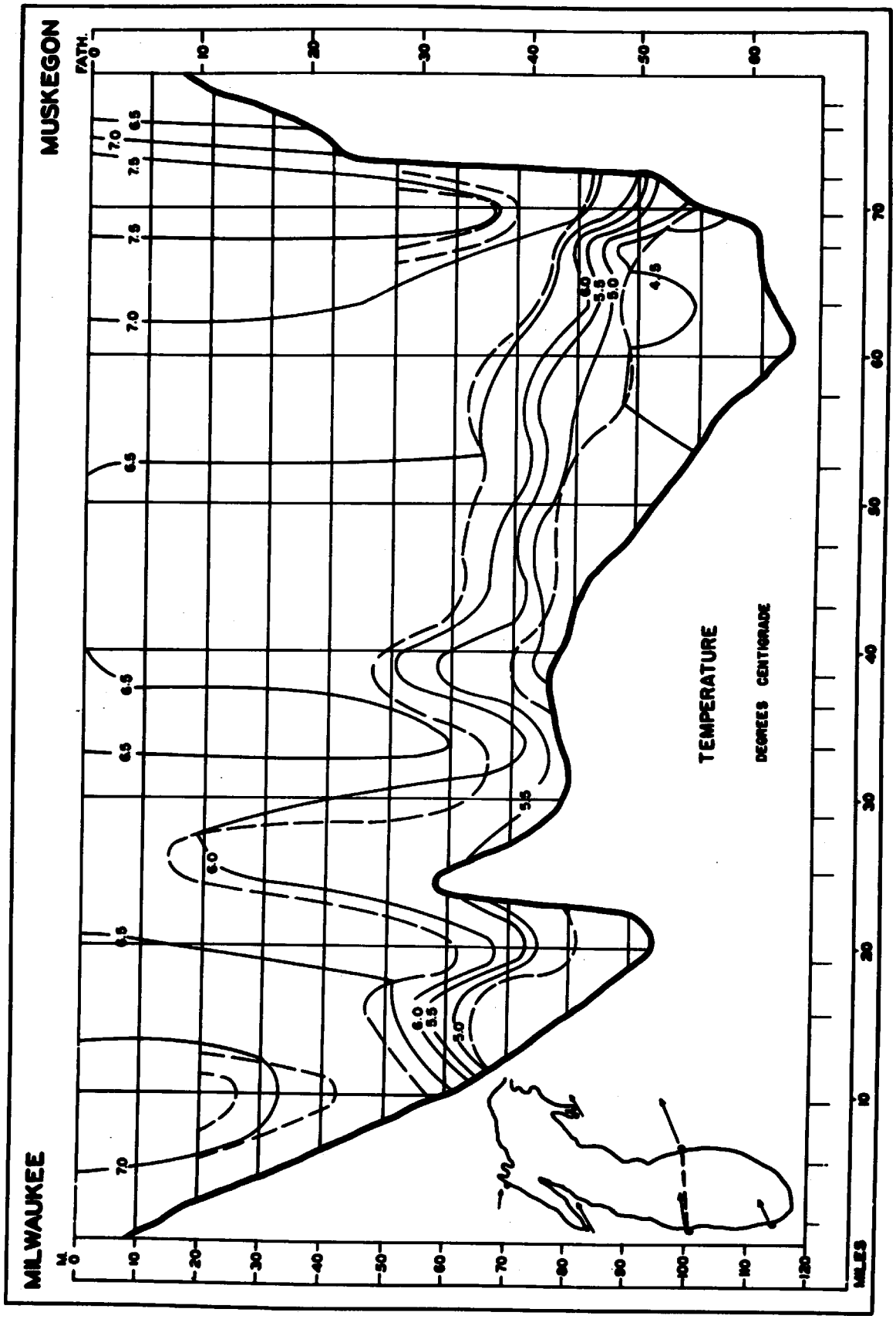


Figure 28. November temperature distribution across the Milwaukee-Muskegon section in Lake Michigan (from Church, 1942a,b).

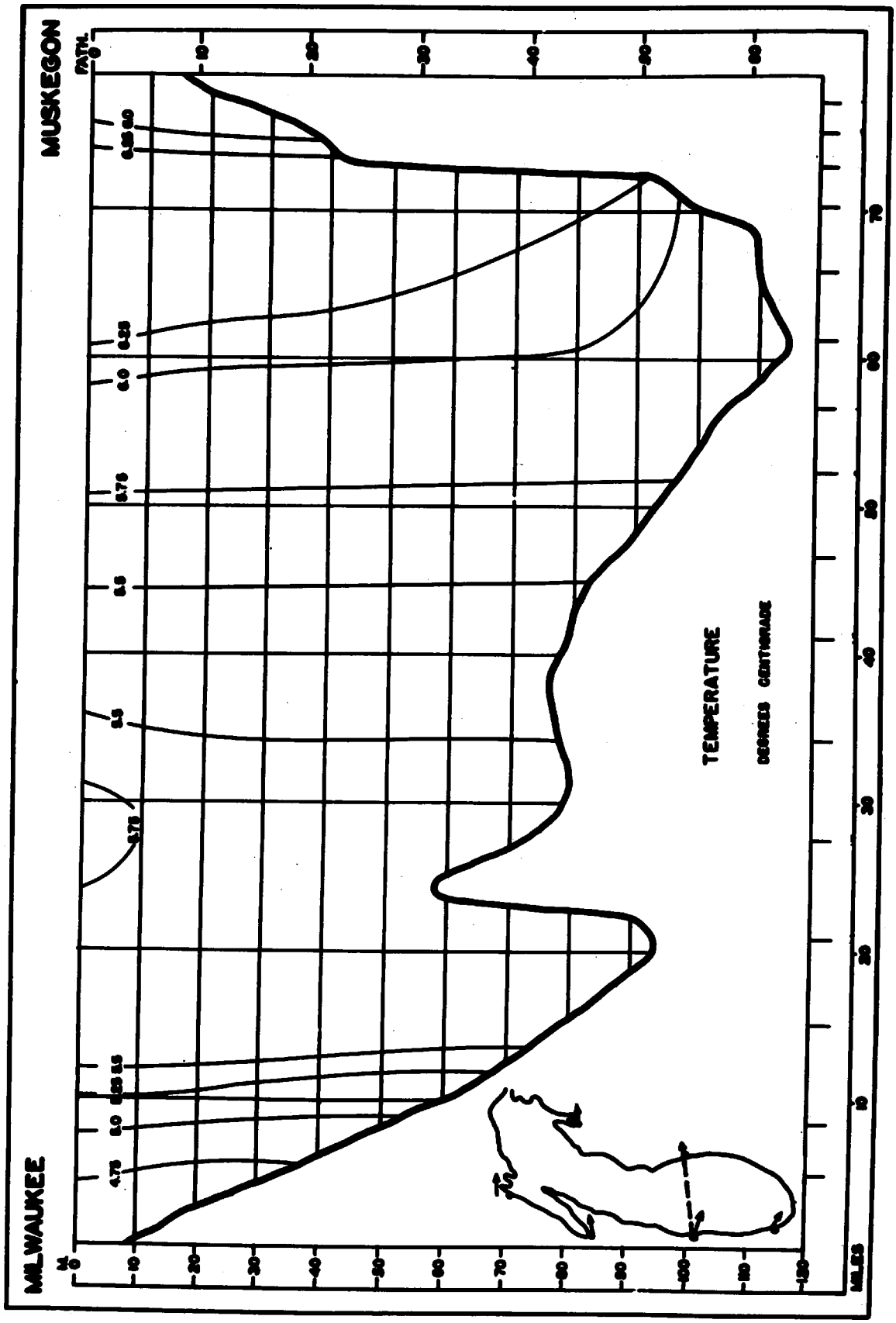


Figure 29. December temperature distribution across the Milwaukee-Muskegon section in Lake Michigan (from Church, 1942a,b).

Comparison of Velocity Field

MERIDIONAL VELOCITY

The configuration of surface current during the navigation season found by Harrington (1895) by means of drift bottles (drawn by Millar, 1952) was reproduced in Figure 1. His general mean current pattern in Lake Michigan shows a cyclonic circulation. There are also two cyclonic cells together with the general lake circulation, one well developed cell in the southern basin and another weaker cell in the northern basin. The northward current on the east side of the lake is very well defined. The southward current on the west side of the lake is weaker. The current in Lake Michigan varies in speed from 10 to 20 cm/sec.

Harrington's current pattern has no specific time correspondence with our defined time periods. However, the summer-heating period, the spring thermal bar period, the strong stratification period, and the autumn-cooling period are within the navigational season. Of course, the strong stratification period is out of our prediction. Of the other three periods, the two longer periods show cyclonic circulation in the lake. During the summer-heating period, the meridional velocity shown in Figure 17 gives a surface current pattern like that of Harrington. During the thermal bar period, the meridional velocity is shown in Figure 19 which shows that the currents close to both shores have cyclonic circulations while the middle portion of the lake has anticyclonic circulation. The circulation of the autumn-cooling period is reversed. In our model study, the current magnitudes may reach a maximum of 20 cm/sec during the summer-

heating season, 12 cm/sec during the spring thermal bar period which coincide with Harrington's measurements. However, due to the lack of precise time correspondences, the comparison between our theoretical solutions and Harrington's field results is very loose. The meridional circulations of the spring-thermal bar and the summer-heating periods agree qualitatively with Harrington's, but the autumn-cooling period does not. Furthermore, our simple model study does not show detailed eddy patterns in the lake.

Ayers et al. (1958) made four cruises of synoptic survey in Lake Michigan in 1955 and studied the current by using drift bottles, then computed the current circulation by the modified dynamic height method (Ayers, 1957). Their August current circulation, while the lake is strongly stratified at that time, is not predicted in our homogeneous model study. Their June surface currents have been reproduced here as shown in Figure 30. Though a relatively weak thermocline has already been formed during the time of their cruises, our summer-heating period circulation pattern should still be observed if there is no drastic change in the lake dynamic system. Ayers' June currents show, in general, a cyclonic circulation with two weaker cells in the northern and southern basin similar to that of Harrington's; but in addition, they found another large clockwise gyre near Benton Harbor, Michigan City area at the southern Lake Michigan basin. The magnitudes of currents they found are generally less than 10 cm/sec. Our meridional current of the summer-heating period is shown in Figure 17. Qualitatively, the general circulation pattern and speed magnitude agree well with Ayers' surface currents. Note that the detailed eddy circulations have been neglected in our model study.

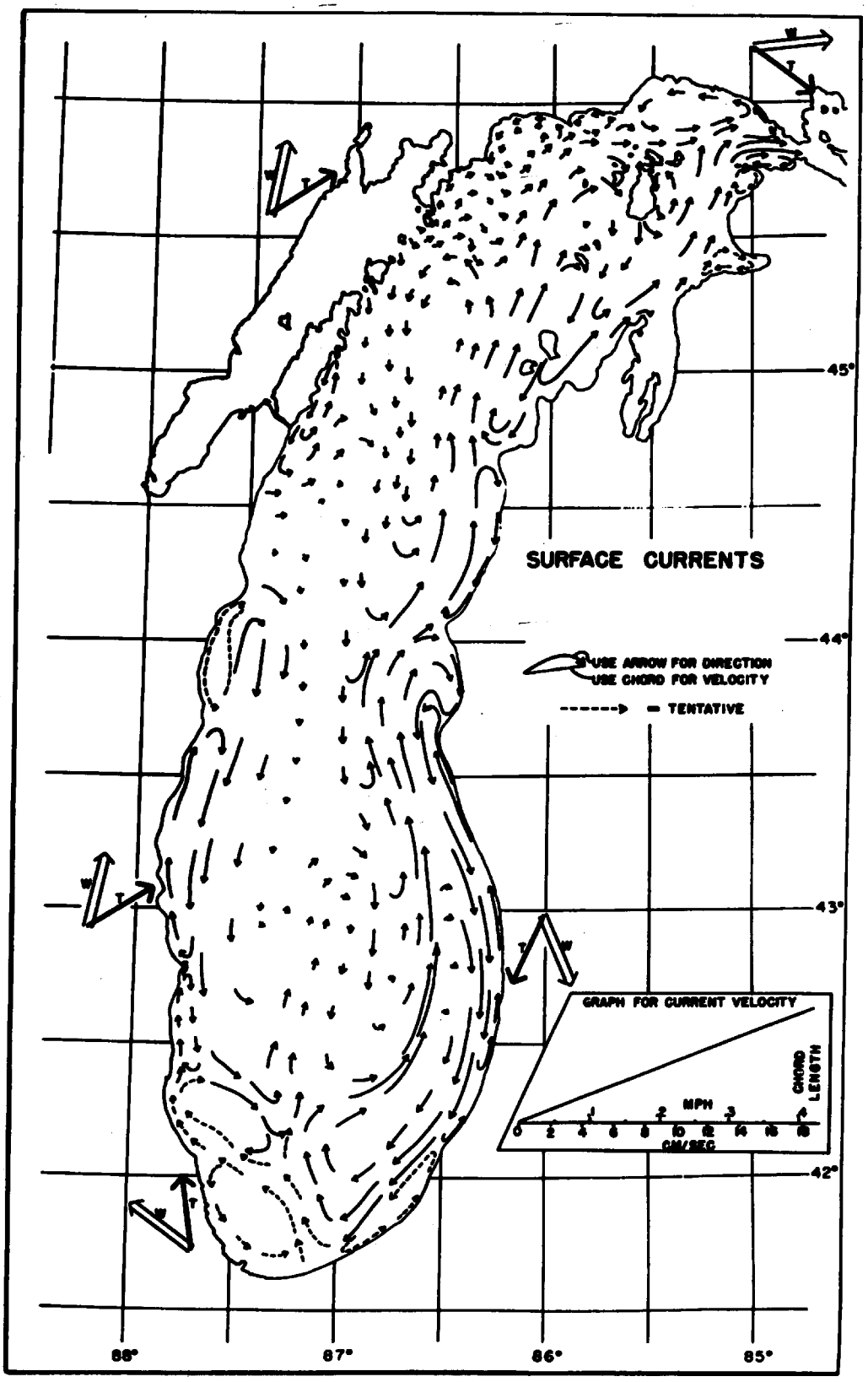


Figure 30. June surface currents in Lake Michigan (from Ayers et al., 1958).

In 1962 and 1964, the FWPCA deployed numerous temperature and current recording instruments at more than thirty stations all over the lake. At each station there was an instrument pair consisting of temperature recorder and current meter at each fixed depth of 10, 15, 22, 30 m and at each succeeding 30-m level. Unfortunately, these finely spaced, long period, lakewide recorded data have not been analyzed and published. Their preliminary report (U. S. Dept. of Interior, 1967) indicates that, generally speaking, surface currents in Lake Michigan are weak and southbound near the west shore, more intense and northbound near the east shore. No permanent type of circulation pattern has been found in Lake Michigan, but four basic patterns have been observed, two in winter and two in summer. Neglecting the summer patterns, their roughly defined winter surface circulation patterns are reproduced as shown in Figures 31 and 32. Figure 31 is the winter pattern which normally occurs from January to April though not necessarily in a continuous manner. This pattern accounts for 20 to 25 percent of the water movements during the year. This current pattern shows a general cyclonic circulation with an elongated gyre on the northern basin and another large gyre in the southern basin. The corresponding time in our categorization is the winter-cooling period which has shown in general the same circulation pattern indicated in Figure 17 as that in Figure 31. The other winter pattern they reported is shown in Figure 32 which is usually found after November through March intermittently. This time period is relevant for comparison with our autumn-cooling period which occurs after the thermocline is very deep and weak, or after it disappears. They both show an anticyclonic circulation. The eddy gyres and nearshore flows of the winter patterns do not agree

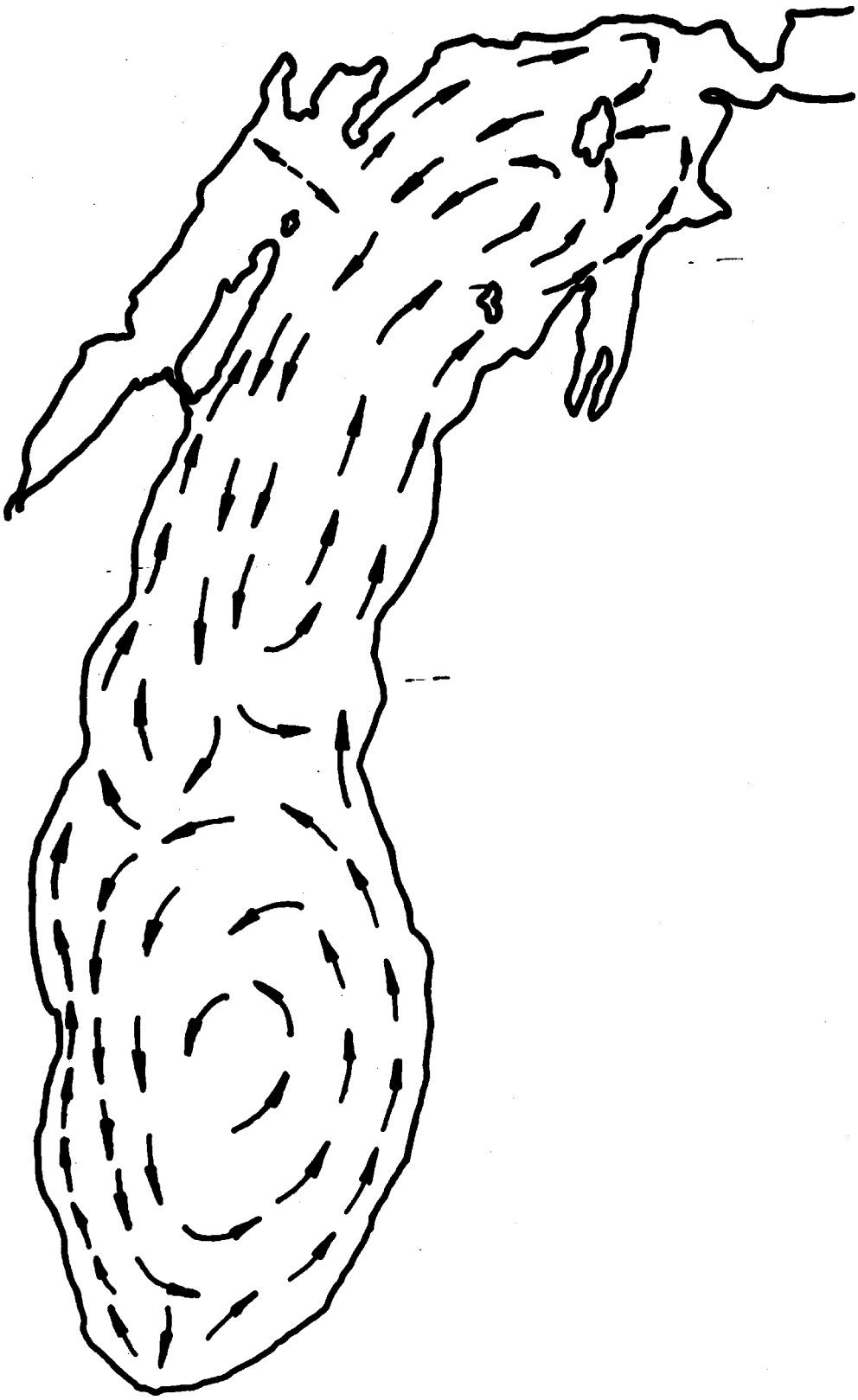


Figure 31. First basic winter surface current pattern in Lake Michigan (from U. S. Dept. of Interior, 1967).

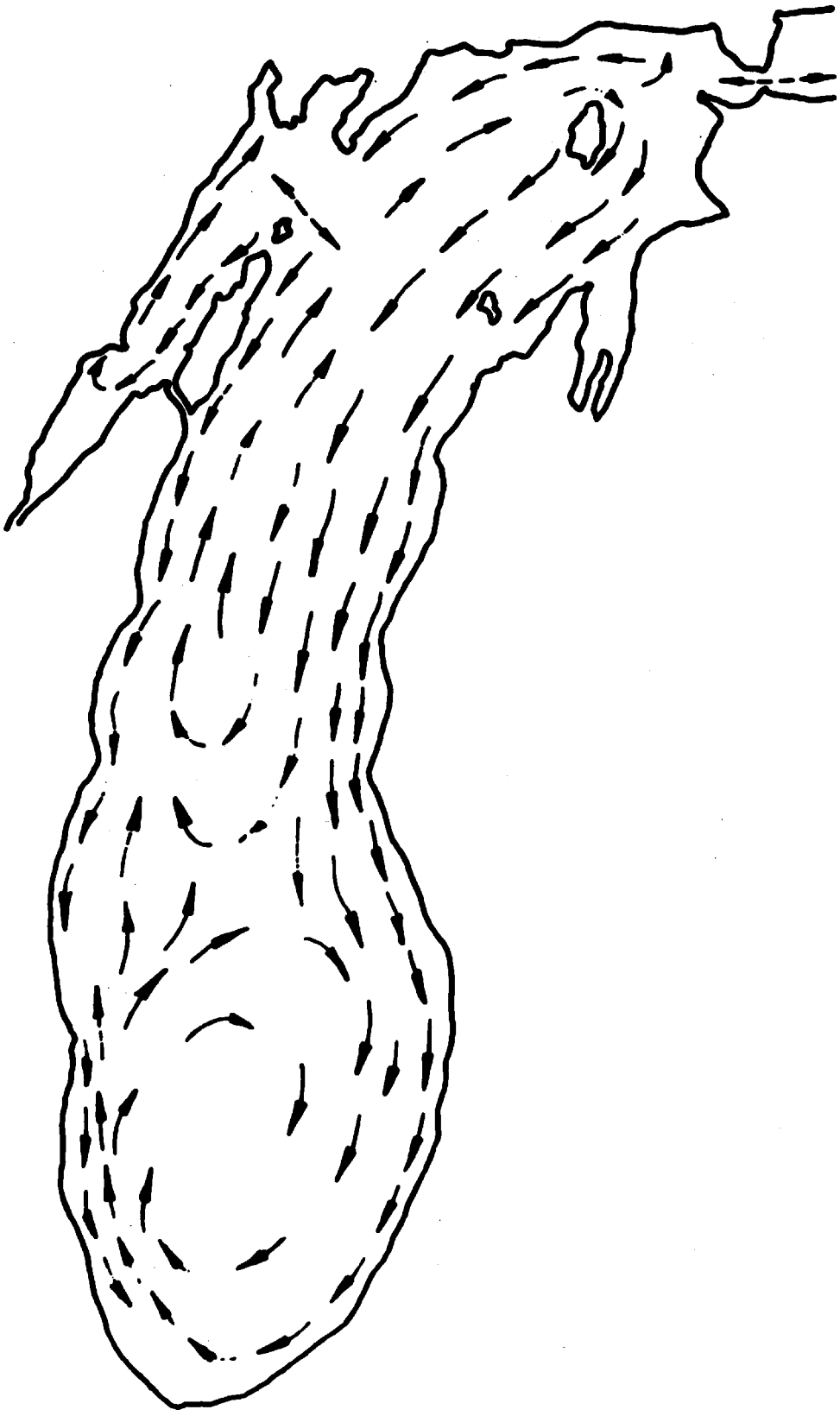


Figure 32. Second basic winter surface current pattern in Lake Michigan (from U. S. Dept. of Interior, 1967).

well with our theoretical prediction. This may be due to our neglect of wind stresses which is important to fluctuating currents, especially in the very shallow area as well as the uppermost surface layer of the lake.

On 10 May and 27 June 1968, we ran two sets of drogues for the current study in the west side of Lake Michigan outside of Milwaukee Harbor as indicated in Figure 33. The wind conditions, positions of each fixed point, running time, and current speed are shown in Table 13. Currents were flowing southward in

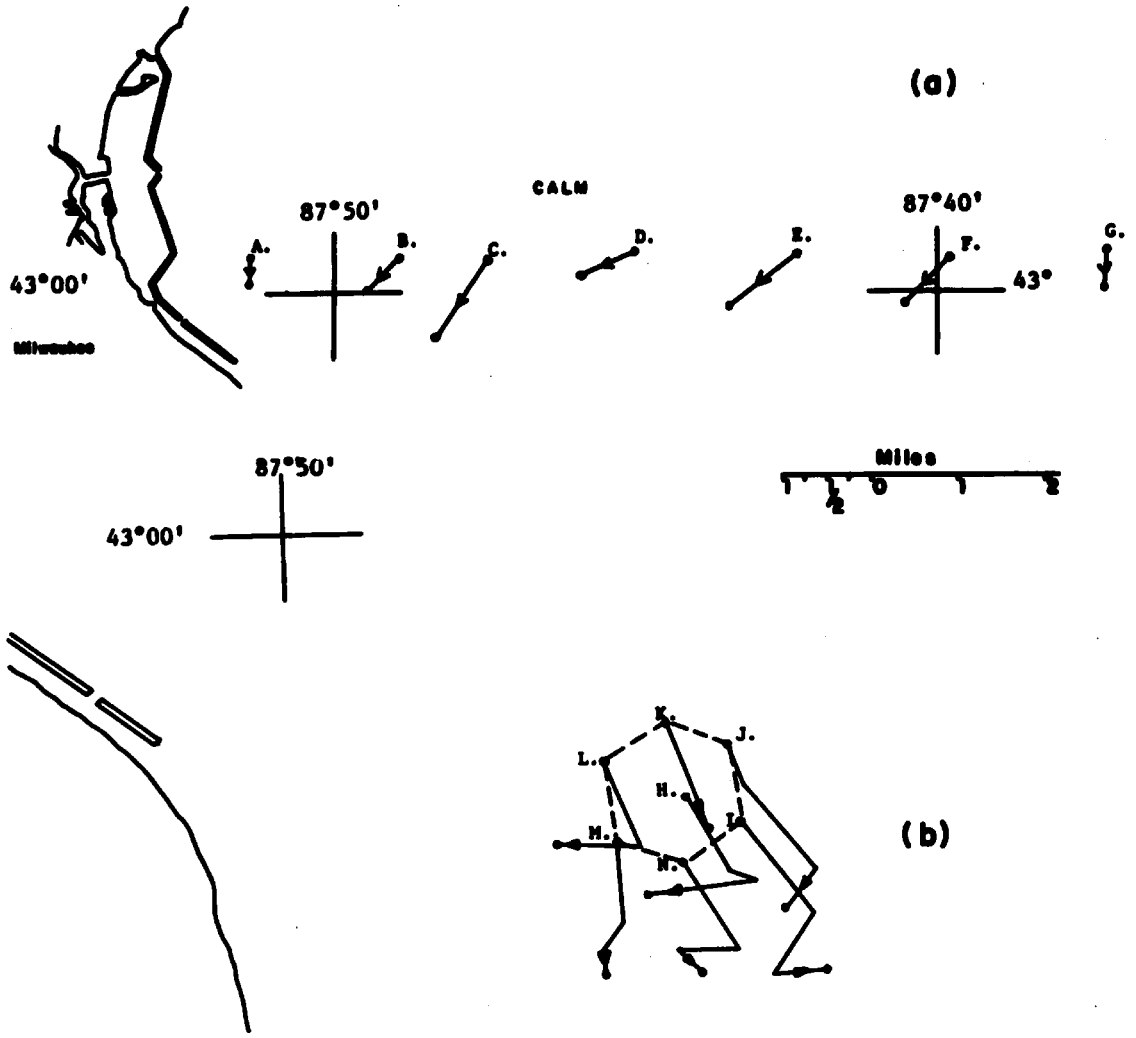


Figure 33. Drogue studies for surface current measurements near western shore. (a) 10 May 1968. (b) 27 June 1968.

TABLE 13

Drogue Studies of Surface Current on the West Side of Lake Michigan

Date		10 May 1968					27 June 1968				
Wind		N, 4 kt					NxW, 6 kt				
Lake Condition		Calm					1 ft Wave				
	Station	Time		Speed, cm/sec	Mean, cm/sec	Station	Time		Speed, cm/sec	Mean, cm/sec
		Start	Finish				Start	Finish		
Drogue Study	A	0800	1506	3.12		H	1245	1848	4.91	
	B	0815	1520	4.73		I	2151	1820	9.86	
	C	0821	1532	8.02		J	1301	1813	10.74	
	D	0837	1548	4.91	5.39	K	1308	1805	7.14	7.6
	E	0848	1604	7.58		L	1314	1856	4.91	
	F	0859	1620	5.36		M	1321	1840	8.47	
	G	0912	1635	4.01		N	1327	1831	7.14	

agreement with our meridional currents on the west side of the lake during the summer-heating period. On the east side of the lake, a tripod-supported pendulum current meter was installed 230 m offshore at a depth of 5 m from 11 May to 11 October 1967 under Dr. Ayers' direction. The late spring and early summer current directions are summarized in Table 14. We notice that most of the currents flow northward near the east shore of the lake during the summer-heating period, which agrees well with our meridional velocity solution prediction.

TABLE 14

Percentage of Hours Current Flowed Northward, Westward, and Southward on the East Side of Lake Michigan Near Benton Harbor, Michigan

Month	Current, %		
	Northward	Westward	Southward
May	96.7	3.0	0.3
June	95.2	4.8	0
July	97.1	2.9	0

ZONAL AND VERTICAL VELOCITIES

Due to the smallness in magnitudes of the zonal and vertical velocities there are not much field data available for comparisons with our theoretical current circulations in the cross-section of Lake Michigan. However, the thermal bar phenomenon in a large dimictic lake is quite well observed and documented by Tikhomirov (1963), Rodgers (1965, 1966), and others. The thermal bar is established in the spring-warming-up season when the shallow inshore edges of the lake have been warmed to above 4°C, while the deep open-lake-water is still less than 4°C. At the junction of the two waters, a boundary band of water (the thermal bar) of nearly 4°C is created by mixing of the warmer inshore water and the colder offshore water. The 4°C water formed at the thermal bar is denser and it sinks. The sinking water is replaced by a shoreward surface flow from the deep open-lake toward the thermal bar, and by a lakeward surface flow from the inshore region toward the thermal bar. The convergence zone is readily observed by the windrows of dead fish, trash, and garbage accumulated along the thermal bar.

Rodgers (1965) has deduced a thermal bar circulation as shown in Figure 34. There are four cells circulating contratotationally in the cross section with sinking motion along the 4°C isotherms at the thermal bars and upwellings at the middle as well as on both edges of the lake. This kind of current pattern is exactly our thermal bar circulation as shown in Figure 20. Note that we use a smoother temperature profile in our model investigation which results in moving the thermal bar farther out to the open lake.

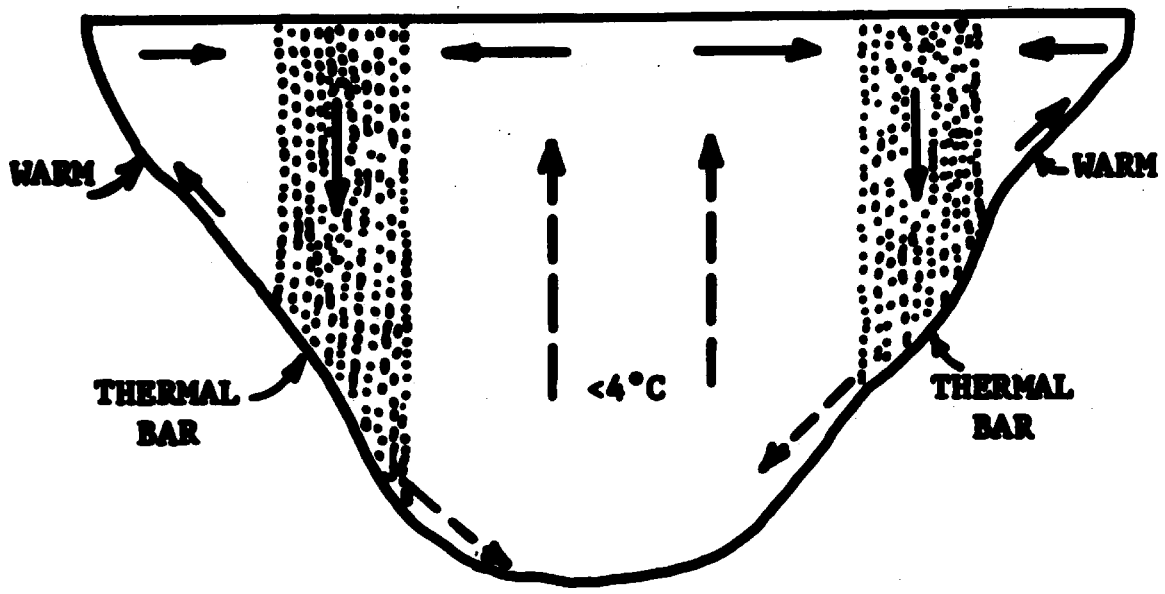


Figure 34. Thermal bar circulation (after Rodgers, 1965).

The actual condition of the thermal bar mixing phenomenon is considerably more complex as indicated in the aerial photograph (Figure 35) taken along the thermal bar near Grand Haven in Lake Michigan during the spring of 1968. Zonal and vertical current measurements of the thermal bar circulation are very difficult, not only because of their small magnitudes but also because of their being obscured by other factors.

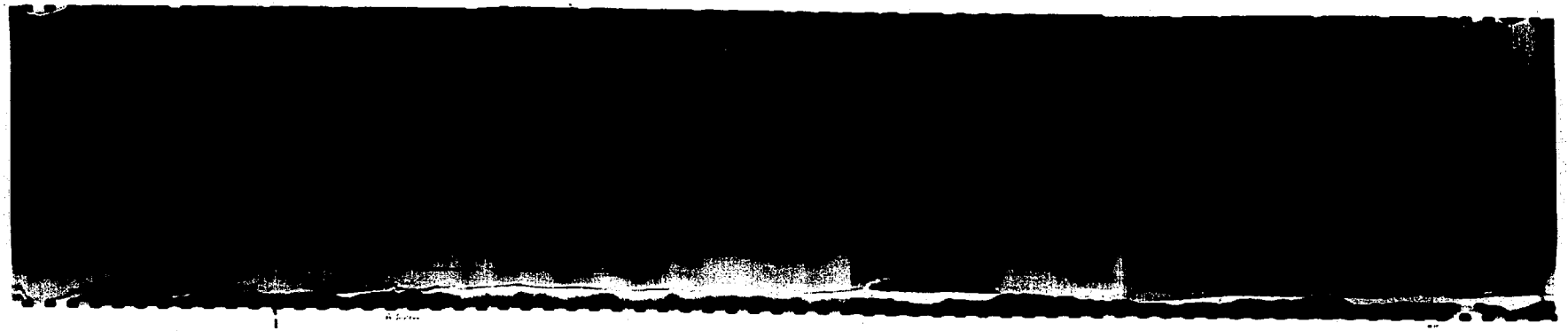


Figure 35. Aerial photograph of thermal bar phenomena on 7 May 1968 near Grand Haven, Michigan. The darker part is at the temperature around 4°C (kindly supplied by Mr. F. C. Polcyn, Infrared and Optical Sensor Laboratory, The University of Michigan, in cooperation with NASA Flight.)

IX. CONCLUSIONS

We have theoretically investigated the thermally induced current in Lake Michigan. Using the procedure of double perturbation expansions outlined in Chapter III, approximate solutions have been obtained for the whole flow field, except for four unimportant corners. Approximation errors of the solutions are estimated to be the order of (Rossby number)^2.

Two types of nondimensional temperature distributions have been found. One type prevails during all the general thermal current periods, namely winter-cooling, spring-heating, summer-heating, and autumn-cooling periods, with the temperature distributions as shown in Figure 15. The other type prevails during thermal bar periods, both spring and autumn, as shown in Figure 16. Three types of circulation pattern have been found in the model study. There are the type-A and the type-B circulation patterns, the general thermal currents (Figures 17 and 18), and the type-C circulation pattern (Figures 19 and 20). The type-B currents are exactly the opposite of the type-A currents. The type-C circulation is unique for the thermal bar phenomena.

In trying to verify the theoretical thermal circulation currents, some field measurements for currents and eddy viscosities were conducted in 1967 and 1968 in Lake Michigan. Comparisons have been made between predictions obtained from our mathematical study and previously published field data such as those of Harrington (1895), of Church (1942a,b), of Ayers et al. (1958), and of Rodgers (1965). Qualitatively, the theoretical temperature distribution and the thermal current structure agree very well with the real field

observations in Lake Michigan during the corresponding seasons. This leads one to postulate that the thermal body force does play an important role in generating the mean lake circulation patterns.

Our theoretical solutions do not show large eddies in the southern and northern basins which have been observed. This is perhaps because the model assumes a flat bottom.

The agreements between the theoretical solutions and the field observations are rather poor in the shallow regions. This may well be the result of the faster response of the shallow water current to wind stresses and of the irregularities of the coastlines. Due to the neglect of wind stresses, the model current circulation is not expected to coincide with instant current measurements, especially in the shallow water or at the upmost surface layer, but it is expected to be valid for the prediction of the mean current circulation pattern in the lake.

As to the thermal currents in Lake Michigan during the strongly stratified period in the summer and early autumn, further theoretical work needs to be done.

REFERENCES

Ayers, J. C. 1957. A dynamic height method for the determination of currents in deep lakes. Limnology and Oceanography, 2:150-161.

_____. 1962. Great Lakes Water, their circulation and physical and chemical characteristics. Amer. Assoc. Adv. Sc., Publ. No 71: 71-89.

_____, D. C. Chandler, G. H. Lauff, and C. F. Powers. 1958. Currents and water masses of Lake Michigan. Univ. of Michigan, Great Lakes Research Division, Publ. No. 3, 169 p.

Barcilon, Victor. 1964. Role of the Ekman Layers in the stability of the symmetric regime obtained in a rotating annulus. J. of the Atmospheric Sciences, 21:291-299.

Batchelor, G. K. 1953. The theory of homogeneous turbulence. Cambridge University Press, 193 p.

_____ and A. A. Townsend. 1956. Turbulent diffusion. Surveys in Mechanics. Cambridge University Press, pp. 352-399.

Bellaire, F. R. 1965. The modification of warm air moving over cold water. Proc. 8th Conf. on Great Lakes Research, Univ. of Michigan, Great Lakes Research Division Publ. No. 13, pp. 249-256.

Boussinesq, J. 1877. Theorie de l'ecoulement tourbillant. Mem. Proc. Acad. Sci. XXII, 46. Paris.

Bowden, K. F. 1964. Turbulence. Oceanographic and Marine Biology Annual Review, 2:11.

_____, K. F. 1965. Horizontal mixing in the sea due to a shearing current. J. Fluid Mech., 21:83-95.

Bowles, P., R. H. Burns, F. Hudswell, and R.R.P. Whipple. 1958. Sea disposal of low activity effluent. Proc. 2nd International Conf. Peaceful Use of Atomic Energy. United Nations, N. Y., 18:376-389.

Brindley, J. 1960. Stability of flow in a rotating viscous imcompressible fluid subjected to differential heating. Royal Soc. London, Phil. Trans., A253:1-25.

Carrier, G. T. 1953. Boundary layer problems in applied mechanics. Adv. in Applied Mech., 3:1-19.

Charnock, H. 1959. Tidal friction from currents near the sea bed. Geophys. J., 2:215-221.

Church, P. E. 1942a. The annual temperature cycle of Lake Michigan. Univ. of Chicago, Institute of Meteorology, Misc. Report No. 4, 48 p.

_____. 1942b. The annual temperature cycle of Lake Michigan. Univ. of Chicago, Institute of Meteorology, Misc. Report No. 18, 100 p.

Csanady, G. T. 1963. Turbulent diffusion in Lake Huron. J. Fluid Mech., 17:360-383.

_____. 1964. Turbulence and diffusion in the Great Lakes. Univ. of Michigan, Great Lakes Research Division Publ. No. 11:326-339.

_____. 1966. Accelerated diffusion in the skewed shear flow of lake currents. J. Geophys. Res., 71:411-420.

_____. 1967. Large-scale motion in the Great Lakes. J. Geophys. Res., 72:4151-4162.

_____. 1968a. Motions in a model great lake due to a suddenly imposed wind. J. Geophys. Res., 73:6435-6447.

_____. 1968b. Wind-driven summer circulation in the Great Lakes. J. Geophys. Res., 73:2579-2589.

Davies, T. V. 1956. The forced flow due to heating of a rotating fluid. Royal Soc. London, Phil. Trans., A249:27-64.

_____. 1959. On the forced motion due to heating of a deep rotating liquid in an annulus. J. Fluid Mech., 5:593-621.

Davis, R. A. and D.F.R. McGeary. 1965. Stability in near-shore bottom topography and sediment distribution, southeastern Lake Michigan. Proc. 8th Conf. on Great Lakes Research, Univ. of Michigan, Great Lakes Research Division Publ. No. 13:222-231.

Deacon, E. L. 1962. Aerodynamic roughness of the sea. J. of Geophys. Res., 67:3157-3172.

Deason, H. J. 1932. A study of surface currents in Lake Michigan. The Fisherman, 1:3-4, 12.

Defant, A. 1961. Physical oceanography. MacMillan Co., N. Y., Vol. I, 729 p.

Eady, E. T. 1949. Long waves and cyclone waves. Tellus, 1:33-52.

Ekman, V. W. 1905. On the influence of the earth's rotation on ocean currents. Arkiv. Mat. Astr. Fysik., 2:1-52.

Elder, F. C. and H. S. Soo. 1967. An investigation of atmospheric turbulent transfer processes over water. Univ. of Michigan, Great Lakes Division Special Report No. 29, 46 p.

Farlow, J. S. 1965. A field technique used for horizontal diffusion studies in Lake Michigan and Lake Erie. Proc. 8th Conf. on Great Lakes Research, Univ. of Michigan, Great Lakes Research Division Publ. No. 13:299-303.

Fowlis, W. W. 1963. An experimental study of the transitions between the flow regimes of thermal convection in rotating annulus of liquid. Ph.D. Thesis, Univ. of Durham, England, 188 p.

_____ and R. Hide. 1965. Thermal convection in a rotating annulus of liquid; effect of viscosity on the transition between axisymmetric and non-symmetric flow regimes. J. Atmosph. Sc., 22:541-558.

Foxworthy, J. E. and G. M. Barsom. 1967. Comments on paper by G. T. Csanady "Accelerated diffusion in the skewed shear flow of lake currents." J. Geophys. Res., 72:2683-2691.

Fultz, D. 1953. A survey of certain thermally and mechanically driven fluid systems of meteorological interest. Fluid models in geophysics. Proc. 1st Symposium on the Use of Models in Geophysical Fluid Dynamics. Baltimore, Maryland, pp. 27-63.

Greenspan, H. P. and L. N. Howard. 1963. On the time-dependent motion of a rotating fluid. J. Fluid Mech., 17:385-404.

Hadley, G. 1735. Concerning the cause of the general trade winds. Royal Soc. London, Phil. Tans., 39:58-63.

Harrington, M. W. 1895. Surface currents of the Great Lakes. U. S. Dept. of Agriculture, Weather Bureau, Bull. B.

Hide, R. 1953. Some experiments on thermal convection in a rotating liquid. Royal Meteorological Soc., Quart. Jour., 79:161.

_____. 1958. An experimental study of thermal convection in a rotating liquid. Royal Soc. London, Phil. Trans., A250:441-478.

_____. 1964. The viscous boundary layer at the free surface of a rotating baroclinic fluid. Tellus, 16:523-529.

Hill, M. N. Ed. 1962. The sea. Vol. I. Physical oceanography. Interscience, Wiley, N. Y., 864 p.

Hinze, J. O. 1959. Turbulence. McGraw-Hill, N. Y., 586 p.

Hough, J. L. 1958. Geology of the Great Lakes. University of Illinois Press, Urbana, Ill., 313 p.

Hunt, I. A. 1959. Winds, wind set-ups, and seiches on Lake Erie. U. S. Lake Survey, Detroit, Michigan, 59 p.

Hunter, C. 1967. The axisymmetric flow in a rotating annulus due to a horizontally applied temperature gradient. J. Fluid Mech., 27:753-778.

Hutchinson, G. E. 1957. A treatise on limnology. Vol. I. Geography, Physics, and Chemistry. Wiley, N. Y., 1015 p.

Kolmogoroff, A. N. 1941. The local structure of turbulence in an incompressible viscous fluid for very large Reynolds number. Doklady Akad. Nauk U.S.S.R. Geophys., Ser.3:405-413.

Kuo, H. L. 1957. Further studies of thermal motions in a rotating fluid. J. Meteorology, 14:553-558.

Lamb, H. 1932. Hydrodynamics. Dover, N. Y., 673 p.

Lesser, R. M. 1951. Some observations of the velocity profile near the sea floor. Amer. Geophys. Union, Trans. 32:207-211.

McFadden, J. D. and R. A. Ragotzkie. 1963. Aerial mapping of surface temperature pattern of Lake Michigan. Proc. 6th Conf. on Great Lakes Research, Univ. of Michigan, Great Lakes Research Division Publ. No. 10:55-58.

Millar, F. G. 1952. Surface temperatures of the Great Lakes. Fish Res. Bd. Canada Jour., 9:329-376.

Mortimer, C. H. 1963. Frontiers in physical limnology with particular reference to long waves in rotating basins. Proc. 6th Conf. on Great Lakes Research, Univ. of Michigan, Great Lakes Research Division Publ., 10: 9-42.

Munk, W. H. 1950. On the wind-driven ocean circulation. J. Meteorology, 7:79.

Noble, V. E. 1966. Vertical current structure in the Great Lakes. University of Michigan, Great Lakes Research Division Special Report No. 27, 42 p.

_____. 1967. Evidences of geostrophically defined circulation in Lake Michigan. Proc. 10th Conf. on Great Lakes Research, pp. 289-298. International Association for Great Lakes Research.

Noble, V. E. and R. F. Anderson. 1968. Temperature and current in the Grand Haven, Michigan vicinity during thermal bar conditions. Proc. 11th Conf. on Great Lakes Research, pp. 470-479. International Association for Great Lakes Research.

Noble, V. E. and J. C. Ayers. 1961. A portable photocell fluorometer for dilution measurements in natural waters. Limnology and Oceanography, 6:457-461.

Okubo, A. 1962. A review of theoretical models for turbulent diffusion in the sea. J. Oceanographical Society of Japan, the 20th annual volume, 286 p.

_____ and S. Farlow. 1967. Analysis of some Great Lakes drogue studies. Proc. 10th Conf on Great Lakes Research, pp. 299-308. International Association for Great Lakes Research.

Pierson, W.J., Jr. 1964. The interpretation of wave spectrum in terms of the wind profile instead of the wind measured at a constant height. J. Geophys. Res., 69.

Richardson L. E. 1926. Atmospheric diffusion shown on a distance neighbor graph. Proc. Royal Soc. London, Phil. Trans., A110:709-727.

_____ and H. Stommel. 1948. Note on eddy diffusivity in the sea. J. Meteorology, 5:238-240.

Richardson, W. S. 1962. Instruction manual for recording current meter. Woods Hole Oceanographic Instituttion, Ref. No 62-6, 10 p.

Robinson, A. R. 1959. The symmetric state of a rotating fluid differentially heated in the horizontal. J. Fluid Mech., 6:599-620.

Rodgers, G. K. 1965. The thermal bar in the Laurentian Great Lakes. Proc. 8th Conf. on Great Lakes Research, Univ. of Michigan, Great Lakes Research Division Publ. No. 13:358-363.

_____. 1966. The thermal bar in Lake Ontario, spring 1965, and winter 1965-66. Proc. 9th Conf. on Great Lakes Research, Univ. of Michigan, Great Lakes Research Division Publ. No. 15:369-374.

Schlichting, H. 1968. Boundary-layer theory. McGraw-Hill, N. Y., 737 p.

Stoermer, E. F. 1968. Nearshore phytoplankton populations in the Grand Haven, Michigan vicinity during thermal bar conditions. Proc. 11th Conf. on Great Lakes Research, pp. 137-150. International Association for Great Lakes Research.

Stommel, H. 1955. Lateral eddy viscosity in the Gulf Stream system. Deep-Sea Res., 3:88-90.

Strong, A. E. and F. R. Bellaire. 1965. The effect of air stability on wind and waves. Proc. 8th Conf. on Great Lakes Research, Univ. of Michigan, Great Lakes Research Division Publ. No. 13:283-289.

Sverdrup, H. U., M. W. Johnson, and R. H. Fleming. 1942. The oceans. Their physics, chemistry, and general biology. Prentice-Hall, N. Y., 1087 p.

Tikhomirov, A. I. 1963. The thermal bar of Lake Ladoga. Bull. (Izvestiya) All-Union Geograph. Soc. 95, American Geophys. Union Transl. Soviet Hydrology, selected paper No. 2:182-191.

U. S. Department of Commerce, Weather Bureau. 1959. Climatology and weather services of the St. Lawrence Seaway and Great Lakes. Prepared by Marine Area Section, Office of Climatology, U. S. Dept. of Commerce, Weather Bureau Technical Paper No. 35, 75 p.

U. S. Department of the Interior, Federal Water Pollution Control Administration. 1967. Lake currents. A technical report containing background data for a water pollution control program. Water Quality Investigations, Lake Michigan Basin, U. S. Dept. of the Interior, Federal Water Pollution Control Administration, Great Lakes Region, Chicago, Ill., 364 pp.

Van Dyke, Milton. 1964. Perturbation methods in fluid mechanics. Academic Press, N. Y., 229 p.

Verber, J. L. 1964. Initial current studies in Lake Michigan. Limnology and Oceanography, 9:426-430.

_____. 1965. Current profiles to depth in Lake Michigan. Proc. 8th Conf. on Great Lakes Research, Univ. of Michigan, Great Lakes Research Division Publ. No. 13:364-371.

Welch, P. S. 1952. Limnology. 2nd ed. McGraw-Hill, N. Y., 538 p.